# SYNTHESIS OF GOLD COMPLEXES FROM DIPHOSPHINE LIGANDS AND SCREENING REACTIONS OF HETEROCYCLIC ACETYLACETONATO (ACAC) LIGANDS WITH TRANSITIONAL METAL COMPLEXES

Rogers Nyamwihura, B.Sc.

Thesis Prepared for the Degree of

MASTER OF SCIENCE

UNIVERSITY OF NORTH TEXAS

August 2015

APPROVED:

Michael G. Richmond, Major Professor
Martin Schwartz, Committee Member
William E. Acree, Jr., Committee Member and Chair of the Department of Chemistry
Costas Tsatsoulis, Interim Dean of Toulouse Graduate School

Nyamwihura, Rogers. *Synthesis of gold complexes from diphosphine ligands and screening reactions of heterocyclic acetylacetonato (ACAC) ligands with transitional metal complexes.* Master of Science (Chemistry), August 2015, 122 pp., 14 tables, 44 figures, 98 numbered references.

Syntheses of diphosphine gold (I) complexes from gold THT and two ligands, 4, 5-bis (diphenylphosphino)-4-cyclopenten-1, 3-dione (BPCD) and 2,3-bis(diphenylphosphino)-N-phenylmaleimide (BPPM), were done separately. The reactions happened under ice conditions followed by room temperature conditions and produced two diphosphine gold (I) complexes in moderated yield. Spectroscopic results including nuclear magnetic resonance (NMR) and X-ray crystallography were used to study and determine the structures of the products formed. Moreover, X-rays of all newly synthesized diphosphine gold (I) complexes were compared with the known X-ray structures of other phosphine and diphosphine gold (I) complexes. There were direct resemblances in terms of bond length and angle between these new diphosphine gold (I) complex structures and those already published. For instance, the bond lengths and angles from the newly prepared diphosphine gold (I) complexes were similar to those already published. Where there were some deviations in bond angles and length between the newly synthesized structures and those already published, appropriate explanation was given to explain the deviation.

Heterocyclic ligands bearing acetylacetonate (ACAC) side arm(s) were prepared from ethyl malonyl chloride and the heterocyclic compounds 8-hydroxylquinoline, Syn-2-peridoxyaldoxime, quinoxalinol and 2, 6-dipyridinylmethanol. The products (heterocyclic ACAC ligands) from these reactions were screened with transition metal carbonyl compounds in thermolytic reactions. The complexes formed were studied and investigated using NMR and X-

ray crystallography. Furthermore, the X-ray structures of the heterocyclic ACAC ligand or ligand A and that of rhenium complex 1 were compared with similar published X-ray structures. The comparison showed there were some similarities in terms of bond length and bond angles.

ACKNOWLEDGEMENTS

This thesis would not have been possible without the support and guidance of my thesis committee members. My first gratitude goes to my advisor, Professor Michael Richmond, for his unstinting support, constructive criticism, and willingness to allow me to work in his laboratory. I would also like to thank my other committee members, Professor Martin Schwartz and Professor William Acree, for their support.  all, I would like to express my sincere gratitude to comrade Dr. Vladimir Nesterov for his encouragement and help in analyzing the X-ray structures of my compounds. Furthermore, I thank Dr. Bidisha Mallik for the immense support she has given to me in correcting and organizing my thesis. Moreover, I would like to thank my laboratory mate, Dr. Li Yang, for the training he has given me; without his support, this work would not have materialized. Finally, I would like to thank the University of North Texas for giving me financial help and support and for enabling me to complete this project in the first place.

TABLE OF CONTENTS

Page

LIST OF TABLES

Page

LIST OF FIGURES

Page

LIST OF SCHEMES

Page

LIST OF ABBREVIATIONS

| | |
|---|---|
| BINAP | 1,1′-Binaphthalene-2,2′-diyl)bis(diphenylphosphine |
| BMA | 2,3-Bis (diphenylphosphino) maleic anhydride |
| BPCD | 4, 5-Bis (diphenylphosphino)-4-cyclopenten-1, 3-dione |
| BPPM | 2,3-Bis(diphenylphosphino)-*N*-phenylmaleimide |
| DCE | Dichloroethane |
| DCM | Dichloromethane (methylene chloride) |
| e.e | Enantiomeric excess |
| FW | Formula weight |
| Gold THT Chloride | Gold tetrahydrothiopene chloride |
| HOMO | Highest occupied molecular orbital |
| IR | Infra-red |
| LUMO | Lowest unoccupied molecular orbital |
| NMR | Nuclear magnetic resonance |
| $R_f$ | Retention factor |
| THF | Tetrahydrofuran |
| TLC | Thin layer chromatography |

# CHAPTER 1

# INTRODUCTION

*Science may set limits to knowledge, but should not set limits to imagination.*

Bertrand Russell

## 1.1 Introduction

Ligands are important compounds in organometallic and organic chemistry. They are used in the synthesis of desirable compounds. This is because ligands in some ways behave like enzymes by organizing the transition state as well as stabilizing the metal center during reaction; in this way, it is easy for chemists to have stereo and regiochemical control of the desirable products. This thesis focuses on diphosphine and acetylacetonate (acac) ligands. These are commonly used ligands in organometallic and organic chemistry.

Phosphine ligands are at the center of transition metal chemistry. They have been well studied and utilized by chemists in areas such as organic synthesis, redox chemistry, and catalysis. For instance, (R)-(+)-(1, 1'-binaphathalene-2, 2'-diyl) bis (diphenylphosphine) or (R-BINAP) is a commonly used ligand in the synthesis of chiral compounds. Phosphines are useful because of their important electronic and structural properties which give them versatility. The electronic and structural properties of phosphines can be manipulated by simply varying different substituent groups attached to the phosphorous. This results in a dramatic change in ligand properties. Some of the visible outcomes of electronic and structural properties which make phosphines superior over other ligands such as amine and N-heterocyclic carbene (NHC) include the following: first, unlike NHC ligands, phosphines are spectactor ligands; they do not participate in chemical reactions or interfere in any way with metal activities. Second, because of their large inversion energy barrier, phosphines can exist as enantiomeric pure compounds,

unlike amine ligands which have a low inversion barrier and tend to exist as racemic mixtures. Enantiomeric pure phosphines are useful in the synthesis of chiral compounds. Third, phosphine can stabilize the metal center in a complex; this is because phosphines are good sigma electron donors and can behave as a good π-acids. Detailed information on phosphine properties is discussed in Section 1.3.

Acetylacetonate and its derivatives such as β-diketonates, are also important ligands. Their use depends on their chemical reactivity, volatility, and thermal and solvolytic stability. These properties have made their metal complexes to have wide application in solvent extraction as well as in gas chromatography extraction of various metals. Furthermore, in N.M.R. spectroscopies, lanthanides containing β-diketonate are widely preferred because of the very insignificant line broadening they cause.

Substituents in acac ligand have a remarkable impact on the properties and behavior of the corresponding complex. For instance, the presence of fluoride in the acac ligand tends to confer higher Lewis acidity on metal atoms. Moreover, it has been found that the volatility and stability of metal β-diketonate is widely increased by the substitution of fluoride in the diketonate ligand.[1]

## 1.2 Gold Compounds in Catalysis

This section discusses gold compounds and their phosphine complexes used in catalysis. In addition, it elaborates on how both gold (I) complexes are used in the synthesis of various organic compounds. Before going deeper into the application of gold compounds in homogenous catalysis, it is better to understand why gold is preferred over other available transition metal catalysts such as $Co_2(CO)_8$, $PdL_n$, $PtL_n$ and $AgL_n$ ( where L stands for “ligand”

and n is the number of ligands attached to the metals). The following are some reasons why gold compounds are better than other transition metal catalysts. First, gold, being a soft transition metal, prefers to bond to other soft elements such as carbon, which makes it perfect for organic synthesis. Second, unlike palladium, gold has a slight tendency to undergo hydride elimination. Third, reactions catalyzed by gold happen at a faster rate than those catalyzed by other transition metals. This high reactivity of gold compounds cannot be explained by ligand exchange rate alone. Fourth, organogold compounds have a propensity to undergo protodemetellation at a faster rate.[2]

One drawback with the use of gold compounds in catalysis is their intransigent nature toward oxidation and their tendency to undergo reduction. For this reason, gold is not a good catalyst for cross-coupling reactions.[3]

### 1.2.1 Gold Phosphine in Catalysis

Gold (I) phosphine complexes have long been used in catalysis; for instance, [$AuCl(PPh_3)$] has been used in oxidative carbonylation of amine. This reaction is done in the presence of oxygen, which acts as an oxidant. Since gold is resistant to oxidation, the catalyst used works well in the presence of air. As reported by Shi, [4] the reaction proceeds at 200$^{o}$ C and 5 atm. to afford carbamate products in high yield (93%).

Acid-promoted intermolecular hydroamination of alkyne to afford ketimine has been done in the presence of [$AuMePPh_3$] catalyst. This reaction has been carried out previously using other metal catalysts such as mercury, ruthenium, zirconium, thallium, rhodium, and palladium, but none has ever achieved both the efficiency and the yield necessary to allow its use on a practical scale. In the presence of [$AuMePPh_3$], the reaction's yield ranges from 59% to 99%.

This reaction proceeds in a solvent-free environment and cannot happen without the use of an acid promoter such as $H_3PW_{12}O_{40}$[5]

In 1999, Hosomi and his co-workers[6] reported on the dehydrogenative dimerization of trialkylstannanes using an Au(I)catalyst. During their studies they conducted a series of parallel reactions using [$AuClPPh_3$] as a catalyst with various trialkylstannate hydrides. From these studies they determined that all reactions afforded high yield between 91-99%. The reaction proceeds faster when triphenyl phosphine ($PPh_3$) is added to the mixture. Without the addition of $PPh_3$ in the reaction mixture, a precipitation of insoluble materials is observed. Addition of $PPh_3$ helps to avoid inactivation of catalytic species and subsequent precipitation.

In 2000, Hosomi[7] reported on the first selective hydrosilylation of aldehyde and aldimiide using [$AuClPPh_3$] catalyst. The reaction achieves both regio and chemoselective reduction of carbonyl compounds. Hydrosilylation of benzaldehyde and subsequently removal of silicon from intermediate product to afford alcohol was done. The reaction was carried out in a series of different solvents and phosphine ligands. It was found that reaction proceeds well under mild temperature ($70^o$ C), and yield was 92% when $PBu_3$ and tetrahydrofurane (THF) were used instead of $PPh_3$ in DMF, which resulted in a 0% yield. $PBu_3$ was added to the reaction to prevent the deactivation of the catalyst. This was evident because the yield of the product was directly related to the addition of more $PBu_3$. $PBu_3$ prevents the formation of gold clusters and reduction of Au (I) to Au (0).

In 2004, Roembeke[8] reported on the successful application of phosphine gold (I) carboxylates and its sulfonates derivative in hydration of alkyne. The products in this reaction are ketone (as a major) and enol ether (as minor product). This reaction has been done with other compounds such as Ru (II and III), Rh (I) and Pt (II) with limited success. With the use of

(triphenylphosphine) gold (I)-p-tolylsulfonate, for instance, it was found that the reaction proceeds with high regioselectivity to afford Markovnikov product in high yield. Moreover, the reaction proceeds well when $BF_3{\cdot}Et_2O$ is used as a co-catalyst.[8]

## 1.3 Phosphine: Properties

At the center of phosphine ligands is phosphorous; an element unlike nitrogen, it can expand its valence shell and use its 3d orbitals in bonding. Furthermore, phosphines are good sigma donors and pi-acceptors. In this way they (phosphines) can help to stabilize metals during bonding. Unlike other ligands such as N-heterocyclic carbene (NHC), phosphines are known to be good spectator ligands: they do not interfere with metal during catalysis.[9] Their bulky size, which depends on the substituent (R) group, can be effectively used by chemists to induce asymmetric induction through stereochemistry or regiochemistry. Moreover, large and bulky phosphine prefers lower coordination numbers, unlike small-size ligands such as carbonmonoxide, which prefers higher coordination numbers.

Studies have shown that when the substituent (R) group present in the ligand is an alkyl such as methyl or ethyl, the acidic strength of phosphine is weakened, whereas with a more powerful electron-rich substituent such as methoxyl or amino group the π-acidity is enhanced. In the phosphine ligand, a low-lying empty orbital (σ*) or (Lowest Unoccupied Molecular Orbital) LUMO of the P-R bond is the one that is responsible for π-acidity.[10] In the case of the electronegative substituent group attached to the phosphine ligand, there is a general tendency to lower the energy level of the LUMO (σ*) of the phosphorous-substituent (P-R) bond. This in turn has a stabilizing effect on the LUMO. The more electronegative R is, the lower the energy of the LUMO or σ*. For instance, the P-F bond has lower energy than the P-O bond, which is

also of lower energy than the P-N bond, which is also of lower energy than the P-C bond. As the LUMO (σ*) becomes lower in energy, it tends to be a better pi-acceptor of electrons from the metal donor through backbonding. Back donation lengthens and weakens the P-R bond. The lengthening impact on the P-R bond of back donation from metal is vitiated by phosphorous' donation of its lone pair to the metal orbital.[11]

One important thing to remember is that though phosphines are excellent ligands in homogenous catalysis, their limitation in industry arises from the fact that they tend to undergo oxidative addition. This leads to their degradation as well as to the deactivation of the metal center during catalysis. Figure 1.1 shows some common examples of phosphine ligands.

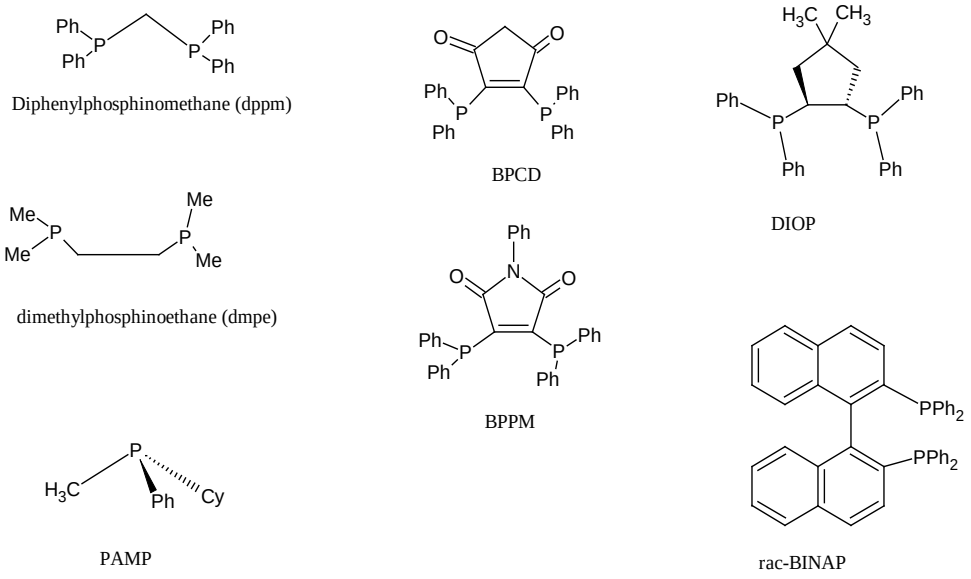


Figure1.1 Some Common Examples of Phosphine Ligands

The order of increasing π-acidity character of phosphine ligands is given as follows:

$$PMe_3 = P(NR_2)_3 < PAr_3 < P(OMe)_3 < PCl_3 < CO = PF_3$$

As one can see, $P(NR_2)_3$ is a good electron donor because lone pair electrons in nitrogen compete with metal $d_\pi$ orbitals in donating to P-R LUMO (σ*). [12] Ligands on the left such as

$PMe_3$ are great electron donors and poor π-acids, while the opposite is true at the opposite end: $PF_3$ is a great π-acid and poor electron donor.

### 1.3.1 Phosphine's Basicity

Free trialkylphosphines and trialkylamine have similar protic basicity. For instance, the $pK_a$ of $HPEt_3$ in DMSO is 9.1, whereas the pKa of $HNEt_3$ in the same solvent is 9.[13] However, phosphine binds more strongly to the transition metals than amine. The answer lies in the nature of the interaction between phosphine and metal. This is due to the fact that phosphorous in phosphine is a soft element and most transition metals are soft acids. Nitrogen being a hard element, it does not bind with higher affinity with soft transition metals.

Phosphine ligands can be more easily oxidized than amine ligands because of the formation of stable phosphorous (V). This explains why some phosphine ligands are air-sensitive; for instance, some alkylphosphines are-air sensitive, whereas aryl phosphine as well as phosphites are less air sensitive. In addition, alkylphosphine with bulky substituents (with a high degree of steric hindrance) are less air-sensitive than is alkylphosphine with less bulky substituents.[14] Table 1.1 shows the pKa's of selected phosphine ligands. From the table it can be seen that electron withdrawing groups such as fluorides and chlorides lower the pKa value and basicity, while electron donating groups such as methyl and methoxyl increase the basicity of phosphine.

Table 1.1 Selected pKa of Phosphine Ligands[15]

| $PR_3$ | pKa |
|---|---|
| $(p\text{-}ClC_6H_4)_3P$ | 1.03[c] |
| $(p\text{-}FC_6H_4)_3P$ | 1.97[c] |

| | |
|---|---|
| $Ph_3P$ | 2.73[d] |
| $(o\text{-}MeC_6H_4)_3P$ | 3.08[c] |
| $(p\text{-}MeC_6H_4)_3P$ | 3.84[c] |
| $(pMeOC_6H_4)_3P$ | 4.57[c] |
| $MePh_2P$ | 4.59[e] |
| $Me_2PhP$ | 6.50[d] |
| $Me_3P$ | 8.65[d] |

Note, permission to reproduce these data in Table 1.1 was granted by the ACS publisher, and the data are from the work of Angelici, R.J.; Bush, R.C. *Inorg. Chem.* **1988**, 27, 681-686.[15]
[c] source: Allman, T.; Goel, R.G. *Can.J.Chem.* **1982**, 60, 716.
[d] source: Streulli, C.A. *Anal.Chem.* **1960**, 32, 985.[e] source: Golovin, M.N.; Rahman, M.M.; Belmonte, J.E.; Giering, W.P.*Organometallics* **1985**, 4, 1981.

### 1.3.2 The Phosphorous Inversion Barrier

Phosphorous has a higher inversion barrier than nitrogen. The inversion barrier energy ranges from 29-35 kcal/mol. The higher inversion barrier makes it easier to prepare optically active phosphines. The amine ligand with different substituent group exists as a racemic mixture of two different conformers due to the low inversion barrier of nitrogen. Optical active phosphines ligands are important in synthesis of enantioselective catalysts which are used in asymmetric synthesis.

### 1.3.2 Tolman's Electronic Parameter and Its Importance

Phosphine metal bonding happens in two ways. In the first way, the phosphine sigma ($\sigma$) orbital donates lone pairs of electrons to an empty orbital of metal as shown in Figure1.2a. In the second stage, metal donates back electrons to the phosphine ligand as shown in Figure1.2b. The electrons from metals are donated to the d-orbital of phosphorous, or they can be donated to the

antibonding orbital which is σ*. Now it is widely agreed that the donation happens to the σ*, because the d-orbital of phosphorous is at a much higher energy level.

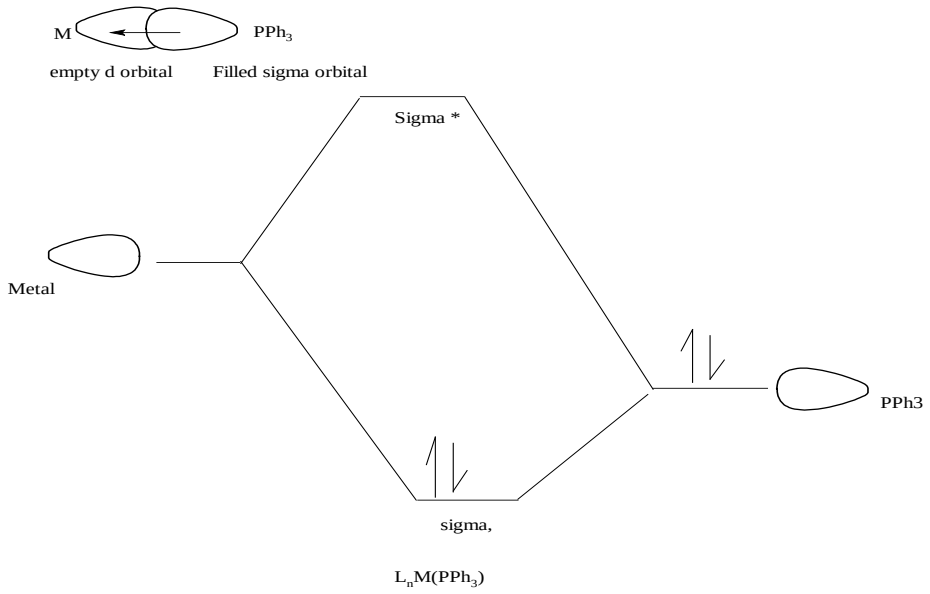


Figure1.2a The top diagram shows Phosphine Donation of Electrons to the Metal Center

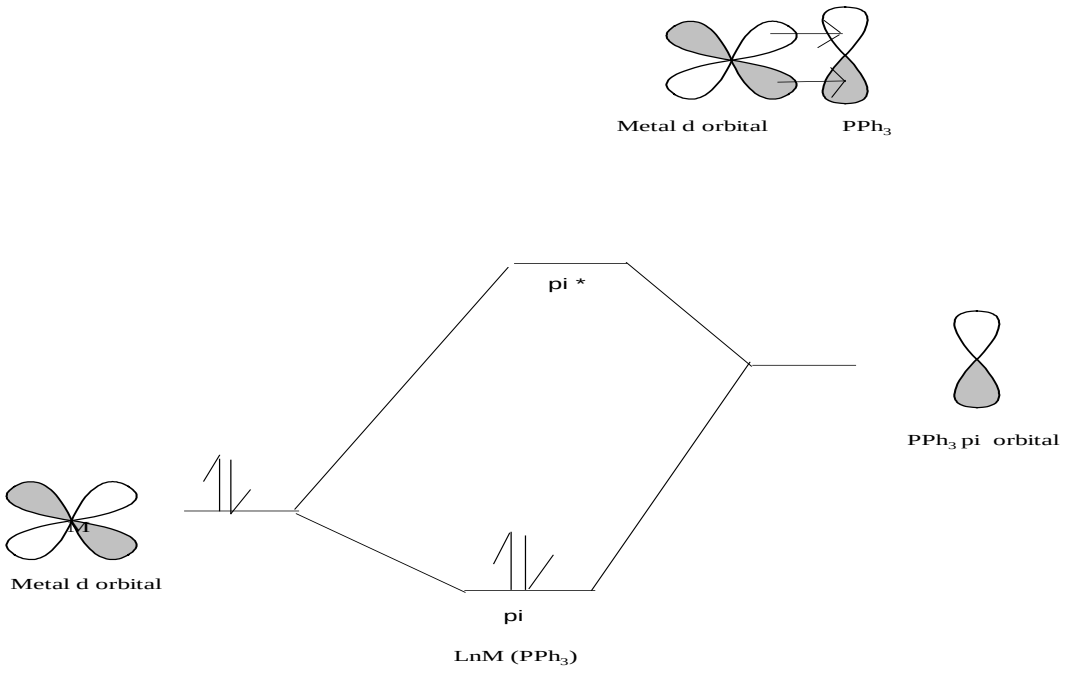


Figure1.2b Metal Donates Electrons to the Phosphine Ligand

The ability or tendency of phosphine to donate electrons through sigma bonding is reduced when R is an electron withdrawing group such as fluorido, phenyl, or chloride. This has significant impact on the energy level of σ*. It tends to lower it, which means more backbonding can happen. The opposite is true if R is a donating group such as methoxy, or alkyl. Therefore, it is possible to manipulate and alter the electronic properties of the metal complex without altering its steric aspect. This can be done by substituting an R group of the same size but different electronic properties or by using isosteric phosphine.

Tolman has done extensive studies on phosphine ligands to determine how the substituents' R group in $PR_3$ influences the electronic properties of the metal in metal complexes. In his studies he compared vibrational frequencies of carbonyl ligands, $^{v}$(CO), from series of complexes of $LNi(CO)_3$ that contained different $PR_3$ ligands. He discovered that electron density on Ni increases when the stronger donor phosphine is present, and some of the electron density from Ni is passed to the CO ligands through back donation. This has an effect of lowering the vibrational frequency $^{v}$(CO). The stronger the donor ligand, the more electron density is passed from the metal to the carbonyl. If the donor ligand competes with the carbonyl ligand for back donation to the metal, the vibrational frequency of CO is increased. Metal carbonyl backbonding is formed between the metal d orbital and π* of carbonyl, which leads to the strengthening of the metal-carbon bond (M-C), and at the same time it weakens the carbon-oxygen bonding (C-O) of the carbonyl. The notable effect of increasing the electron donating power of the ligand is found in the change in equilibrium between oxidative addition and reductive elimination. In this case the increase in ligand donating power favors the oxidative addition product.[16] Table 1.2 illustrates the relationship between phosphine ligand electronic donating ability and its impact on the vibrational frequencies of the carbonyl carbon-oxygen bond. From the table it can be seen that there is a small decrease in

vibrational frequency as hydrogen is replaced by methyl. The increase in the electron donating ability of alkyl group, R, in turn leads to a decrease in frequency, $\nu$(CO). In general, the lower the value of the vibrational frequency of the carbonmonoxide, the greater the backbonding to the metal; this means more electron density at the metal. In other words, the more electron density phosphine donates to the metal, the more the π-back donation to the carbonyl ligands, and thus the weaker the CO triple bonding, thereby lowering $\nu$(CO) frequency.

Table 1.2 Tolman's Electronic Parameter of Various Phosphine Ligands and their Impact on Vibrational Frequencies of Carbonyl in $Ni(CO)_3L$

| Phosphine Ligand, L | Vibrational Frequencies, $\nu$($cm^{-1}$) |
|---|---|
| $PF_3$ | 2112.0 |
| $P(p\text{-}Tol)_3$ | 2066.7 |
| $P(o\text{-}Tol)_3$ | 2066.6 |
| $P(Me)_3$ | 2064.1 |
| $PEt_3$ | 2061.7 |
| $P\ (i\text{-}Pr)_3$ | 2059.2 |
| $P\ (t\text{-}Bu)_3$ | 2056.1 |

Note, data in this table were taken from the journal article by Tolman, C.A. *Chem.Rev.* **1977**, 77, 313-348.[11] Permission to use these data was granted by the ACS publisher.

Tolman reasoned that the more strongly electron donating phosphines are associated with electron rich metals, the better the CO backbonding, and thus the lower the vibrational frequency, $\nu$CO. This means better donor ligands tend to lower the $\nu$CO. For instance, $PF_3$ is a very small ligand with a small cone angle and yet it results in higher vibrational frequency of $\nu$CO, while $P\ (t\text{-}Bu)_3$ is a good donating phosphine with a bulky size and results in lower $\nu$CO.

### 1.3.3 Tolman's Cone Angle

Phosphorous' ability to compete for coordination positions on Ni (0) can only be explained by the ligand cone angle. The ligand cone angle is used to measure the size of the ligand, and it is defined as an angle formed at center vertex of the metal and hydrogen atoms around the perimeter of the cone.

The ligand cone angle concept has been applied in organic synthesis, particularly in homogenous catalysis. This is due to the fact that the size of the ligand tends to affect metal reactivity. Studies were conducted by Uttley[17] and his group on the reaction between $H_3IrCI_6$ and phosphine ligands. When very bulky ligands $PPh(^tBu)_2$ and $P(^tBu)_3$ react with $H_3IrCI_6$, the product is dihydride $H_2IrCIL_2$. One hydride and five chloride atoms are replaced by two ligand molecules, but when less bulky ligands $PMe(^tBu)_2$ and $PEt(^tBu)_2$ are used, the product is monohydride $HIrCI_2L_2$. This implies that bulky ligands prefer hydrogen over chloride because the hydride ligand causes less steric strain.

In general, one can control the reactivity of a metal complex by controlling the size of the ligand; for example, bulky phosphine ligands tend to dissociate faster than small size ligands; this allows reactions to happen faster when bulky ligands are used. Conversely, if dissociation is to be done slow, small size ligands are preferred, and in this way one can lower the reaction rate. It is possible change electronic effects without changing steric effects or to change steric effects without changing electronic effects. Table 1.3 provides information on the relation between cone angle and ligand size; note that there is a direct correlation between the two: as the ligand gets bigger so does the cone angle.

Table 1.3 Phosphine Ligands and Cone Angles

| Ligand | Angle (°) |
|---|---|
| $PH_3$ | 87 |
| $PF_3$ | 104 |
| $P(OMe)_3$ | 107 |
| $P(Me_3)_3$ | 118 |
| $PEt_3$ | 132 |
| $P(Ar)_3$ | 145 |
| $P(Cy)_3$ | 179 |
| $P(t\text{-}Bu)_3$ | 182 |
| $P(C_6H_5)_3$ | 184 |

Note; data from this table were taken from the journal article by Tolman, C.A. *J. Am. Chem. Soc.*, **1970**, *92*, 2956–2965.[18] Permission was granted by the publisher, American Chemical Society.

## 1.4 Phosphine Ligands in Catalysis

All transition metals, especially late transition metals, form complexes with trivalent phosphorous compounds.[19] Phosphine complexes are excellent catalysts because of the following factors. First of all, when a molecule coordinates to the metal center, the reactivity of the functional group(s) of that molecule is radically altered. Secondly, reactive species of the molecules become stabilized and react in a controlled manner. Thirdly, two or more molecules coordinate to the same metal center, and their proximity at the metal centers increases the probability the molecules will react. Forth, the presence of the phosphine ligand not only stabilizes the intermediate complex but also controls the manner in which the molecules react, thus inducing selective conversion.

qPhosphine ligands are important ligands in organic synthesis; some of their advantages over other known ligands include their inertness in chemical reaction; as has been pointed out, phosphines are spectator ligands. Moreover, they are easy to manipulate in order to induce enantioselectivity, diastereoselectivity and regioselectivity. Several applications of these ligands

that are important in asymmetric hydrogenation and coupling reactions are discussed in the following sections.

### 1.4.1 Phosphine in Asymmetric Hydrogenation

In industry, asymmetric hydrogenation is an important reaction in the synthesis of various products and intermediates such as L-menthol, carbapenem and β-amino acids. In order to induce asymmetry in a molecule, chiral ligands such as BINAP [20] have been designed and prepared. Asymmetric hydrogenation is often carried out using complexes of Ruthenium (Ru), Iridium (Ir) and Rhodium (Rh). Ruthenium is an excellent metal because it is relative cheap compared to rhodium, and it has a high performance compared to iridium. Although BINAP has been used because of its performance, occasionally it has failed to produce adequate results. It is for this reason that other chiral ligands such as BIPHEMP and SEPHOS were developed. For instance, in a study by Shimizu and his co-workers on asymmetric hydrogenation of hydroxylacetone it was found that BINAP produced 89 % e.e, BIPHEP produced 92.5% e.e, and MeO-BIPHEP produced 96% e.e. This observation was carefully studied, and it was postulated that as the dihedral angle becomes smaller, the interaction between the ligand and substrate becomes stronger; hence, the enantioselectivity is enhanced.[21] Figure1.3 shows various chiral ligands used in hydrogenation. The ligands shown have axial chirality instead of chiral centers.

The SEGPHOS ligand, which has a smallest dihedral angle of 64.99º, was synthesized and later modified to produce various analogies by changing the R group. These analogies include Tol-SEGPHOS, DM-SEGPHOS, and DTBM-SEGPHOS. For more information about these analogies please see reference 21.[21]

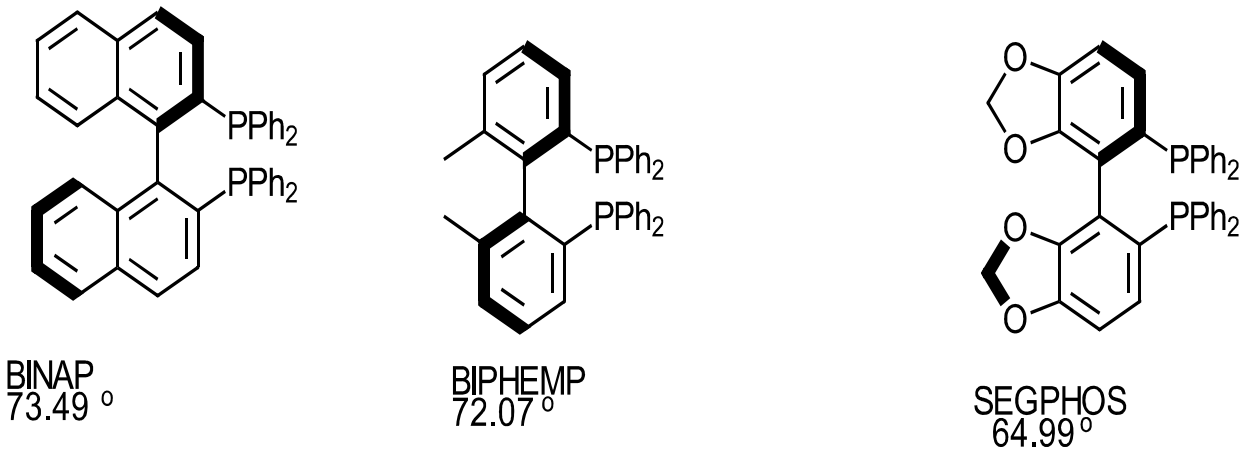


Figure 1.3. Dihedral Angle and Enantioselectivity in the Asymmetric Hydrogenation of Hydroxyacetone

Asymmetric hydrogenation of hydroxyl acetone proved that the SEGPHOS ligand had a higher performance in terms of catalytic activities and enantioselectivities than BINAP. The ligand achieved 98.5 e.e and a turnover number (TON) up to 10000 compared to 3000 for BINAP. Despite high enantioselectivity, SEGPHOS, like BINAP, showed low diastereoselectivity. In order to overcome this problem, it was found from studies that substitution at the 3, 5-position of the phenyl appendages on the ligand enhances diastereoselectivity. This led to the design of DTBM-SEGPHOS. Figure 1.4 shows some of the analogies of the SEGPHOS ligand.

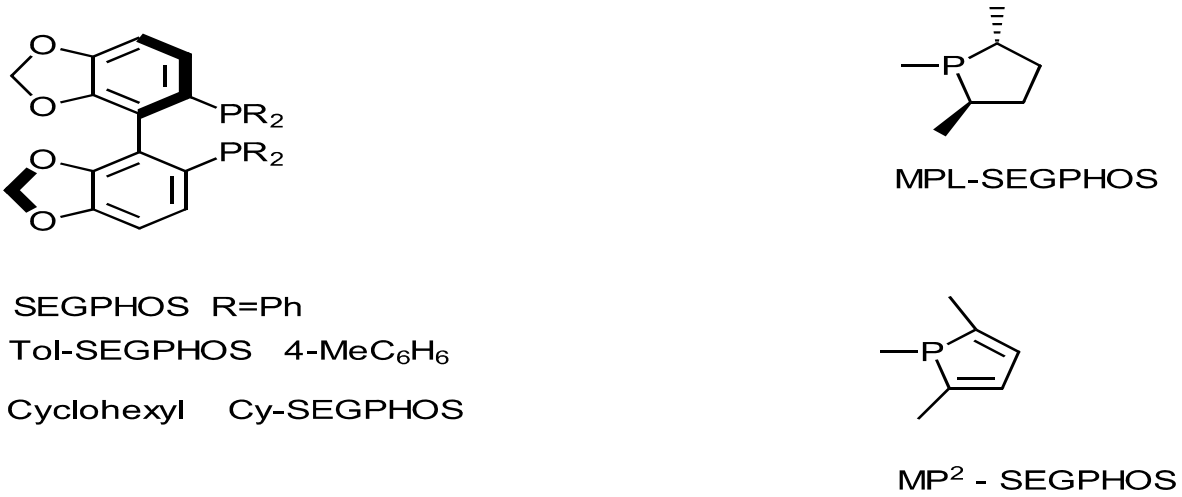


Figure1.4**.** SEGPHOS Analogies

### 1.4.2 Phosphine in Coupling Reactions

Transition metals such as palladium and platinum have been used as catalysts in synthesis of organic compounds both on a small scale and on an industrial scale. Some of the common reactions that employ the use of these transition metals include coupling reactions such as C-H bond activation, carbon-phosphorous bond activation, and carbon-carbon and carbon-nitrogen bond formation. Coupling reactions involve complex steps such as insertion, cyclometallation, oxidative addition, reductive elimination, and sometimes transmetallation. Some of the common coupling reactions include Heck, Suzuki, and Sonagashira coupling. Phosphine ligands are commonly used to stabilize metal centers during the catalytic cycle. Scheme 1.1 illustrates the Heck-Mizoroki coupling reaction and catalyst regeneration. This reaction has been well studied; it starts with oxidative addition, which involves the changes from Pd(0) to Pd(II). In this step there is an increase in the oxidation number of the metal, leading to formation of Pd-C bonds and Pd-R bonds. This step is followed by carbometallation or insertion of Pd(II) into the olefin substrate and subsequent transfer of alkyl (R) from Pd(II) to the olefin to generate a palladium(II) alkyl complex. Elimination of palladium hydride (β-elimination) from the complex affords the final product, which is olefin. The catalyst is regenerated from the base assisted elimination.

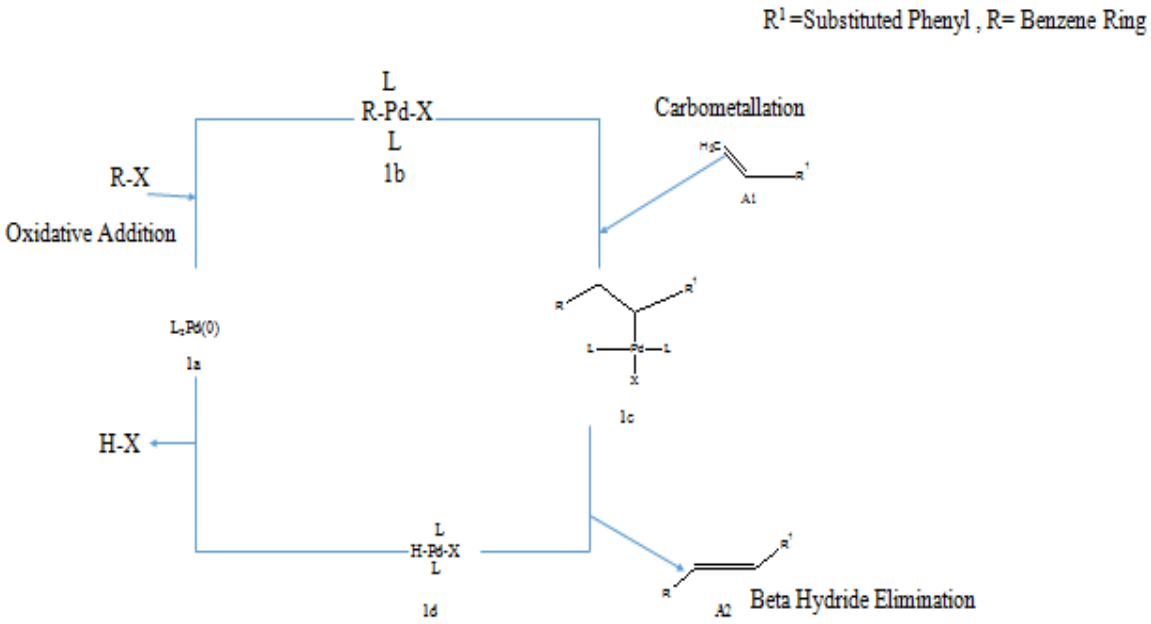


Proposed Mechanism of Heck-Mizouri Coupling Reaction

Scheme 1.1. Heck-Mizouri's Proposed Mechanism of Reaction. For the reference concerning the scheme1.1 please refer to the journal from which it was taken, Knowles, J.P et al. *Org. Biomol. Chem*., **2007**, 5, 31-44.[22]

Palladium cross-coupling reactions such as Stille, Sonagashira, or Suzuki coupling involve similar processes such as oxidative addition and reductive elimination. The difference arises with transmetallation, which is a transfer of a ligand from one metal to another. This is followed by isomerization of ligands at the metal center from the anti-position to the *syn*-position. This is in turn followed by reductive elimination, which is a reverse of oxidative addition. During reductive elimination, the two ligands are joined together to form a carbon-carbon bond. Scheme 1.2 illustrates the general cross-coupling mechanism which involves transmetallation and reductive elimination.

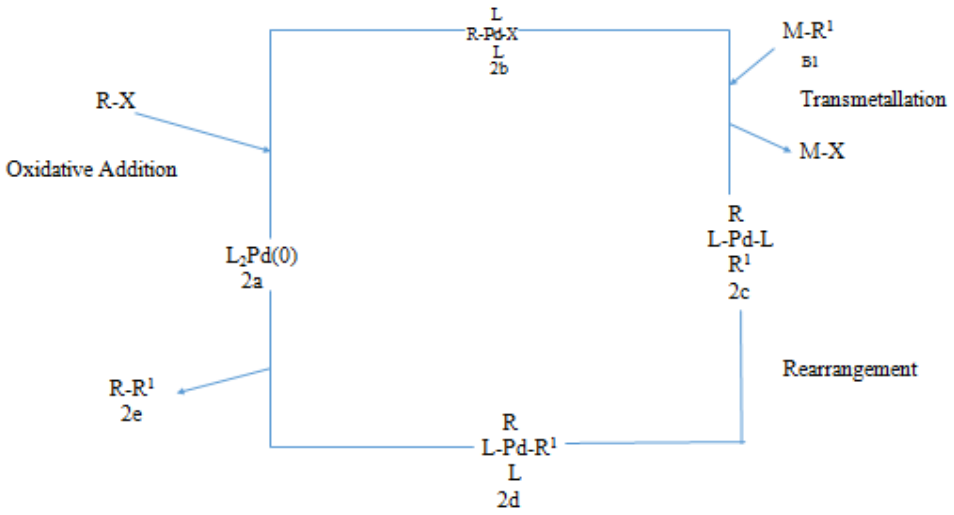


Scheme 1.2. Cross-Coupling Mechanism. For the reference concerning scheme1.2 please refer to this journal from which it was taken. Knowles, J.P et al. *Org. Biomol. Chem*., **2007**, 5, 31-44.[22]

Coupling reactions such as one mentioned have a wide range of industrial and pharmaceutical applications. In this section I have explored some of the applications of the phosphine ligand complex in the design and synthesis of various organic compounds which could not have been accomplished without the phosphine ligand complex.

### 1.4.3 Phosphine in Aliphatic Dehydrogenation of Alkane

Selective functionalization of aliphatic alkane has been a considerable challenge to chemists, first because of the lack of an active functional group in alkane and second due to the lack of selectivity in the functionalization of alkane. Various methods and techniques have been introduced with mixed success. For instance, in 1979 Crabtree[16] reported the first dehydrogenation of alkane using a transition metal catalyst, and this was followed in 1983 when Baudry[23] made a breakthrough in the same area by using a homogenous catalyst. Other complexes were later designed. These complexes work by the transfer of hydrogen from the

alkane to the hydrogen acceptor. These methods have two serious setbacks, the first that they are slow and the second that they suffer from catalyst decomposition.

With the PCP pincer complexes, $IrH_2\{C_6H_3(CH_2PR_2)2\text{-}2,6\}$ where R = $^tBu$ or $Pr^i$, which are effective and powerful catalysts for selective aliphatic dehydrogenation, dehydrogenation happens without the use of a sacrificial hydrogen acceptor. Furthermore, this homogenous catalyst has been used effectively in cyclic alkane dehydrogenation, for instance, conversion of tetrahydorfuran to furan and of cycloalkane to arene. Catalytic conversion of the mentioned compounds is highly inhibited by the presence of nitrogen, even in the smallest amounts. This is due to the formation of the dinitrogen complex, $[Ir\{C_6H_3(CH_2PR_2)2\text{-}2,6\}]_2(\mu\text{-}N_2)$, which poisons the catalyst and renders it useless. Mechanistic studies have shown that aliphatic phosphine in pincers plays an agnostic role in enhancing the catalytic activities of the catalyst.[24] Figure 1.5 shows one of the common catalysts used in dehydrogenation reactions.

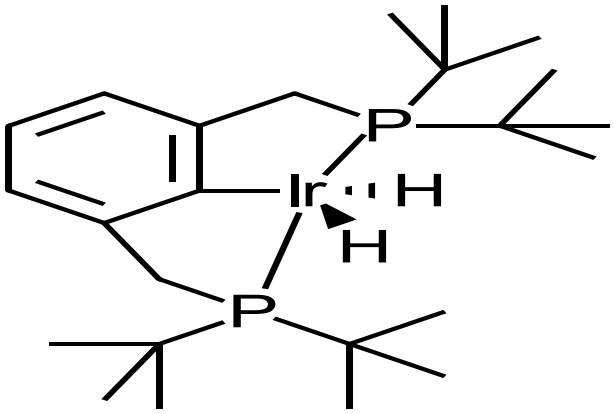


Figure 1.5. PCP Complexes Used in Dehydrogenation Reaction

### 1.4.4 Phospha-Palladacycles in Heck Coupling

Treatment of palladium acetate with sterically demanding tri-ortho-toly phosphine $P(o\text{-}Tol)_3$ in toluene at 50° C furnishes a yellow cyclometallated *trans*-di(μ-acetato)-bis[o-(di-o-

tolylphosphino)benzyl]dipalladium(II), which is an air-moisture-stable compound. This compound as shown in Figure1.6 has been used as a catalyst in arylation of olefin with aryl halides. This Mizoroki-Heck coupling reaction involves the formation of a carbon-carbon bond. In industry, this reaction is used in the synthesis of cinnamic ester derivatives from n-butyl acrylate and aryl bromides. The cinnamic ester products are often used in industries as UV-absorbers, as anti-oxidants in plastics, and as intermediates in pharmaceuticals. The catalyst has a BKMK high turnover number (TON) of up to $10^6$ [mol product/mol palladium] and the yields ranges from 92% to > 99% depending on the substituent on the aryl halide ring.[25] The catalytic activities of this cyclometallated palladium (II) decrease when an alkyl group such as cyclohexyl or tert-butyl is bound to the phosphorus atom, but higher reaction rates are observed with aryl substituents such as *o-tol*, phenyl, and $Me_2S$ when they are bound to phosphorous atom. Also, monomeric complexes like acetylacetonato- [o-(di-o-tolylphosphino)-benzyl] palladium (II) have low catalytic activity in comparison to the dimer.[26] One important industrial application of phospha-palladacycles is in the synthesis of key step intermediates used in making the pain killer naproxen**.**[25]

In 1997 Rawal also reported the synthesis of substituted benzo-fused heterocyclic (indole, benzofurans and benzopyrans). In this synthesis he employed the use of a phospha-palladacylce catalyst, and the reaction proceeded through anionic intramolecular cyclization. Better yields were achieved under mild conditions of 70°C, and the catalyst proved to be superior to traditional $Pd(PPh_3)_4$, $Pd(OAc)_2$ and $Pd(o\text{-}toly)_3$.The main side product produced during the reaction is resorcinol.[27]

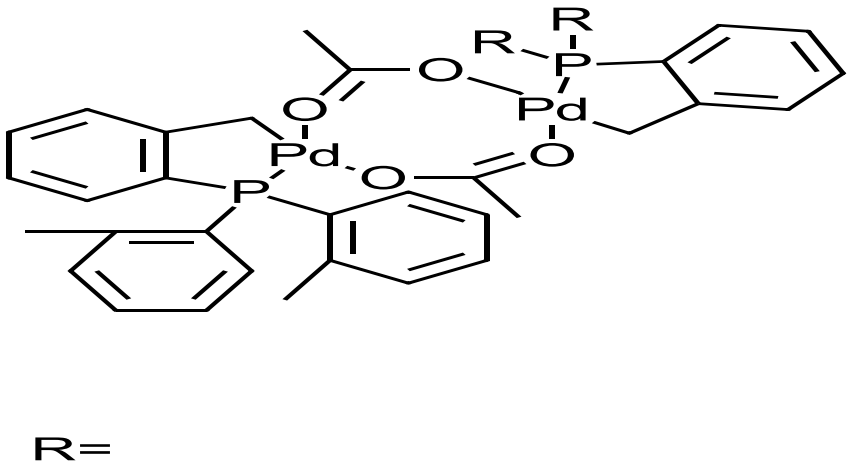


Figure 1.6 Cyclometallated transdi(μ-acetato)-bis[o-(di-o- lylphosphino)benzyl]dipalladium(II)

### 1.4.4 The Application of Phospha-Palladacycles in Stille Coupling

Stille coupling involves the use of aryl or vinyl stannanes with aryl halides or triflate. The reaction also involves transmetallation and reductive elimination. Toxic organotin compounds are used because they are not air or moisture sensitive; besides that, they have high chemoselectivity and can therefore tolerate most functional groups. The palladacycle catalyst has been used by Hartwig and his group in the Stille coupling reaction of 4-bromoacetophenone and $PhSnMe_3$ using toluene as the solvent.[28 and 25]

## 1.5 Current on Diphosphine: BPCD and BPPM Ligands

In my research, I have focused on two rigid tertiary bidentate diphosphine ligands, BPCD and 2, 3-bis (diphenylphosphino)-*N*-phenylmaleimide (BPPM). The two ligands 4, 5-bis (diphenylphosphino) cyclopentene-1, 3-dione (BPCD) and BPPM [29] are known to be redox active when complexed with transition metals such as platinum. They have been used (for instance by Richmond's group) in the synthesis of different types of organometallic complexes such as clusters.[30] In addition, BPCD and BMA (the latter ligand, BMA, were not used in this

study) have been demonstrated by Richmond's group to have one electron reduction at a relatively low potential (<-1.1 V). Moreover, their ability to act as electron reservoirs[31] has been implicated in their tendency to control ligand substitution in reactions involving mononuclear compounds with an excess of 18 electrons. This has been demonstrated by Mao and his co-workers.[32] When functionalized with electron rich organic compounds, the localized HOMO (Highest Occupied Molecular Orbital) of the BPCD ligand can be switched on and off via a substituent such as 4-$Me_2N$ through protonation and quaternization.[33,34] In addition, as far as can be determined from the literature, the ligands BPCD and BPPM have not been used to chelate gold atoms; as they redox active and good donating ligands, it is expected the complex formed from them would have better electrochemical and luminescent activities.

## 1.6 Acetylacetonate (ACAC) and Its Derivatives

Acetylacetonate is a common ligand used in organic chemistry; it has several advantages compared to other known ligands. Some of advantages include that it is very easy to characterize using common techniques such as IR and $^1$H-NMR. The ligand is fairly simple to make and inexpensive. It exists as a tautomer between the keto and enol forms.

### 1.6.1 ACAC Complex Interatomic Distances

Braun[35] reported the average bond lengths (Å) and angles (°) of acac complexes. Selected bond lengths and bond angles of the acac ligand are shown in Figure1.7 . Note that the letter M stands for the metal used.

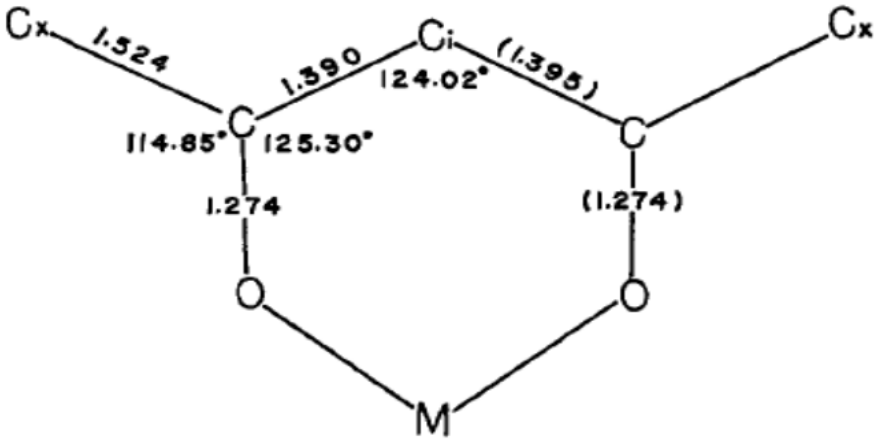


Figure1.7. Selected Bond Angles and Lengths of the Acac complex. Braun, R.L, Lingafelter, E.C. *JACS*, **1966**, 88, 2951-2956. Permission to reproduce this figure has been granted by the ACS publisher.

### 1.6.2 Acetylacetonate (Acac) Ligand Binding Modes

The Acetylacetonato (acac) ligand binds metal ions in different ways. The type of bonding depends on the nature of the metal ions. The first mode of bonding is through the ligand's two oxygen atoms; thus, it behaves as a bidentate ligand (as shown in Figure 1.8 ). In the case of electronegative elements (such as $Au^{1+}$, $Au^{3+}$, $Ir^{3+}$, $Hg^{2+}$ and $Pt^{4+}$), acac prefers to use its acidic carbon atom for bonding. In some cases, both types of bonding appear in one compound.[36] The IR spectra for *O,O'*-coordination are 1630-1500 $cm^{-1}$ for the $^{\nu}$(C=O) and $^{\nu}$(C=C) band. Koda and his group have investigated the binding mode of [$NiBr_2$ (acacH)]; from their studies they have discovered that $Ni^{2+}$ binds the acacH ligand through its oxygen pair (or in neutral keto form).[37] The second binding mode, which involves metal-carbon sigma bond (M-C) bonding, often happens with soft metal ions such as $Pd^{2+}$ and $Hg^{2+}$. This form of binding is sometimes referred to as anion organometallic (M-C) bonding.

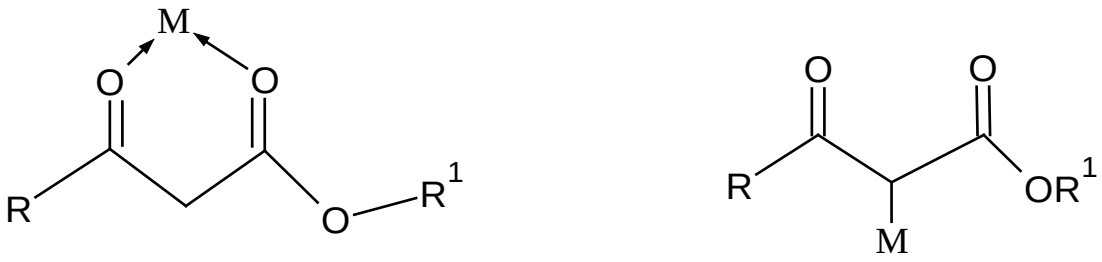


M= Cu ,Re, Zn, $Pt^{2+}$, Pd, etc

$R^1$, R= Me, Et, OMe, OEt, etc

Figure1.8. Acac Binding Modes

The other mode of binding between acac and metal cation includes the neutral enol form. In this binding mode acac tautomerizes in its keto form and produces six–membered rings through coordination with hydrogen, and at the same time one oxygen coordinates to metal cation in a monodentate fashion. In real life sometime more than one binding mode can happen; for instance, studies done by Thornton and his group on $[UO_2(acac)_2(acacH)]$ have shown that two acac ligands bind to the metal center in anionic keto form, while the third ligand is bound to the metal through neutral enolic form.[38]

The anionic keto form is another binding mode which is similar to the neutral keto form (or *O,O*-donor coordination). The only major difference is that in the anionic keto form the acac ligand is keto formed from tautomerization, which means the metal cation forms a six-membered ring with the ligand. Studies by Shalhoub and his group on $[Co(acac)_3]$ have found that the acac ligand binds the cobalt metal center using the anionic keto form binding mode. Infrared spectrum data showing that $^{\nu}CO = 1580\ cm^{-1}$ also support the existence of anionic bonding between oxygen and the metal atom. Furthermore, $^1$H-NMR data also supported their claim, since they show only a 6:1 signal from methyl and methinic protons with a chemical shift of 2.2 and 5.6 ppm respectively.[39]

The last mode of binding is neutral organometallic π-bonding. In this case the metal center forms a bond with the carbon-carbon double bond (C=C) of enolate. Furthermore, the hydrogen covalently bonded to the enolate anion is coordinated to the neutral oxygen of C=O. This mode of binding is very common among platinum compounds. Figure1.9 illustrates the four forms of bonding.

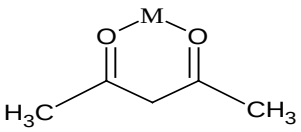


Neutral Keto form

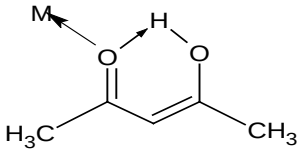


Neutral Keto form

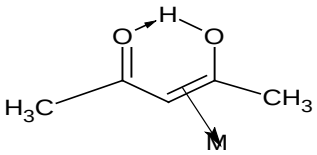


Neutral, Organometallic Pi-bonding

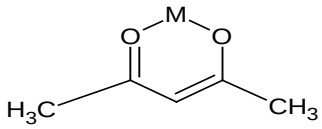


Anionic Keto Form

Figure1.9 Various Modes of Bonding in the ACAC Metal Complex

### 1.6.3 Acac and Its Derivatives: Catalytic Activities

Acac is a versatile organic ligand with a wide range of applications in chemistry. Here, I present some of the general applications of the ligand in chemistry. The acac complex and its derivative 1, 3-diketonate are used as fuel additives[40] and also as a supercritical fluid for waste removal;[41] they are used in luminescent hybrid materials[42] and in extraction of metals;[43] they are used as precursors in metal-organic chemical vapor deposition (MOCVD);[44] in industry they are used in superconducting thin film development;[45] and in organic chemistry they are used in

preparation of homogenous and heterogeneous catalysts[46,47] The catalytic activities of acac ligands are discussed **.**

### 1.6.3.1 $Fe(acac)_3$ as a Redox Catalyst

In the natural gas industry, hydrodesulfurization, the removal of toxic hydrogen sulfide gas ($H_2S$) from natural gas is an important process. It is carried out by oxidation of $H_2S$ to its elemental sulfur $S_8$. The reaction is done by passing oxygen in the presence of a redox iron catalyst. Quite often $H_2S$ is oxidized to unwanted sulfate: $SO_4^{2-}$, sulfite, $SO_3^{2-}$, and $S_2O_4^{2-}$.Unlike $S_8$, which precipitates out, these anions are not easily separated from the reaction mixtures. In order to avoid the formation of unwanted anions, $H_2S$ is separately oxidized by a $Fe^{3+}$ catalyst in the absence of oxygen to $S_8$ and hydrogen, while the iron catalyst is reduced to $Fe^{2+}$. The second step is the regeneration of $Fe^{3+}$ from $Fe^{2+}$ through oxidation by oxygen, which results in the formation of water from hydrogen. Aminopolycarboxylic acid is often used as the ligand to chelate the iron catalyst, but this ligand suffers oxidative degradation through radical reaction. This renders the catalyst useless or inefficient. To overcome this problem, $Fe(acac)_3$ is used instead because the acac ligand is resistant to degradation by radical formation as Dhar and his coworker reported.[48] Moreover, by varying the end R groups in the acac ligand, one can alter its basicities and the formation constant of the complex, in this case $Fe(acac)_3$. For instance, the electron withdrawing group trifluoromethyl ($CF_3$) has been found to lower electron density on carbonyl oxygen, which in turn decreases the basicity of acac, thereby leading to a decrease in the stability of the metal chelating complex. A moderate electron donating group such as phenyl increases both basicity and the formation constant.[49]

### 1.6.3.2 Acetylacetonate (acac) in Oxidation of Hydrocarbon

The acac ligand shows catalytic activities when complexed with transition metal elements such as vanadium. $VO(acac)_2$ is a commonly used catalyst in the oxidation of anthracene or any polyaromatic hydrocarbon. Hydrogen peroxide is an oxidizing agent in this reaction, but the reaction happens only in the presence of $VO(acac)_2$.[50] The product of this reaction is ketone, and the catalyst itself can be prepared from reaction between hydrated $VOSO_4$ and 2, 4-pentanedione in the presence of sodium carbonate and water.[51]

### 1.6.3.3 Acac in Polymerization

$Al(acac)R^2$ where $R=CF_3$ has been reported to have catalytic activities in the polymerization of epoxides. [52] In addition, in recent years much attention has been focused on the potential use of aluminum alkoxide complexes derived from a fluorinated acac ligand. Such complexes are known to have catalytic activities in ring opening polymerization (ROP) of cyclic esters such as ε-caprolactone and lactide. The catalyst has been found to exhibit a high degree of control over polymerization. The polyester produced tends to have a narrow molecular weight distribution and controlled molecular weight. Also, polymerization results in well-controlled stereochemistry. For instance, racemic lactide monomers have been used to produce isotactic-containing polylactides.[52]

$Co(acac)_2$ is another catalyst which has now been employed in the polymerization of vinyl acetate. Traditionally, poly(vinyl acetate) or PVAc has been produced largely by radical polymerization of its monomer vinyl acetate, although coordination polymerization has been used successfully in the production of copolymers with a limited incorporation of vinyl acetate. The use of the radical polymerization of vinyl aceate suffers one serious setback: the radical

monomer tends to react head to head instead of head to tail. Head to head addition results in the formation of primary radicals. The primary radicals react further with the trapping agent, resulting in dormant species which are stubborn to reactivate, thereby slowing down the polymerization reaction and the molecular weight distribution. This problem can be overcome by using $Co(acac)_2$ . Cobalt diacetylacetonate {$Co(acac)_2$ } has been shown to be able to change its reactivity radically by significantly reducing head-head addition or the formation of dormant species.[53] Also, the $Co(acac)_2$ catalyst exerts a high degree of control by increasing its high monomer conversion rate and degree of polymerization.

Group (IV) transition metal acac such as bis(β-diketonate) titanium and zirconium (IV) complexes have been used in the homogenous polymerization of olefin, where their efficiency and effectiveness have eclipsed those of the metallocene catalysts. The advantages these catalyst have over metallocene include their stability and that they are simple and cheap to make and can be modified; for instance, dichlorobis (β-diketonate) titanium together with the co-catalyst methylaluminoxane has been used in the polymerization of styrene, and the polymer produced has high syndiotacticities of 94-98% .[54]

#### 1.6.3.4 $Co(acac)_2$ in Synthesis of Cyclopentenone

A low valent cobalt compound in carbonylation reaction has been widely used in the synthesis of cyclopentenone systems; this reaction is also known as the Pauson-Khand Reaction (PKR). In most cases, $Co_2(CO)_8$ is used as a catalyst in PKR. Cyclopentenone systems are ubiquitous in natural and unnatural products, and as a result, many cobalt based catalysts such as (Indenyl)Co(COD) have been developed to overcome various challenges during cyclopentenone system synthesis and at the same time to keep a high yield. For instance, (Indenyl)Co(COD),

despite being a good catalyst, has little tolerances to some functional groups such as halides and esters, and it has not done well in reactions containing the acetylene functional group. $Co(acac)_2$, together with $NaBH_4$, has proven to be an effective and efficient catalyst capable of overcoming the challenges to which (Indenyl)Co(COD) succumbs. Studies done by Chung's group have shown that the use of $NaBH_4$ enhances the catalytic activities of $Co(acac)_2$ well when phenylacetylene and norborene are substrate. When used with or without $NaBH_4$ salt, cobalt compounds such as $CoCl(PPh_3)$, $CoCl_2$, and $CpCo(CO)_2$ showed little catalytic activity. Furthermore, $Co(acac)_2$ catalyzes both the intramolecular cyclization of enyne compounds and the intermolecular reaction between acetylenic compounds and norborene, even in the case of PKR intolerance toward halides, esters, and alcohols.[55] $Co(acac)_2$ together with $NaBH_4$ still produces moderate to high yield (see reference 84 in Tables 1 and 2), unlike (Indenyl)Co(COD), which perfomed very poorly[55] with these functional groups. The reaction catalyzed by $Co(acac)_2$ involves the formation of cobalt carbonyl; this was proven to be true after isolation of (1-hexyne)$Co_2(CO)_6$ when 1-hexyne and ethylene were used as a substrate. The use of $NaBH_4$ in the reaction is to block the formation of cobalt clusters and or inactive cobalt species; [55] this prolongs the catalyst's life span. The reaction conditions and the yields in these reactions are found in reference 84.[56]

# CHAPTER 2

# EXPERIMENTS

## 2.1 Introduction

This chapter presents the experimental section. It discusses in detail the synthesis and purification of the compounds prepared. In addition, this chapter discusses how solvents and reagents were prepared prior to their use and the instruments used to analyze the prepared compounds. Lastly, this chapter discusses how X-ray testing was done to analyze the newly-synthesized compounds.

## 2.2 Solvents

Methylene chloride was directly obtained through the use of a special machine employed for drying solvents. All solvents were degassed and stored under argon. The rest of the solvents used in the reaction, tetrahydrofuran (THF), ethanol, and 1, 2-dichloroethane (DCE), were degassed before use for at least 40 minutes using argon in a Schlenk vessel.

## 2.3 Reagents

Gold THT and all metal complexes were obtained directly from my advisor, Professor Richmond. Other reagents such as ethyl malonyl chloride and 1, 2-dithiolbenzene were purchased directly from Aldrich.

## 2.4 Instrumentation

All reactions were carried out in an argon environment to exclude air. Schlenk vessels and specialized NMR tubes were used to carry out the reactions. The infrared spectra were

obtained from a Nicolet 20SXB FT-IR spectrometer, using a desktop computer control and OMNIC software in 0.1 mm NaCI cells. The reported NMR spectra were obtained from a 400 MHz Varian instrument, and $^{31}$P-NMR was referenced to external $H_3PO_4$ (85%) with a $\delta$=0 chemical shift.

## 2.5 Preparation of Diphosphine Gold (I) Based Complexes

In this section I present the synthesis of diphosphine gold (I) complex from the phosphorous ligands BPCD and BPPM. All reactions presented in this section were carried out under argon conditions and monitored by TLC. Light was excluded from the reaction in order to avoid decomposition of the gold (I) complex into nanoparticles.

### 2.5.1 Synthesis of $Au_2C_{29}H_{22}O_2Cl_2P_2$ or [$Au_2Cl_2$(bpcd)]

In the preparation of the gold (I) complex as shown in Scheme 2.0 , 0.1 g (0.3125 mmol) of gold THT was dissolved in 50 ml of methylene chloride (DCM) under argon using a Schlenk flask. The solution was stirred using a magnetic bar at 0$^o$ C in an ice-water bath. Into this solution, 0.093g (0.156 mmol) of the BPCD ligand was dissolved in 50 ml of methylene chloride, which was added via cannula method under argon conditions. The stirring continued for 1 hour, and then ice was removed and the reaction was allowed to run at room temperature for another hour. The reaction was monitored using normal phase TLC, and it was found that the product has a retention factor ($R_f$) of 0.26 while BPCD has an Rf of 0.68. The TLC was accomplished using diethyl ether as a mobile phase. Since our desired product is insoluble in diethyl ether but soluble in methylene chloride (DCM), purification of the product was done using solvent extraction. Afterwards, a DCM-ether mixture was used to remove the impurities

from the reaction mixture, and extraction was done twice. The mass of the gold (I) complex product, which precipitated after purification, was found to be 0.0591g, and yield was 40.7% of the pure product. The $^{31}$P-NMR result showed the new peak at 14.12 ppm, which is consistent with the results of past studies.[57] The product obtained was dissolved in DCM and layered with benzene, which resulted in the formation of nice yellowish crystals. Scheme 2.1 shows the reaction between BPCD and gold THT.

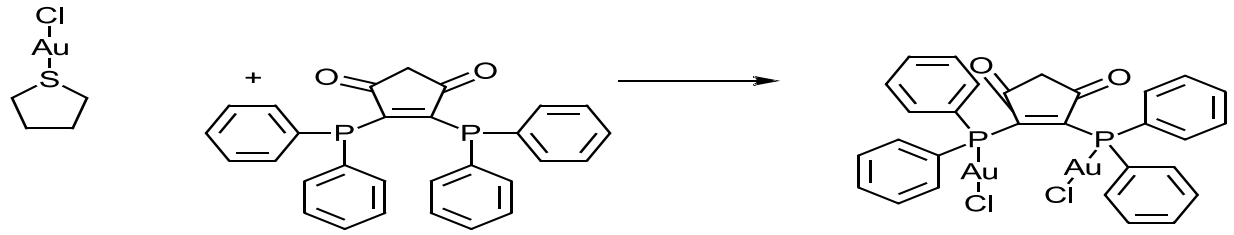


1

Scheme 2.1. Synthesis of Gold (1) Complex from the BPCD Ligand

### 2.5.2 Synthesis of $Au_2Cl_2C_{34}H_{25}O_2N_1P_2$

In the second experiment, 0.1 g (0.3139 mmol) of gold THT and 0.085g (0.1569 mmol) of BPPM ligand were dissolved in 20 ml of DCM under argon conditions. The two reagents were mixed together using a solvent transfer method. The reaction was stirred in an ice-water bath at around 0$^{o}$ C for an hour, after which the ice was removed, and then it was stirred at room temperature for another hour. The reaction was covered with aluminum foil to prevent light from ruining the gold (I) compound. The reaction mixture turned golden orange after approximately an hour. The reaction is shown; see Scheme 2.1. The TLC results were obtained using DCM as the mobile phase, and the product was found to have an $R_f$ value of 0.24. After two hours of

running the reaction, the solvent was removed under reduced pressure. Purification was done using ether extraction. About 2 ml of diethyl ether was used twice to precipitate the product. Afterwards, the product was freeze-dried using benzene. The mass of the pure product finally obtained was 0.0565g, constituting 35.8% of the net yield. The $^{31}$P-NMR result of the product showed a large single peak at 14.2 ppm, this was the same as the result reported by Fenske.[57]

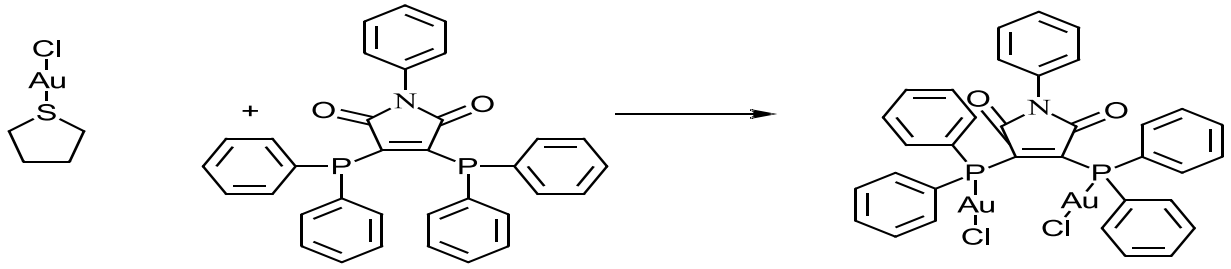


1

Scheme 2.2. Synthesis of Gold (1) Complex from BPPM

## 2.6 Synthesis of Heterocyclic-Based Acac Ligands

Heterocyclic ligands such as syn-2-peridoxyaldoxime, 8-hydroxylquinolinol, and 2, 6-pyridinyldimethanol are known in the literature for their chelating ability. These ligands have been used in metal complexation because of their ability to act as bidentate and sometimes as polydentate ligands. Furthermore, because of their conjugation, these ligands have become a primary target in the synthesis of redox active complexes. In addition, 8-hydroxylquinolinol complexes have been known to have antimicrobial activities which make them a good candidate in drug development. In addition, 8-hydroxyquinoline is a common non-innocent ligand and has dramatic potential to be used as a redox active ligand when complexed with a transition metal

complex. A non-innocent ligand as defined by Jonathan **(**Rochford, J et al. *Organometallics*, **2013**, 32, 1832-1841)[58] "is a ligand whose electronic coupling with central metal d orbitals is so effective that the resulting bonding /antibonding molecular orbital formed cannot be unambiguously assigned to either metal or ligand entities".[58,59] The nature of the metal-ligand bonding is covalent, and the resulting interaction dramatically alters the physical and electronic properties of the metal complex formed.[60,61 ,62 and 63] The π-orbitals of ligand 8-hydroxylquinoline comprehensively overlap with metal $d_\pi$ orbitals, which has a dramatic outcome on the photophysical and electrochemical properties of the complex and make it useful in photocurrent generation in dye-sensitized solar cells. Moreover, the electronic properties of the complex can be further manipulated and modified by the addition of substituents in ligands. Groups such as fluorine, nitro, or chloride are known for their electron withdrawing ability, and this can have a large impact on the energy level of the LUMO of ligands. Such groups are known to lower the LUMO of ligands such as phosphine, thus making the LUMO accessible for metal electron donation.

Despite the plethora of complexes made from these heterocyclic ligands, there has been little interest in the design and synthesis of polydentate ligands from syn-2-peridoxyaldoxime, 8-hydroxylquinolinol or 2, 6-pyridinyldimethanol and acetyl acetonate (acac) ligands. In theory the addition of acetylacetonate to any of these heterocyclic ligands has ability to increase the coordination ability of the product formed. Also, the union with acac greatly modifies and improves the chemical properties of the product. It is because of these reasons that our group decided to take on the synthesis and the acac adduct and prepare their metal complexes in order to determine their complex structure. The next section discusses the synthesis of heterocyclic ligands A, B, and C from ethyl malonyl chloride and heterocyclic compounds. These ligands

were used in the screening reaction with transition metal complexes in order to prepare heterocyclic metal complexes.

### 2.6.1 Synthesis of Ligand A

In the synthesis of ligand A, as shown in Scheme 2.3 , 0.5 g (3.44 mmol) of 8-hydroxylquinolinol was dissolved in 30 ml of dichloromethane (DCM) in a Schlenk flask. This was followed by purging of the flask to remove any air. Argon gas was introduced into the flask to displace the air. To the solution in the flask, 0.34 g (3.37mmol) of $Et_3N$ was added using a syringe. The solution was allowed to stir in an ice-water bath for at least 10 minutes. In the beginning, the reaction had a shiny golden yellow, the color of the ethyl malonyl chloride. The reaction was monitored using TLC and stirred overnight for an approximate 12 hours.

Then the solvent was removed using a high vacuum line, and a dark greenish yellow solution remained together with a white suspension of ammonium salt. An approximate 30 ml of DCM was added to the reaction mixture followed by another 30 ml of deionized water to extract the ammonium salt. The extraction was repeated three times. The organic layer was then treated with $CaCl_2$ to remove any water remaining in the solution. TLC was performed using DCM/ether 4:1 as the mobile phase and revealed the existence of the starting material. The starting material, 8-hydroxyquinolinol, has a $R_f$ value of 0.61, while the product has the $R_f$ value of 0.41. Column chromatography was used to separate the product from the starting material, using the same 4:1 ratio of DCM/ether, but the yield was not recorded. The following are the $^1$H-NMR results: 8.74-8.75 ppm (d, J= 3.2 Hz), 8.12-8.14 ppm (d, J= 8.4 Hz), 7.29-7.31 ppm (d, J= 8.0 Hz), 7.14-7.16 (d, 7.6 Hz), 3.57 (s) and 4.18-4.24 (q).

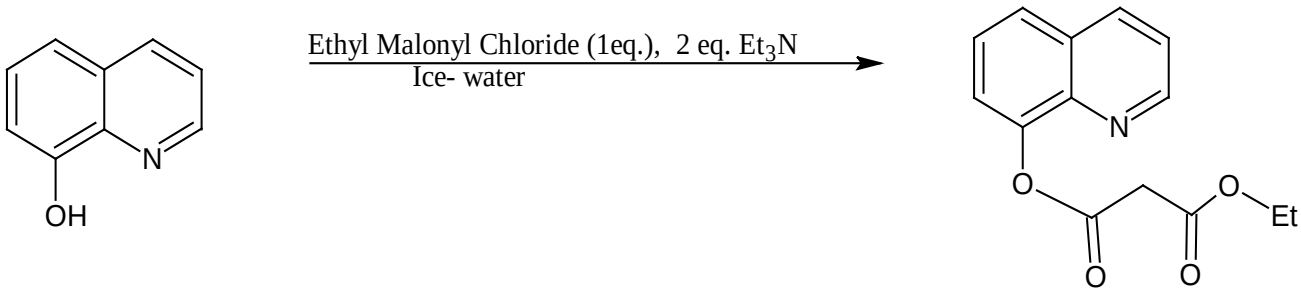


Ligand A

Scheme 2.3. Synthesis of Ligand A

2.6.2 Synthesis of Ligand B

In the synthesis of ligand B, as shown in Scheme 2.4**,** 0.5 g (4.09 mol) of syn-2-peridoxyaldoxime was dissolved in 30 ml of dichloromethane (DCM) in a Schlenk flask. The flask was vacuumed twice and filled with argon using a vacuum line. An excess amount of $Et_3N$ was added to the solution via syringe, and the solution was stirred in an ice-water bath for at least 10 minutes. To this solution, 0.93 g (4.09 mol) of ethyl malonyl chloride was added using a syringe, and the solution was stirred for 3 hours. At the start, the reaction was a shiny golden yellow, the color of the ethyl malonyl chloride. The reaction was monitored using TLC and stirred overnight for an approximate 12 hours.

Then the solvent was removed under vacuum, and a deep red solution remained together with white suspension of ammonium salt from triethylamine. An approximate 30 ml of DCM was added to the reaction mixture. This was followed by another 30 ml of deionized water to extract any ammonium salt. The extraction was repeated three times, and the organic layer was treated with $CaCl_2$ to remove water. After solvent extraction and drying, the reaction mixture turned a slightly golden red. TLC was done using ethyl acetate and DCM in 4:2 ratios that revealed there were three spots with $R_f$ of 0.59, 0.33, and 0.16. The following are the $^1$H-NMR chemical shift δ in ppm: 8.66- 8.65, (dq, J=1.2 and 1.6 Hz), 8.65-8.64, (dq, J=1.2 and 1.6 Hz),

8.05, 8.04, 8.04- 8.02 (t, J= 0.8, 1.2 and 8.0 Hz), 7.78-7.77, (ddt, J= 0.4, 0.8, 1.6 and 2.0 Hz), 7.6-7.75, (d, J=1.6 Hz ), 7.74- 7.73, (dd, J= 0.4, 1.6 and 7.6 Hz), 7.38-7.39, (d, J=1.2 Hz,) and 37-7.36, (dd, J=1.2, 2.8 Hz), and 7.35-7.35 (d, J=1.2 Hz).

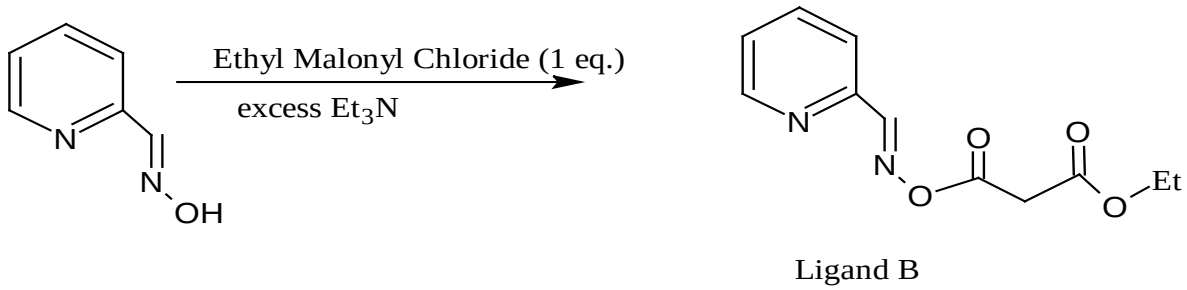


Ligand B

Scheme 2.4. Synthesis of Ligand B

2.6.3 Synthesis of Ligand C

In the synthesis of ligand C as indicated in Scheme 2.5**,** 0.2 g, (1.44 mmol) of 2, 6-pyridinyldimethanol was dissolved in 30 ml of dichloromethane (DCM) in a Schlenk flask. The flask was vacuumed twice and filled with argon using a vacuum line. To the solution in the flask, 0.29 g, (2.87 mmol) of $Et_3N$ was added using a syringe. The solution was stirred in an ice-water bath for at least 10 minutes. At the beginning the reaction was shiny golden yellow, the color of the ethyl malonyl chloride. TLC was used to monitor the reaction. The reaction was stirred overnight for an approximate 12 hours. The next day, the solvent was removed under vacuum. A bright greenish yellow solution remained together with a white suspension of ammonium salt. An approximate 30 ml of DCM was added to the reaction mixture. This was followed by another 30 ml of deionized water to extract any ammonium salt. The extraction was repeated three times. The organic layer was treated with $CaCI_2$ to remove any water remaining in the solution. The obtained product was purified using column chromatography with DCM as the solvent. The mass

of pure product (ligand C) obtained was 0.34 g, which corresponded to a 65.14% yield. The following are the NMR results of ligand; the chemical shifts (δ) are in ppm: δ, 7.950-7.912, (t, J =7.6 Hz), δ, 7.54-7.52, (d, J=7.6 Hz), 5.48 (s), 3.68 (s), and $^{13}$C-NMR: δ, 166.321 and 166.17.

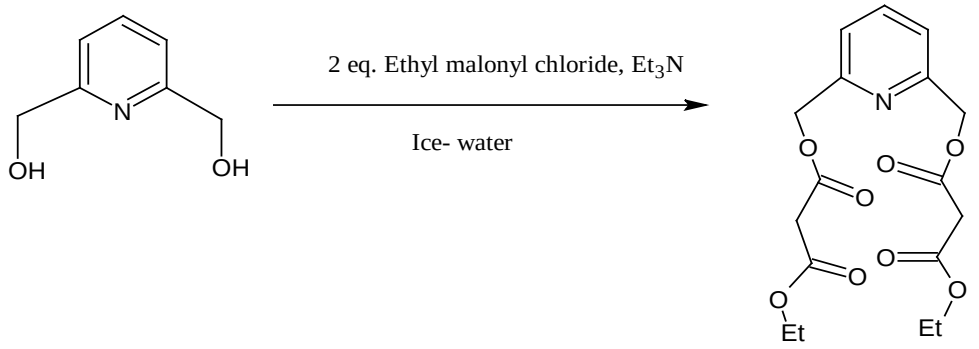


Ligand C

Scheme 2.5. Synthesis of Ligand C

# CHAPTER 3

# THE REACTIONS OF LIGANDS A-C WITH METAL CARBONYL

## 3.1 Introduction

This chapter discusses the preparation of metal complexes from ligands A, B, and C and transition metal carbonyl. The aim of this research is to investigate the binding modes of the acac ligand in metal complexes. Therefore, great interest has been paid and effort has been made toward the investigation of whether there is a reaction between the ligand and the metal complex, and what the structure of the complex formed from thermolytic reaction.

### 3.1.1 Synthesis of Rhenium Complex 1

The method used to prepare these complexes was derived from reference 21.[64,65,66 and 67] An approximate 0.05g (0.136 mmol) of ligand C and 0.0442g (0.136 mmol) of $ReBr(CO)_5$ were added to the Schlenk flask and vacuumed using a high vacuum line. This was followed by the addition of 0.1 g of NaOH solid. Argon gas was added after vacuuming, and 30 ml of dichloroethane (DCE) was added. The solution was warmed to a higher temperature slowly. Finally, the temperature was raised to 125° C. The reaction mixture changed from fading yellow (the color of the ligand) to bright yellow. The reaction was allowed to reflux overnight. The next morning, the TLC was taken using ether-DCM in a 3:1 ratio. TLC revealed the presence of the ligand and two spots with $R_f$= 0.18 and the baseline $R_f$ = 0.00. An approximate 0.01 g of $ReBr(CO)_5$ was added, and reaction was refluxed until all the ligand was consumed. The solvent was removed, and crude NMR was taken. After the NMR studies, the reaction mixture was dissolved in a small amount of DCM and layered with benzene; after a few weeks a colorless single crystal was obtained. X-ray was used to analyze the structure. The structure of the product

is shown in Scheme 3.1. The $^{1}$H-NMR results are as follows, in which all chemical shifts are in ppm: δ, 8.29-8.25 (t, J=8.0 Hz), δ, 7.77 -7.75 (d, J=8.0 Hz), 4.28 (s), 3.73 (s) and 3.57 (s). The IR results are 1924 cm$^{-1}$, 2023 cm$^{-1}$, 2253 cm$^{-1}$ and 2375 cm$^{-1}$.

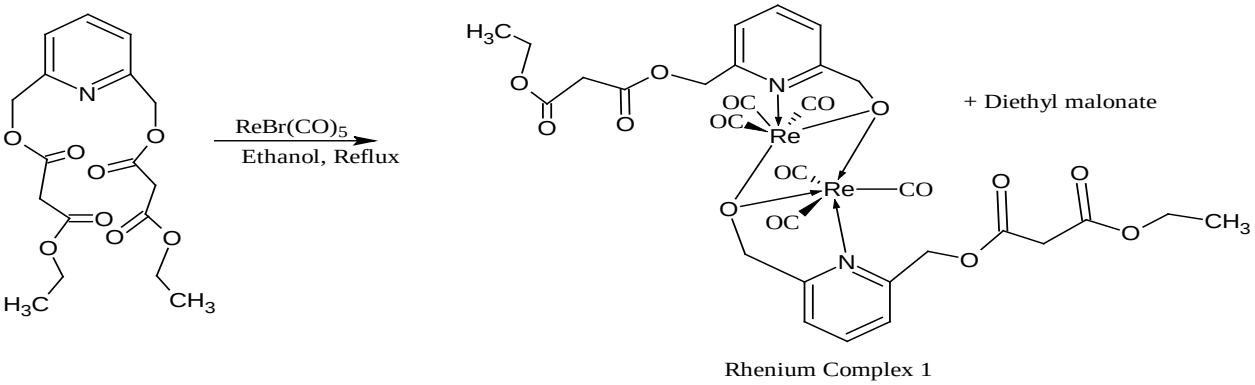


Scheme 3.1. Attempted Synthesis of Rhenium Complex 1

### 3.1.2 Attempted Synthesis of Rhenium Complex 2

In an attempted synthesis of rhenium complex from ligand A, 0.11 g (0.41 mmol) of ligand A and 0.13 g (0.33 mmol) of $ReBr(CO)_5$ were added to the Schlenk flask, which was vacuumed. This was followed by the addition of argon gas and 25 ml of DCE solvent to the mixture. The solution was warmed slowly to 110° C. The reaction mixture changed from green (the color of the ligand) to a dark honey-brown solution after an overnight of reflux. TLC was performed using diethylether: DCM in 3:1 ratio revealed there were ligand starting materials. Then 0.2 equivalent (0.03 g) of $ReBr(CO)_5$ was added to the mixture and the mixture was refluxed. After 4 hours of refluxing at 110° C, the solvent was removed and an NMR was taken. The results of the NMR are shown and discussed under “discussion and results.” The TLC showed a new spot with $R_f$ of 0.21. The proposed structure from the reaction is shown in Scheme 3.2.

The following are the $^{1}$H-NMR results from the reactions; note that all chemical shifts (δ) are in ppm: δ, 9.04-9.03 (d, J= 4 Hz), δ, 8.33-8.31 (d, J= 8.4 Hz), δ, 7.96-7.94, (dd, J=1.6, .4.8 Hz,), δ, 7.78-7.76, (dd, J=1.2, 8.4 Hz) and δ, 7.42-7.40, (dd, J=0.8, 1.2, 8.0 Hz). The IR vibrational peaks of the products are: 1900 cm$^{-1}$, 2025 cm$^{-1}$, and a small sharp peak at 2300 cm$^{-1}$.

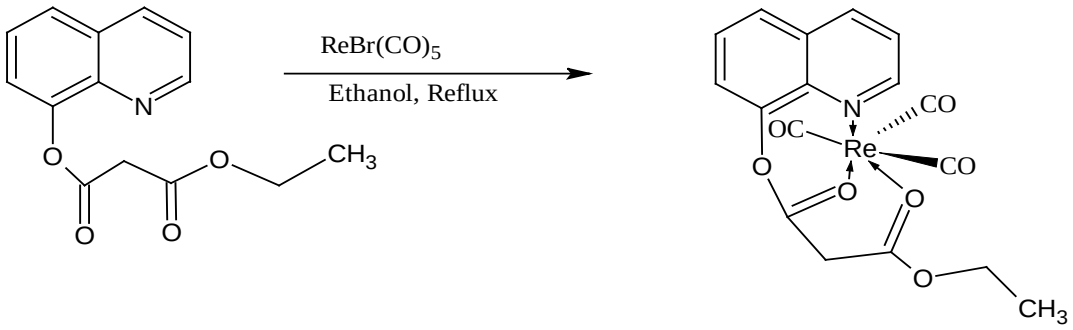


Scheme 3.2. Synthesis of Rhenium Complex 2

## 3.2 X-Ray Crystallography

The crystal structure determination of compounds diphosphine gold(I) complex 1 or [$Au_2Cl_2$(bpcd)], [$Au_2Cl_2$(bppm)], ligand A, and rhenium complex 1 were carried out using a Bruker SMART APEX2 CCD-based X-ray diffractometer. The instrument was equipped with an Oxford low-temperature cryostat and a Mo-target X-ray tube (wavelength = 0.71Å). The X-ray data for the compounds were collected at 100(2) K. Data collections, indexing, and initial cell refinements were carried out using APEX2.[68] The frame integrations and final cell refinements were carried out using SAINT.[69] An absorption correction was applied using the program SADABS[70], and all non-hydrogen atoms were refined anisotropically. H- Atoms in the investigated compounds were placed in idealized positions and were refined using a riding model. The structures were examined using the Addsym subroutine of PLATON to ensure that

no additional symmetry could be applied to the finalized models.[71]All structures were solved and refined using the SHELXTL program package software.[72]

# CHAPTER 4

# RESULTS AND DISCUSSION

## 4.1 Introduction

This section reports the NMR and X-ray results from the reactions detailed in Chapters 2 and 3. It also discusses the results and how they help to confirm the success of my research. In some experiments X-ray quality crystals were not obtained, so NMR and IR results were solely relied upon to confirm the success of the reaction. In some cases, as in the case of rhenium complex 2, NMR did not reveal the structure of the co-ordination of complexes, but it provides a clear indication of the existence of new compounds formed and of the disappearance of the starting materials in the reaction mixture. Therefore, the NMR studies confirmed whether reaction had happened or not. Moreover, the X-ray structure of the compounds prepared were compared with similar structures of known published compounds.

## 4.2 $[Au_2Cl_2(bpcd)]$: Spectroscopic Results and X-ray Structural Comparisons

Synthesis of the diphosphine gold(I) complex 1 or $[Au_2Cl_2(bpcd)]$ from BPCD was done under ice conditions. The temperature was gradually allowed to increase as the ice melted. The reaction was stirred at room temperature, and after an hour it turned bright orange. Later observations indicated that the reaction would run well over a short period of time in the absence of light. This is because light decomposes gold compounds into nanoparticles. Table 4.1 provides information on X-ray crystallographic and data processing parameters for diphosphine gold(I) complex 1 or ($Au_2C_{29}H_{22}O_2Cl_2P_2$). Figure 4.1 provides the detailed X-ray structure of $[Au_2Cl_2(bpcd)]$.

Table 4.1 X-ray Crystallographic and Data Processing Parameters for Diphosphine Gold (I) Complex 1 or ($Au_2C_{29}H_{22}O_2Cl_2P_2$)

| | |
|---|---|
| Crystal System | Monoclinic |
| Space Group | P $2_1$/n |
| a, Å | 13.634(1) |
| b,Å | 16.817(12) Å |
| c,Å | 13.708(10) Å |
| β, deg | 102.330(1) ° |
| V ($Å^3$) | 3070.5(4) |
| Emperical formula | $C_{30}H_{24}Au_2Cl_4O_2P_2$ |
| Formula Weight (FW) | 1014.17g/mol |
| Formula Unit per cell (Z) | 4 |
| Density, ($Mg/M^3$) | 2.19 |
| abs coeff (μ) $mm^{-1}$ | 10.03 $mm^{-1}$ |
| Reflection Collected | 36161 |
| F(000) | 1904 |
| R Indeces (All data) | R1 = 0.04,wR2 = 0.13 |
| GOF | 1.04 |

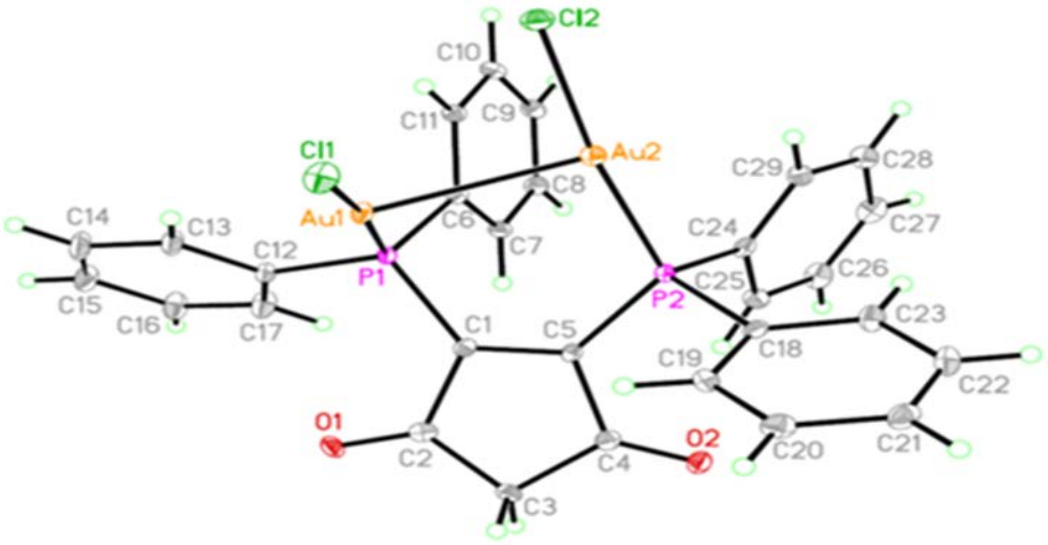


Figure 4.1. X-ray Structure of Diphosphine Gold (I) Complex 1or [$Au_2Cl_2$(bpcd)] or ($Au_2C_{29}H_{22}O_2Cl_2P_2$). The following are some of the selected bond lengths in Angstrom (Å) and bond angles in degrees (°): Au(1)-P(1) 2.231(2), Au(1)-Cl(1) 2.289, Au(1)·····Au(2) 2.916(4), P(1)-C(1) 1.812(6), P(2)-C(18) 1.819(6), C(1)-C(2) 1.515(8), C(2)-C(3) 1.483(9), C(3)-C(4) 1.522(8), O(1)-C(2) 1.214(8), O(2)-C(2) 1.205(8), P(1)-Au(1)-Cl(1) 173.72(6), P(1)-Au(1)-Au(2) 83.37(4), Cl(1)-Au(1)-Au(2) 101.55(4), P(2)-Au(2)-Cl(2) 172.69(6), P(2)-Au(2)-Au(1) 100.46(4), Cl(2)-Au(2)-Au(1) 86.85(4), C(12)-P(1)-C(1) 110.6(3), C(5)-P(2)-Au(2) 117.2(2), C(18)-P(2)-Au(2) 109.7(2), C(24)-P(2)-Au(2) 110.8(2), C(18)-P(2)-C(5) 103.2(3), C(24)-P(2)-C(18) 107.6(3), C(6)-P(1)-Au(1) 121.1(2), C(1)-P(1)-Au(1) 106.7(2), C(12)-P(1)-Au(1) 112.1(2). For more information about bond angles and lengths of [$Au_2Cl_2$(bpcd)], please see Appendix A.

The Au·····Au interaction in [$Au_2Cl_2$(bpcd)] is 2.916(4) Å. This value is within a normal range of Au·····Au interactions in other dinuclear gold(I) phosphine compounds.[73] Au·····Au interaction happens orthogonal to the principal axis of linearly coordinated Au (I) centers. In addition, a typical Au·····Au interaction ranges from 2.75-3.40 Å.[74]

The Au-P bond length (2.231(2) Å) in [$Au_2Cl_2$(bpcd)] is similar to other Au-P bond lengths found in other dinuclear gold(I) compounds. For instance, in [$Au_2(\mu\text{-}S_2(CH_2)_3)$(dppm)] the Au-P bond length is 2.259 Å.[73] In [$Au(dpmaa)_2$]Cl, Au-P bond lengths are 2.387(3) and 2.381(2) Å.[75]

In $[Au_2Cl_2(bpcd)]$, P-Au(1)-Cl(1), bond angles are 172.69(6)$^o$ and 173.72(6)$^o$. This is less than the 180$^o$ expected in Au(I) diphosphine complexes with a coordination number (CN) of 2. This deviation from linearity is attributed to Au·····Au interaction. In order to accommodate this interaction, the complex distorts in such a way as to minimize the steric interaction between phenyl groups and between the chloride ligands. In gold (I) compounds with a very weak or no Au·····Au interaction, the P-Au-Cl angle is often closer to 180$^o$. For an example, in $[PPh_3AuCl]$, the P-Au-Cl is 179.63° and in $[(PhO)_3AuCl]$[76] it is 178.5(2)°, whereas in $[PEt_3AuCl]$ it is 178.5(3)°.[77]

The Au-Cl bond length in $[Au_2Cl_2(bpcd)]$ is 2.289(2) Å, which is consistent with other Au-Cl bond lengths reported in the literature. For example, in $[(Ph_3PSe)AuCl]$ and [(EtImt)AuCl], Au-Cl is 2.26(1) Å. The Au-Cl bond lengthens if the electron withdrawing group (EWG) is attached to the Au atom. This is because EWG leads to the removal of the electron density from the Au-Cl bond. This is true in the case of $[(Ph_3PS)AuCl]$, where Au-Cl is 2.555(1) Å. An electronegative sulfur removes electron density from Au-Cl, thus weakening the bond. Moreover, the Au-Cl bond is the longest in all of the gold (I) complexes.[76]

### 4.2.1 $^{31}$P-NMR Result for ($Au_2C_{29}H_{22}O_2Cl_2P_2$) or $[Au_2Cl_2(bpcd)]$

The $^{31}$P-NMR study of the ($Au_2C_{29}H_{22}O_2Cl_2P_2$) complex shows a chemical shift (σ) of 14.2 ppm. This is in agreement with previous studies done by Fenske.[78] The $^{31}$P-NMR for the ($Au_2C_{29}H_{22}O_2Cl_2P_2$) is given in Figure 4.2.

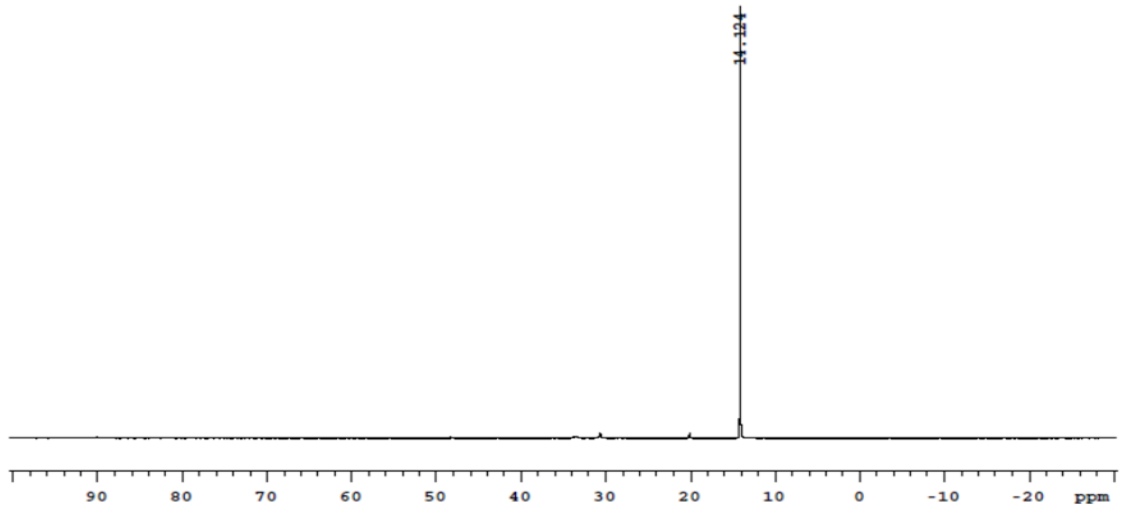


Figure 4.2. $^{31}$P-NMR of diphosphine gold (I) complex 1 after reaction with BPCD Ligand

4.2.2 [$Au_2Cl_2$(bpcd)] versus [4-(Diphenylphosphanyl-9, 9-dimethylxanthene]AuCl

[4-(Diphenylphosphanyl-9,9-dimethylxanthene]AuCl or $C_{27}H_{23}AuClOP$ crystallizes in a monoclinic crystal system with a *C2/c* space group, whereas [$Au_2Cl_2$(bpcd)] crystallizes in a monoclinic crystal system with a $P2_1/n$ space group**.** In both compounds the coordination number and oxidation state of gold (I) complexes are 2 and 1 respectively.

[$Au_2Cl_2$(bpcd)] is a dinuclear complex with a semi supported[79] Au·····Au interaction, whereas ($C_{27}H_{23}AuClOP$) is a mononuclear complex and is most likely to exhibit unsupported Au·····Au interaction. The Au-P bond length in [$Au_2Cl_2$(bpcd)] is 2.231(2) Å, whereas in $C_{27}H_{23}AuClOP$ it is 2.224(9) Å. In both cases, the Au-P bond length is comparable to those found in Au-$PPh_3$ systems [(2.232(4) Å].[80] In $C_{27}H_{23}AuClOP$, the Au-Cl bond length is shorter by 0.16 Å (the actual Au-Cl bond length in $C_{27}H_{23}AuClOP$ is 2.273(1) Å) compared to that of [$Au_2Cl_2$(bpcd)]. Also, it is shorter by 0.18 Å compared to the average bond length of known gold (I) complex.

P-Au-Cl is 178.3(2) in $C_{27}H_{23}AuClOP$, whereas in $[Au_2Cl_2(bpcd)]$ P-Au-Cl values are 172.69(6) ° and 173.72(6) °. Weakness or lack of Au·····Au interaction in $C_{27}H_{23}AuClOP$ could be the reason why the P-Au-Cl angle is larger and closer to linear as expected in complexes with a coordination number (CN) of 2. The X-ray molecular structure of $C_{27}H_{23}AuClOP$ is given in Figure 4.3. .

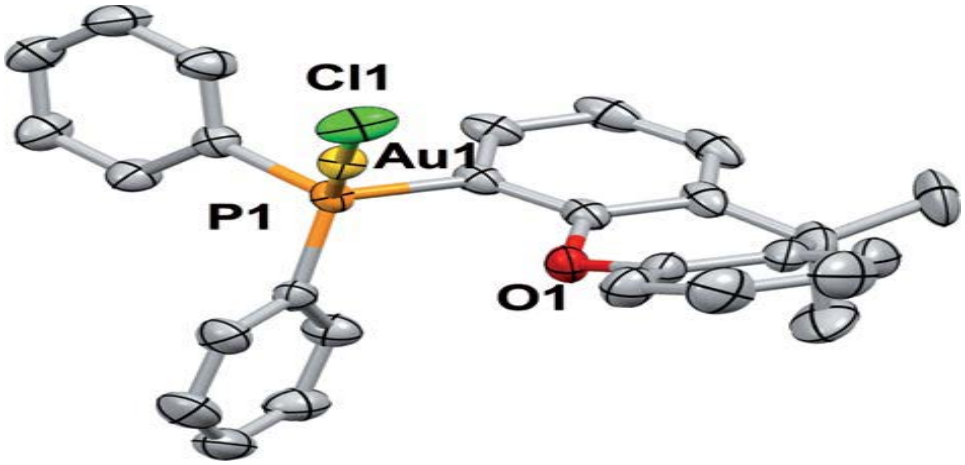


Figure 4.3. Molecular Structure of $C_{27}H_{23}AuCIOP$. Maier, A.F.G et al. *Eur. J.Org*. **2014**, 4515-4522. Permission to reproduce this figure has been granted by ACS.

### 4.2.3 $[Au_2Cl_2(bpcd)]$ versus $[Au(PEt_3)Cl]$

The two compounds bear some similarities. First, both compounds crystallize in a monoclinic crystal system. Second, in both compounds there are four molecules of gold (I) complex per unit cell; therefore, Z = 4. Third, in both compounds the coordination number (CN) of the gold (I) complex is 2. Two ligands connected to gold (I) atoms are *trans* to each other, thereby forcing a linear geometry on a complex. Furthermore, in both cases the oxidation state of gold (I) is +1.

There are also some differences between the two compounds. First, $[Au(PEt_3)Cl]$[77] is mononuclear while $[Au_2Cl_2(bpcd)]$ is dinuclear. In solid state there is very little of the Au·····Au interaction {3.615(2) Å} seen in $[Au(PEt_3)Cl]$. This interaction is strongly observed

in other mononuclear gold (I) complexes as we will see in the case of [Au($PMe_3$)I]. Poor Au·····Au interaction in [Au($PEt_3$)Cl] is attributed to steric hindrance caused by the bulky ethyl group in [Au($PEt_3$)Cl] as compared to the methyl group in [Au($PMe_3$)I]. Steric hindrance by a large ethyl group shields Au atoms from interacting with each other and forming Au·····Au.

Au-Cl bond lengths in [Au($PEt_3$)Cl] are 2.305(8) Å and 2.306(8) Å, whereas in [$Au_2Cl_2$(bpcd)] Au-Cl are 2.289(2) Å and 2.302(2) Å. The two compounds have similar bond lengths which are in agreement with studies in the literature on gold (I) halide complexes.[81] In gold (I) halide complexes, the Au-Cl bond length is the longest of all. The longest Au-Cl bond so far belongs to three coordinate [(P-P) AuCl], and its value is 2.818 Å. [76]

The Au-P bond lengths in [Au($PEt_3$)Cl] are 2.232(9) Å and 2.231(8) Å, whereas in [$Au_2Cl_2$(bpcd)] Au-P, bond lengths are 2.231(2) Å and 2.233(2) Å. In both cases, the bond lengths are unremarkable, being similar and consistent with those found in the literature studies.[80] In [Au($PEt_3$)Cl], (phosphorous-phenyl) P-C bond length ranges from 1.78(4) to 1.82(5) Å, whereas in [$Au_2Cl_2$(bpcd)] it ranges from 1.799(6) to 1.823(6) Å. The two bond lengths are similar, and they are within normal range found elsewhere in the literature on gold (I) phosphine halide.[82]

The Cl-Au-P bond angles in [Au($PEt_3$)Cl] are 178.5(3) ° and 178.9(3)°, whereas in [$Au_2Cl_2$(bpcd)], the bond angles are 172.69(6) ° and 173.72(6) °. In [$Au_2Cl_2$(bpcd)], the Cl-Au-P bond angle is far less than the expected 180°. On the contrary, the Cl-Au-P bond angle is almost linear in [Au($PEt_3$)Cl].

The Au-P-C bond angle in [Au($PEt_3$)Cl] ranges from 113.0(1) to 119.0(2)°, whereas in [$Au_2Cl_2$(bpcd)] the Au-P-C angle ranges from 109.7(2) to 121.1(2)°. This deviation from linearity in [$Au_2Cl_2$(bpcd)] could be attributed to the Au·····Au interaction, [83] which is stronger

[2.916(4) Å] in $[Au_2Cl_2(bpcd)]$ than in $[Au(PEt_3)Cl]$. The Au·····Au interaction is [3.615(2) Å] in $[Au(PEt_3)Cl]$.

### 4.2.4 $[Au_2Cl_2(bpcd)]$ versus $[Au_2Cl_2(bma)]$ and $[PPh_3AuCl]$

$[Au_2Cl_2(bpcd)]$ and $[Au_2Cl_2(bma)]$ are both dinuclear gold (I) complexes. Both compounds crystallize in monoclinic crystal system with a *P 2₁/n* space group. In both compounds there are four molecules of gold (I) complex per unit cell; therefore, Z=4. In both cases, the coordination number (CN) of gold (I) is 2, and the oxidation state at gold center is +1. Furthermore, the two compounds have the semi supported type of Au·····Au interaction.

The X-ray structure of the diphosphine gold (I) complex 1or $[Au_2Cl_2(bpcd)]$ is given in Figure 4.3. The gold (I) compound is a dinuclear complex which crystallizes in the monoclinic space group *P 21/n*. Each atom of gold (I) is linearly connected to a chloride and a BPCD ligand. The interatomic distance between the two gold atoms Au (1) ·····Au (2) is 2.916 Å, which is very close to the known literature values of dinuclear gold (I) complexes (2.935 Å).[78]

The two crystal structures bear some similarities. First, both crystallize in a monoclinic crystal system. Second, they are both dinuclear of gold (I) complexes with a coordination number of 2, and the oxidation state at the metal center is +1.

In $[Au_2Cl_2(bpcd)]$, the P(1)-Au(1)-Cl(1) bond angle is 173.72° compared to 173.88° in $[Au_2Cl_2(bma)]$. Furthermore, the P(2)-Au(2)-Cl(2) bond angle is 172.69° in $[Au_2Cl_2(bpcd)]$ compared to 172.76° in $[Au_2Cl_2(bma)]$. In both cases, the bond angles are highly similar. Au-Cl, Au-P, and P-Au-Cl in $[Au_2Cl_2(bpcd)]$ were also compared with the corresponding bond lengths and angles found by theoretical calculation from the study of $AuClPPh_3$. Aikens[84] and his coworkers have done theoretical studies using the BP86/TZV program. From their studies, they

have calculated the bond length of Au-Cl and found it to be 2.336 Å compared to 2.289(2) Å and 2.302(2) Å in [$Au_2Cl_2$(bpcd)]. The experimental calculation shows the Au-Cl has 2.279 Å. Though the two compounds are remarkably different, their bond lengths are not very different. The only notable difference are the bond angles (P-Au-Cl) of $AuClPPh_3$ (179.68$^o$ and 179.86$^o$), which are larger than those of its corresponding complexes. The difference in bond angle is attributed to steric hindrance. In $AuClPPh_3$, there is less crowding of the phenyl group and thus a decrease in the amount of steric hindrance, while in [$Au_2Cl_2$(bpcd)] and [$Au_2Cl_2$(bma)], the phosphorous atoms are not far apart in a rigid bidentante ligand; this increases the interaction between the phenyl groups, forcing the angle to be smaller in order to reduce the repulsion. Table 4.2 provides more information on bond angles and bond lengths.

Table 4.2 Calculated and Experimental Bond Lengths and Angles of Au(I)Cl(L) where L=Ligand. 1: [$Au_2Cl_2$(bpcd)], 2: [$Au_2Cl_2$(bma)], 3: Calc.$AuClPPh_3$, 4: $Au_2(\mu\text{-}S_2C_6H_4)(PPh_3)_2$, and 5:Exp.[$AuClPPh_3$]

| | 1 | 2 | 3 | 4 | 5 |
|---|---|---|---|---|---|
| Au-Cl | 2.289(2) Å, 2.302(2) Å | 2.2867(9) 2.3004(9Å | 2.336 Å | N/A | 2.279 Å |
| Au-P | 2.231(2) Å 2.233(2) Å | 2.2287(9), 2.2316(9)Å | 2.272 Å | 2.252(4), 2.263(4) Å | 2.235 Å |
| P-Au-Cl | 173.72(6)$^o$ 172.69(6)$^o$ | 173.88(3)$^o$ 172.76(3)$^o$ | 179.86$^o$ | N/A | 179.68$^o$ |
| Au-Au | 2.916(4) Å | 2.935(6) Å | 3.61 Å | N/A | 3.615 Å |
| Au-P-C | 106.7(2) $^o$ 121.1(2)° | 105.97(1)$^o$ 115.(6)$^o$ | N/A | 110.8(5)°, 114.2(5)$^o$ | 113(1) $^o$ 119(2)$^o$ |

For further information about $[Au_2Cl_2(bma)]$, the X-ray structure of the complex is given in Figure 4.4 .

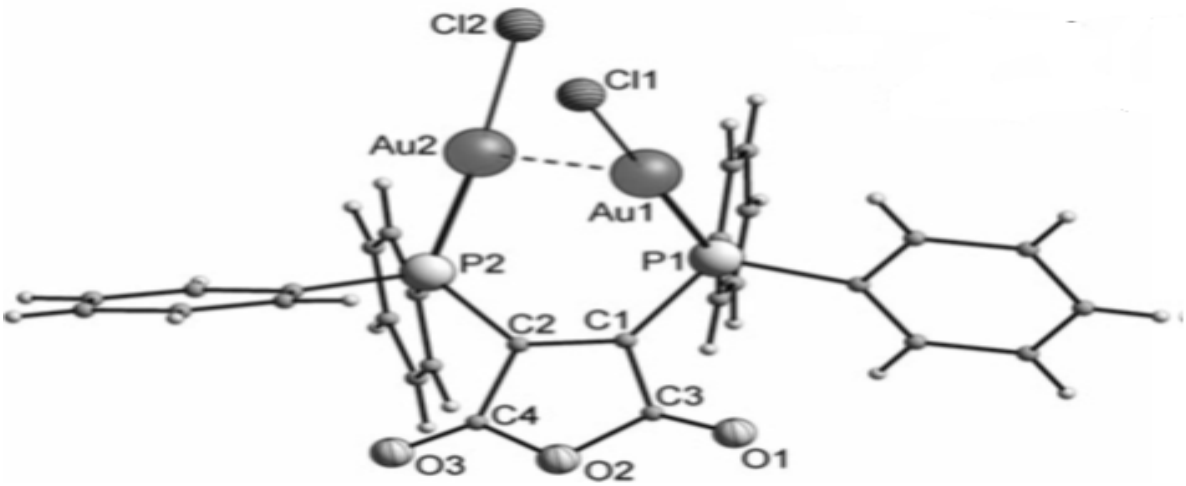


.

Figure 4.4. X-ray Structure of $[Au_2Cl_2(bma)]$ complex. Yu, W; Fenske, D. *J.Clust Sci*. **2012,** 23,757-766. Reproduced with permission from Springer.

### 4.2.5 $[Au_2Cl_2(bpcd)]$ Versus $[Au_2(\mu\text{-}S_2C_6H_4)(PPh_3)_2]$

Further comparison studies were done between $[Au_2Cl_2(bpcd)]$ and $[Au_2(\mu\text{-}S_2C_6H_4)(PPh_3)]$. In the case of $[Au_2(\mu\text{-}S_2C_6H_4)(PPh_3)]$, the two gold atoms are joined together by 1, 2-dithiolene through the Au-S bond. Each phosphine is connected to the Au atom through the Au-P bond. From the X-ray structure of $[Au_2(\mu\text{-}S_2C_6H_4)(PPh_3)]$ (as shown in Figure 4.5 ), the following bond lengths were recorded: Au(1)-P(1) = 2.252 Å, Au(2)-P(2) = 2.263Å, and Au (1) ·····Au (2) = 3.148 Å. These bond lengths were compared to those of $[Au_2Cl_2(bpcd)]$. For instance, Au(1)-P(1) is 2.231 Å, and Au(2)-P(2) is 2.233 Å; $[Au_2(\mu\text{-}S_2C_6H_4)(PPh_3)]$ has a slightly shorter bond length than does $[Au_2Cl_2(bpcd)]$. The Au(1)-Au(2) bond length in $[Au_2Cl_2(bpcd)]$ was found to be 2.9156(4) Å, also shorter than that of $[Au_2(\mu\text{-}S_2C_6H_4)(PPh_3)]$.

In $[Au_2(\mu\text{-}S_2C_6H_4)(PPh_3)]$, there is interaction between S(2) ·····Au(1). Because of this interaction, S(1)-P(I)-Au(I) is slightly perturbed from linearity, S(1)-P(I)-Au(I) is 159.3(1)°.[73]

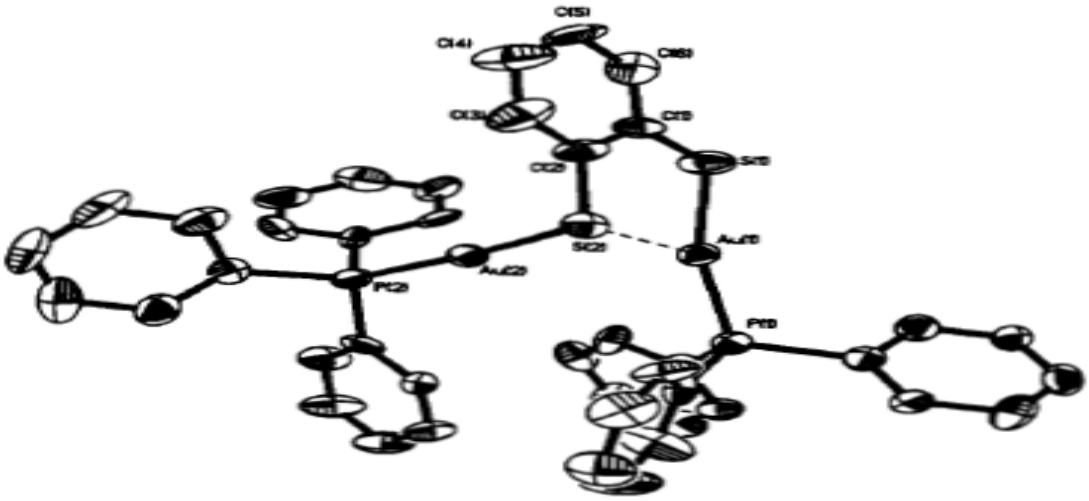

Figure 4.5. X-ray Structure of [$Au_2(\mu\text{-}S_2C_6H_4)(PPh_3)$]. Grant, T et al. *Inorg. Chem*.**1993**, 32, 1749-1755. Reproduced with permission from ACS.

4.2.6 [$Au_2Cl_2$(bpcd)] versus [$Au_2Cl_2(L_2)$]

The L stands for trans-2,3-bis(diphenylphosphino) succinic anhydride ligand.[78] [$Au_2Cl_2(L_2)$], like [$Au_2Cl_2$(bpcd)], is a dinuclear molecule with Au connected to two phosphine ligands. Unlike [$Au_2Cl_2$(bpcd)], which has coordination number of 2, [$Au_2Cl_2(L_2)$] has a coordination number (CN) of 3, the third ligand attached to Au being chloride . Moreover, [$Au_2Cl_2(L_2)$] crystallizes in a triclinic crystal system with a *P-1* space group, whereas[$Au_2Cl_2$(bpcd)] crystallizes in a monoclinic system with a *P* $2_1/n$ space group. There is one molecule of [$Au_2Cl_2(L_2)$] in every unit cell, whereas there are four molecules of [$Au_2Cl_2$(bpcd)] in every unit cell. [$Au_2Cl_2(L_2)$] is not unsaturated (with no C=C bond) and has an inversion center. The two hydrogens and $PPh_2$ are *trans* to one another. In contrast, there are no chiral centers in the BPCD ligand.

The gold atoms in [$Au_2Cl_2(L_2)$] are coordinated in a distorted trigonal fashion as shown in Figure 4.6. This means the individual bond angles have significant variation in their size. For instance, the angle of Cl1-Au-P2 is 101.6°; this angle in [$Au_2Cl_2$(bpcd)] does not exist because

chloride ligands are at the terminal position and do not interact with the opposite gold atoms. In other words, there are no chloride multiple interactions with two gold atoms. In $[Au_2Cl_2(L_2)]$, Cl1-Au-P1 is 98°, whereas the corresponding bond angle in$[Au_2Cl_2(bpcd)]$ is 172.69(6)°, which is closer to 180°. The angle of P1-Au-P2 is 160° in $[Au_2Cl_2(L_2)]$, whereas no such bond exists in $[Au_2Cl_2(bpcd)]$ . In $[Au_2Cl_2(L_2)]$, the Au1-Cl1 bond length is 2.809 Å, and that of Au1-Cl1' is 3.205 Å, even longer than the previous bond length. The longer Au1-Cl1' means weaker interaction. There is no Au1-Cl1' in $[Au_2Cl_2(bpcd)]$ because there is no chloride bridging in the complex. All chloride ligands are terminally connected to gold atoms. Table 4.4 summarizes the relationships in bond angles and lengths among the three complexes. Figure 4.6 shows the structure of the $[Au_2Cl_2L_2]$ complex.

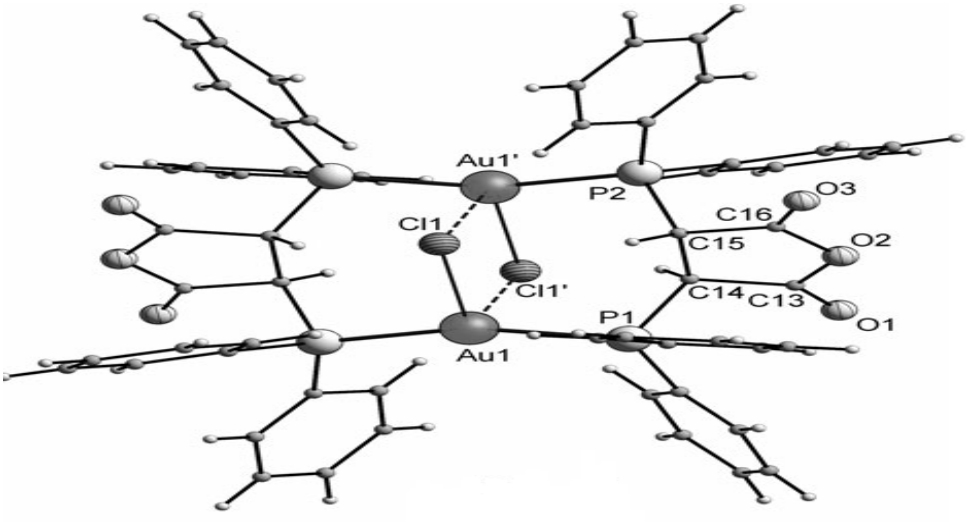


Figure 4.6. The X-ray Structure of $[Au_2Cl_2L_2]$ complex. Figure 4.6 was obtained from Yu, W; Fenske, D. *J.Clust Sci*. **2012,** 23,757-766 [78] Reproduced with permission from the publisher.

Table 4.3 The Bond Angles (°) and Lengths (Å) of the Three Complexes, Note L = Trans-2, 3-bis (diphenylphosphino) succinic anhydride ligand

| | $[Au_2Cl_2(bpcd)]$ | $[Au_2Cl_2(L_2)]$ | $[Au_2Cl_2(bppm)]$ |
|---|---|---|---|
| Au-Cl | 2.289(2), 2.302(2)Å | 2.809 Å | 2.289(2), 2.293(2) Å |
| Au-P | 2.231(2), 2.233(2) Å | 2.304, 2.309Å | 2.23(2) |
| P-Au-Cl | 173.72(6), 172.69(6)° | 98.0, 101.6° | 172.76(6) |
| Au-Au | 2.916(4) Å | N/A<br>107.0(1)° | 2.96(4)<br>106.7(2)°, 121.1(2)° |
| Au-P-C | 106.7(2)Å, 121.1(2)Å | | |
| P-Au-P | N/A | 160.36(4)° | N/A |
| Cl-Au-Cl | N/A | 102.40(3)° | N/A |

4.3 $[Au_2Cl_2(bppm)]$ or $Au_2Cl_2C_{34}H_{25}O_2N_1P_2$

The X-ray structure of $[Au_2Cl_2(bppm)]$ is given in Figure 4.7. This gold (I) compound is a dinuclear complex that crystallizes in the monoclinic crystal system with a *C2/c* space group. Each atom of gold is connected to one chloride ligand and one phosphorous atom of the $PPh_2$ group of diphosphine. The atomic distance between two gold atoms, Au·····Au, was found to be 2.96(4) Å, which is in agreement with the Au·····Au bonding distance.

$^{31}$P-NMR of [$Au_2Cl_2$(bppm)] is given in Figure 4.8 . The chemical shift of the bppm ligand is 14.194 ppm, which also is in agreement with literature studies.[78] For information on X-ray Crystallographic and data processing parameters for [$Au_2Cl_2$(bppm)] or gold (I) complex 2, see Table 4.4 .

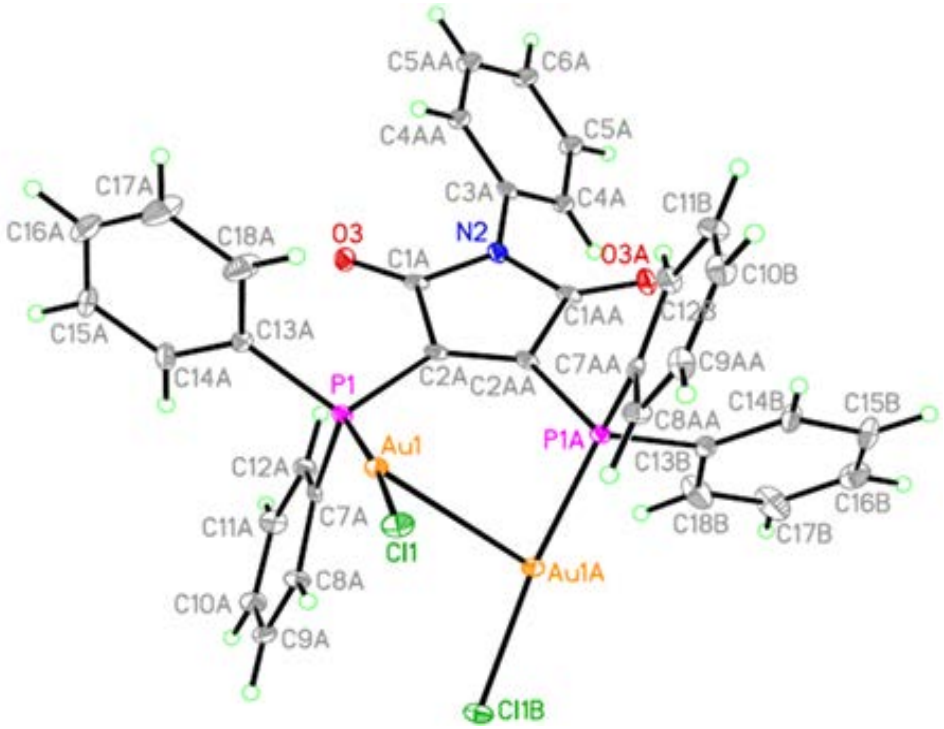


Figure 4.7. The X-ray Structure of [$Au_2Cl_2$(bppm)] or gold(I) complex 2. The bond lengths are given in Armstrongs (Å), and bond angles in degrees (°). The Au·····Au interaction was found to be 2.96(4) Å, Au(1)-P(1) is 2.23(2) Å, Au(2)-P(2) is 2.233(2) Å, Au(1)-Cl(1) is 2.293(2) Å, P(1)-C(1) is 1.805(7) Å, P(1)-Au(1)-Cl(1) is173.88(6), P2-C11 1.800(7), P2-C17 1.824(7), O1-C1 1.191(8), N1-C5 1.435(8), N1-C4 1.389(8), C17-H17 0.95,P1- Au1-Cl1 173.88(6), P1-Au-Au 85.98, P2-Au1-Au2 172.76, P2-Au2-Cl2 172.76, Cl-Au1-Au2 99.66, Cl-Au1-Au2 101.59(5), C7-P1-C13 104.4(3).

Table 4.4 X-ray Crystallographic and Data Processing Parameters for [$Au_2Cl_2$(bppm)]

| | |
|---|---|
| Crystal system | Monoclinic |
| Space Group | *C2/c* |
| a, Å | 34.907(2) |
| b,Å | 14.203(7) |
| c,Å | 26.598(1) |
| α, deg | 90° |
| β, deg | 128.565(1) o |
| V ($Å^3$) | 10310.7(9) |
| Empirical formula | $C_{104}H_{77}Au_6Cl_{12}N_3O_6P_6$ |
| Formula Weight (g/mol) | 3257.1 |
| Formula Unit per cell (Z) | 4 |
| Density, ($Mg/M^3$) | 2.099 |
| abs coeff (μ) $mm^{-1}$ | 8.965 |
| Reflection Collected | 63111 |
| F(000) | 6152 |
| Final R indices | R1=0.0358, wR2=0.1311 |
| G.O.F | 1.057 |

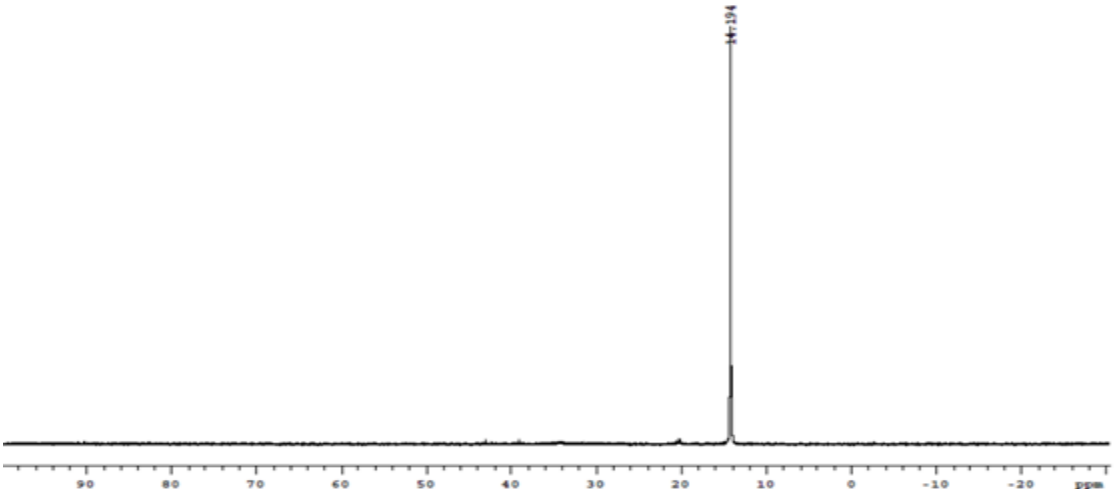


Figure 4.8. $^{31}$P-NMR of [$Au_2Cl_2$(bppm)]

4.3.1 [$Au_2Cl_2$(bppm)] versus [ClAuP(Ph)$_2$($C_6H_4$COLeuMe)]

**[**ClAuP(Ph)$_2$($C_6H_4$COLeuMe)] is a mononuclear which crystallizes in a triclinic crystal system with a *P1* space group In every unit cell there are two molecules of **[**ClAuP(Ph)$_2$($C_6H_4$COLeuMe)]. **[**ClAuP(Ph)$_2$($C_6H_4$COLeuMe)] has a chiral center with an S-configuration. With the exception of Au·····Au, which happens in both cases, there are few similarities between the two compounds. On the other hand, [$Au_2Cl_2$(bppm)] is a dinuclear which crystallizes in a monoclinic crystal system with a *C2/c* space group. There are four molecules of [$Au_2Cl_2$(bppm)] per unit cell.

The Au-P bond length in **[**ClAuP(Ph)$_2$($C_6H_4$COLeuMe)] is 2.230(2) Å, and in the case of [$Au_2Cl_2$(bppm)], the bond length is 2.233(2) Å. The Au-P bond lengths are nearly the same, and this is similar to other gold (I) complexes found in the literature.[78]

The Au·····Au interaction is weaker in **[**ClAuP(Ph)$_2$($C_6H_4$COLeuMe)] by the amount of 3.426 Å as compared to 2.916(4) Å in [$Au_2Cl_2$(bppm)]. This weak interaction in **[**ClAuP(Ph)$_2$($C_6H_4$COLeuMe)] is attributed to the large size of the phenyl groups, which tend to shield the

Au atoms from interacting with each other. Interestingly, during the interaction the two compounds align themselves in crossed sword or scissor like structure, which places the chloride ligands pointing opposite to each other and the phenyls groups away from each other.

The Au-Cl bond length in **[**ClAuP(Ph)$_2$(C$_6$H$_4$COLeuMe)] is 2.272(2) Å, whereas in [Au$_2$Cl$_2$(bppm)] the bond length is 2.289(2) Å; there is not a big difference between the two compounds' Au-Cl bond lengths and Au-Cl bond length found in literature.[78, 85]

The angle of P-Au-Cl in **[**ClAuP(Ph)$_2$(C$_6$H$_4$COLeuMe)] is 173.45(9)°, whereas in [Au$_2$Cl$_2$(bppm)] the angle is 173.72(6)°. In both cases, the angle is less than 180°. This is due to the intermolecular Au·····Au interaction that brings the two gold atoms in close proximity at the expense of P-Au-Cl. The distortion happens in order to avoid more sterics between the halides ligands and between the bulky phenyl groups. The structure of **[**ClAuP(Ph)$_2$(C$_6$H$_4$ CO LeuMe)] is given in Figure 4.9. Permission to reproduce the Figure 4.9 has been granted by the publisher, ACS. The reference where the figure was obtained is Monkowius, U et al. *Inorg.Chem*.**2014**, 53, 10602-10610.

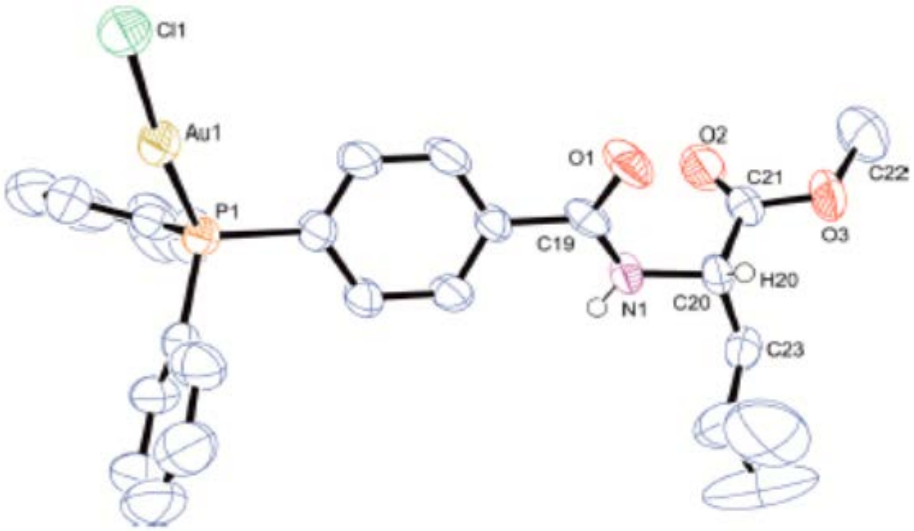


Figure 4.9. The Ortep Stereoscopic Structure of **[**ClAuP(Ph)$_2$(C$_6$H$_4$COLeuMe]

### 4.3.2 $[Au_2Cl_2(bppm)]$ versus $[Au_2Cl_2(dpmaa)]$

The molecular X-ray structure of $[Au_2Cl_2(bppm)]$ was compared with similar structures of mononuclear and dinuclear gold (I) complexes. The same criteria used to compare the first structure $[Au_2Cl_2(bpcd)]$ was used in this case. $[Au_2Cl_2(dpmaa)]$[75]is among several compounds that share similarities with $[Au_2Cl_2(bppm)]$. Both compounds crystallize in a monoclinic crystal system and have the same space group *(C2/c).* In both cases, there is semi supported intramolecular interaction between two gold atoms, Au·····Au; the interaction is made possible by the rigidity imposed by the diphosphine ligand. In $[Au_2Cl_2(dpmaa)]$ the Au·····Au is 3.1913(4) Å, slightly longer than that of $[Au_2Cl_2(bppm)]$, (2.96(4) Å), but both are still within the range of Au·····Au interaction found in other gold (I) complexes.[86] Another similarity seen is the Au-Cl bond lengths: in $[Au_2Cl_2(bppm)]$, the Au-Cl bond lengths are 2.293(2) Å and 2.289(2) Å, which are very close to 2.2889(9) Å, found in $[Au_2Cl_2(dpmaa)]$. Both bond lengths are in agreement with other gold (I) complexes published in the literature.[87]

Furthermore, the Au-P bond lengths in both compounds are also the same and are consistent with the Au-P bond lengths reported in the literature.[88] The Au-P bond length for $[Au_2Cl_2(dpmaa)]$ is 2.2301(8) Å, and those of $[Au_2Cl_2(bppm)]$ are 2.23(2) Å and 2.233(2) Å. The major noticeable difference was seen in P-Au-Cl; this bond is smaller by at least 1° in $[Au_2Cl_2(dpmaa)]$ as compared to those found in $[Au_2Cl_2(bppm)]$. The $[Au_2CI_2(bppm)]$ bond angles are 173.88 for P(1)-Au(1)-Cl(1) and 172.76 $^{o}$ for P(2)-Au(2)-Cl(2), whereas in the previous compound, $[Au_2Cl_2(dpmaa)]$, the bond length is 171.73°. The molecular structure of $[Au_2Cl_2(dpmaa)]$ is given in Figure 4.10 . Note that dpmaa stands for 2,3-bis (diphenylphosphino) maleic acid. The Figure 4.10 was obtained from the following journal article: Berners-Price, S.J et al. *Inorganica Chimica Acta*. **2005**, 358, 4237- 4246. Permission to

reproduce this Figure 4.10 has been granted by the publisher, Elsevier; for more information, please contact the publisher.

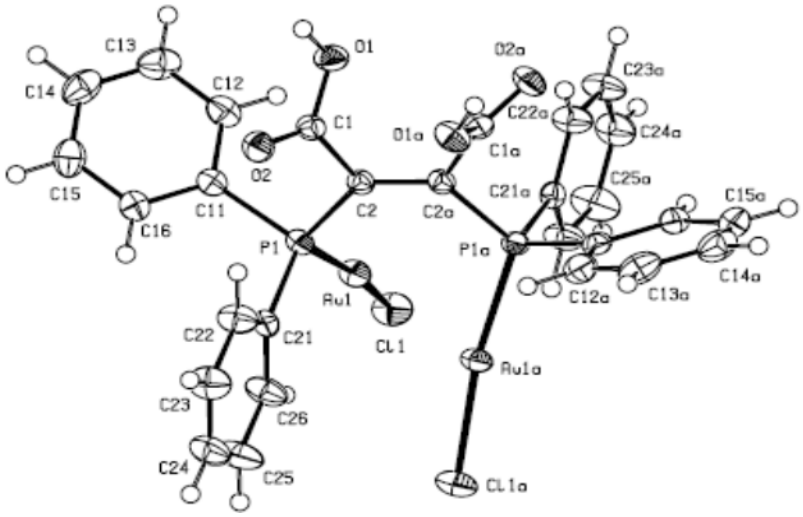


Figure 4.10. Ortep Molecular Structure of the [$Au_2Cl_2$(dpmaa)] Complex

4.3.3 [$Au_2Cl_2$(bppm)] versus Iodo(triphenylphosphine)gold(I) complex

Furthermore, [$Au_2Cl_2$(bppm)] was compared with mononucleariodo(triphenylphosphine) [Au($PPh_3$)I]. The latter structure contains an infinite array of gold atoms. Unlike [$Au_2Cl_2$(bppm)], which has a *C2/c* space group, the space group of [Au($PPh_3$)I] is *Pnca*, and the crystal system is an orthombic, compared to the monoclinic of [$Au_2Cl_2$(bppm)]. In addition, the Au-P bond length is dramatically affected by the type of halogen attached to the gold atom. For instance, Au-P was found to increase as the size of the ligand atom gets bigger and its softness increases: for chloride, it is 2.23 Å, while the iodide Au-P is 2.25 Å, and it is 2.27 Å for a cyanide ligand. This reflects weakening of Au-P bonding with increasing competition from the ligand for bonding with the gold atoms.

The two structures also share some similarities in terms of bond angle and bond length. For instance, the angle of P-Au-I in [Au($PPh_3$)I] is 178.46(6)°, close to 180°, which suggests the

gold is connected linearly to the phosphorous and halogen atoms. The C-P-C bond angle ranges from 104.6(4)-107.1(1) ° in [Au($PPh_3$)I], whereas in [$Au_2Cl_2$(bppm)] the value ranges from 104.4(3)-106.2(3) °.[89] For more detailed comparisons of the bond lengths between the two compounds, refer to the Table 4.5 . Note, that the lack of dimerization in [Au($PPh_3$)I] is attributed to the bulky size of the phenyl group in the ligand, which prevents the two gold atoms from coming closer together and interacting in Au·····Au interaction.

Table 4.5 Complex X-ray Data Comparison of Bond Length and Angles

| [$Au_2Cl_2$(bppm)] | [Au($PPh_3$)I] | [$Au_2Cl_2$(bppm)] |
|---|---|---|
| Au-P | 2.249(2) Å | 2.23(2), 2.233(2) Å |
| P-C | 1.817(9),1.829(8)Å | 1.812(7), 1.828(7) Å |
| Au-P-C | 111.9(3),113.(5)° | 110.2(2), (116.9(2)° |
| C-P-C | 104.6(4),107.1(4)° | 104.4(3), 106.2(3)° |

### 4.3.4 [$Au_2Cl_2$(bppm)] versus [Au($PMe_3$)I]

The third structure to be compared with [$Au_2Cl_2$(bppm)] is [Au($PMe_3$)I]. Unlike the previous structure, [Au($PPh_3$)I] can form a dimer which allows us to measure Au·····Au interaction. Like [Au($PPh_3$)I], [Au($PMe_3$)I] crystallizes as an orthombic rather than a monoclinic crystal system in [$Au_2Cl_2$(bppm)]. Furthermore, the space group in [$Au_2Cl_2$(bppm)] is *C2/c*, whereas that of [Au($PMe_3$)I] is $P2_12_12_1$. The Au·····Au interaction in [Au($PMe_3$)I] is 3.168 Å, slightly weaker than that of [$Au_2Cl_2$(bppm)]. The existence of the unsupported Au·····Au type of interaction in [Au($PMe_3$)I] is evidenced by the fact the observed Au-I bond length is significantly weaker and longer (2.583(1) Å ) than in the monomeric triphenylphosphinegold (I)

complex (2.553(1) Å). Moreover, the I-Au-P configuration is more bent in a dimer, and the direction of bending further suggests Au·····Au interaction. Note that in [$Au_2Cl_2$(bppm)], the kind of Au·····Au which exists as semi supported type of aurophilic interaction, whereas in monomeric [Au($PMe_3$)I] there is unsupported aurophilic interaction with two iodo ligands pointing away from each other.

Au-P in [Au($PMe_3$)I], which is 2.2583(1) Å, is slightly longer than in either [$Au_2Cl_2$(bppm)] and [Au($PPh_3$)I], which are 2.23(2) Å and 2.553(1) Å respectively. The longer Au-P bond in [Au($PMe_3$)I] is explained by the stronger donation tendency of the methyl group in the trimethylphosphine ligand than that of the phenyl group in the triphenylphosphine ligand. In other words, phosphorous donates more strongly in aliphatic phosphine than in aromatic phosphine. Dimerization also tends to lengthening of the Au-P bond. Figure 4.11 shows the structure of [Au($PMe_3$)I]. This structure was obtained from the work of Arhrland and his co-worker; for the reference to this structure, please see this article: Arhrland, S et al. *Acta Chemica Scandinavia A 41*. **1987**, 173-177. For more information on differences and similarities in bond length and angle, please refer to Table 4.6.

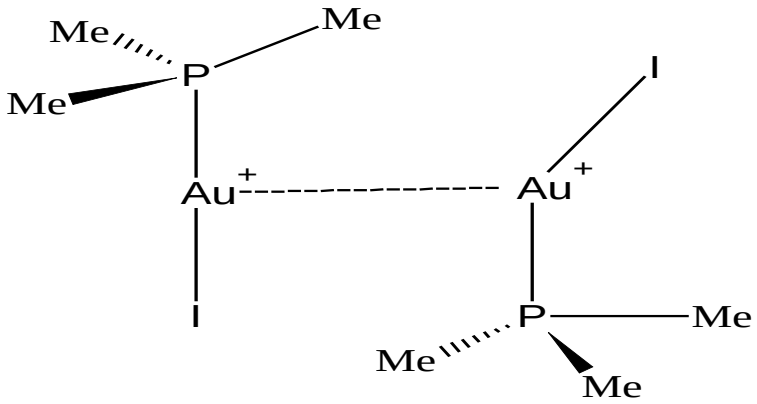


Figure 4.11: The X-ray Structure of [Au($PMe_3$)I]

Table 4.6. X-ray Data Comparison for [$Au(PMe_3)I$] and [$Au_2Cl_2(bppm)$]

| | [$Au(PMe_3)I$] | [$Au_2Cl_2(bppm)$] |
|---|---|---|
| Au-P | 2.256(3) Å | 2.23(2), 2.233(2) Å |
| P-C | 1.80(2), 1.84(2) Å | 1.812(7), 1.828(7) Å |
| Au-P-C | 114.1(6), 114.4(6)$^o$ | 110.2(2)-(116.9(2)$^o$ |
| C-P-C | 103.5(8), 105.6(7) $^o$ | 104.4(3), 106.2(3) $^o$ |
| Au·····Au | 3.168(1) Å | 2.96(4) Å |

4.3.5 [$Au_2Cl_2(bppm)$] versus [2-(Diphenylphosphino-κ-P)benzaldehyde]gold(I) chloride

The fourth compound to be compared with [$Au_2Cl_2(bppm)$] is [2-(Diphenylphosphino-κ-P) benzaldehyde]gold(I) chloride or [$AuCl\{2\text{-}(C_6H_5)_2PC_6H_4CHO\}$]. The compound [$AuCl\{2\text{-}(C_6H_5)_2PC_6H_4CHO\}$] crystallizes in a centrosymmetric space group whereas the asymmetric units contain two independent molecules. Unlike [$Au_2Cl_2(bppm)$], which crystallizes in a monoclinic manner, the latter compound crystal system is triclinic and affords two coordinate complexes with slight variation in both bond length and angle. The intermolecular Au·····Au interaction in [$AuCl\{2\text{-}(C_6H_5)_2PC_6H_4CHO\}$] is extremely weak (5.5900(4) Å compared to 2.96(4) Å in [$Au_2Cl_2(bppm)$]). The Au-P distances are very small, around 2.23 Å, and the P-Au-Cl bond angle is 178.8° for the first crystal and 178.12° for the second crystal [$AuCl\{2\text{-}(C_6H_5)_2PC_6H_4CHO\}$] (both of them are close to 180°), and for [$Au_2Cl_2(bppm)$], the same bond angle is172.76(6) Å, which is less than 180°. The X-ray structures of [$AuCl\{2\text{-}(C_6H_5)_2PC_6H_4CHO\}$] are given in Figures 4.12, and Table 4.7 provides the structural comparisons between the two compounds discussed . The compound crystallizes in a

centrosymmetric space group, and there are two independent molecules as may be seen; the positions of the benzylaldehyde groups in the two X-crystals are not the same.

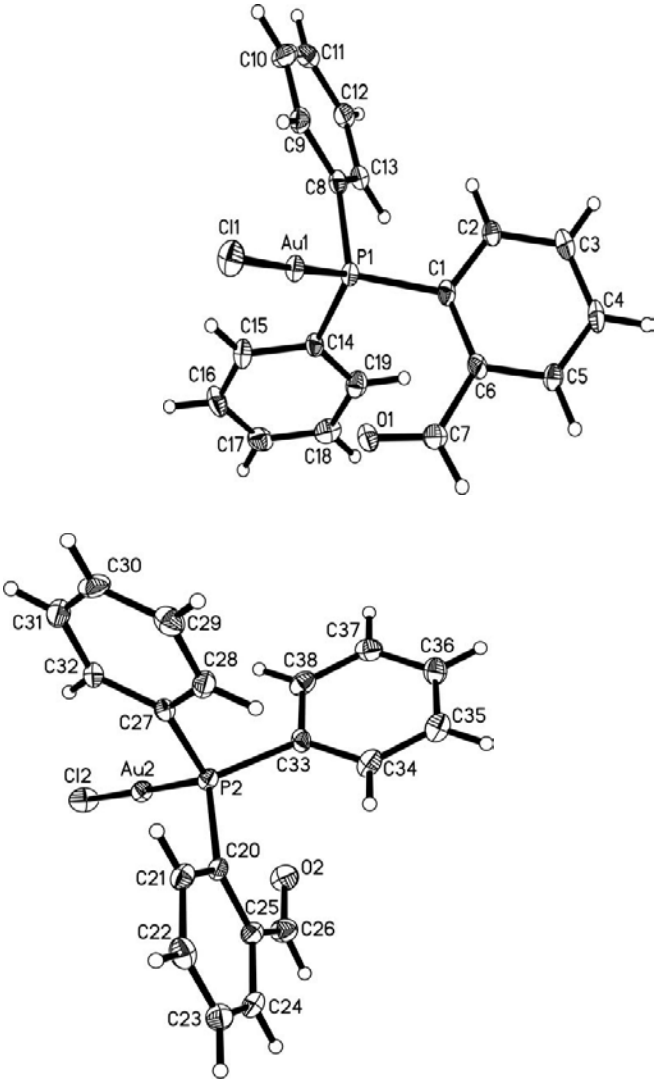


Figure 4.12**.** X-ray Structures of [AuCl{2-$(C_6H_5)_2PC_6H_4CHO$}]. On the left is crystal structure 1 and on the right is crystal structure 2 Smith, M.B et al. *Acta Cryst.***2006.** *E62*, m1850–m1852.

Duplicate: Table 4.3 The Bond Angles (°) and Lengths (Å) of the Three Complexes, Note L = Trans-2, 3-bis (diphenylphosphino) succinic anhydride ligand

| | *Crystal Structure 1* | *Crystal Structure 2* | *[$Au_2Cl_2$(bppm)]* |
|---|---|---|---|
| Au-P | 2.2297(1) Å | 2.2304(1) Å | 2.23(2), 2.233(2) Å |
| | | | 2.293(2) Å, 2.289(2)Å |
| Au-Cl | 2.2819(1) Å | 2.2836(1) Å | |
| | | | 1.828(7) Å |
| P-C | 1.822(5) Å | 1.807(5) Å | |
| | | | 173.72(6)°, 172.69(6)° |
| P-Au-Cl | 178.79(5)° | 179.12(5)° | |

## 4.4 Ligand A

Ligand A was prepared as described in Section 2.6.1. The X-ray structure obtained in the process confirms ligand A. Table 4.9 shows the X-ray crystallographic and data processing parameters for ligand A. The X-crystal is triclinic, and Figure 4.14 shows the X-ray structure. Further information such as bond length and bond angles are discussed in appendix C.

Table 4.7 X-ray Crystallographic and Data Processing Parameters for Ligand A

| | |
|---|---|
| Crystal System | Triclinic |
| Space Group | *P-1* |
| a, | 10.0358(5) Å |
| b | 10.7514(5) Å |
| c | 12.4611(6) Å |
| β | 72.2190(10) ° |

| | |
|---|---|
| V | 1233.37(1) $Å^3$ |
| γ | 83.892(1)° |
| Emperical formula | $C_{14}H_{13}NO_4$ |
| Formula Weight, g/mol | 259.25 |
| Formula Unit per cell (Z) | 4 |
| Density, ($Mg/M^3$) | 1.396 |
| abs coeff (μ) $mm^{-1}$ | 0.103 |
| Reflection Collected | 14975 |
| F(000) | 544 |
| R Indeces (All data) | R1 = 0.0328, |
| | wR2 = 0.0876 |
| GOF | 1.025 |
| Extinction Coeff. | 0.0079(11) |

### 4.4.1 8-Hydroxyquinoline $^1$H-NMR Results

The proton NMR of 8-hydroxyquinoline starting material displays several peaks. The first peak is a doublet of doublets with chemical shifts δ, 8.796, 8.792, 9785, and 8.781, dd, J=1.6 and 4.4 Hz. The second doublets of doublet has the following chemical shifts: δ, 8.185, 8.181, 8.164 and 8.160, J=1.6, and 8.4Hz. The third doublet of doublets has shifts such as δ, 7.356, 7.353, 7.335 and 7.332, J=1.2, and 8.4 Hz. The final set of doublets of doublets reveals chemical shifts at δ, 7.204, 7.201, 7.185 and 7.182, J=1.2, and 7.6 Hz. There was also a doublet peak with the chemical shift δ, 7.487 and 7.466, and J=8.4 Hz.

Ligand A was found to have the following chemical shifts: the first peak was found to be

a doublet with a chemical shift δ of 8.752, 8.744, and J-coupling constant, J=3.2 Hz. The second doublet was observed with a resonance chemical shift of 8.144 & 8.123 and J=8.4 Hz. The last doublet observed includes 7.311and 7.291with J=8.0 Hz. This doublet was found to be further up-field with a chemical shift of 7.156 and 7.137 and J=7.6 Hz. Figure 4.13 shows the detailed NMR spectrum of ligand A.

$^{1}$H-NMR of ethyl malonyl chloride showed the singlet acidic proton in 1, 3-dicarbonyl with a chemical shift of 3.565 ppm as shown in Figure4.13. Quartet methylene and methyl protons have the following chemical shifts: for methylene, the chemical shifts range from 4.236-4.183 ppm and 1.296-1.202 ppm for methyl protons. There is yet another peak at 3.327 ppm for the acidic proton, which is a singlet. In the starting material (ethyl malonyl chloride), the methylene ester proton has a chemical shift ranging from 4.197-4.161 ppm, and the acidic methylene proton has a chemical shift at 3.589 ppm. Both are far downfield in comparison to the ligand A. $^{13}$C-NMR confirmed the presence of the ester bond at 166-170 ppm. The molecular structure of Ligand A is given in Figure 4.14.

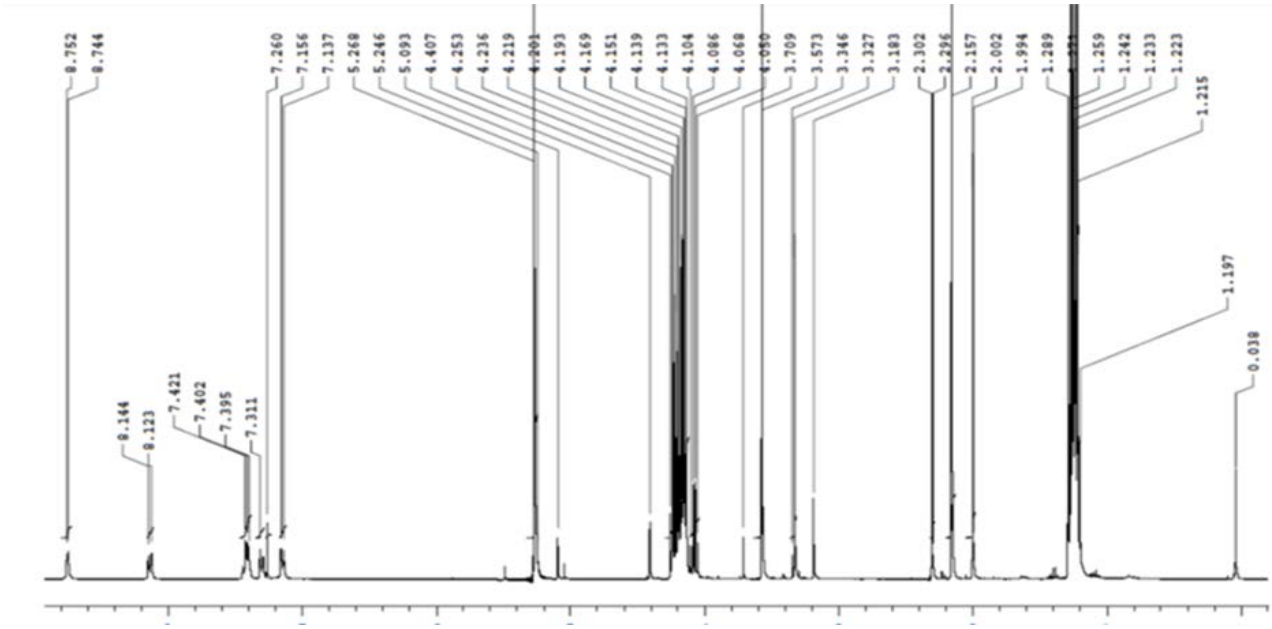


Figure 4.13. The full spectrum of $^{1}$H-NMR of ligand A

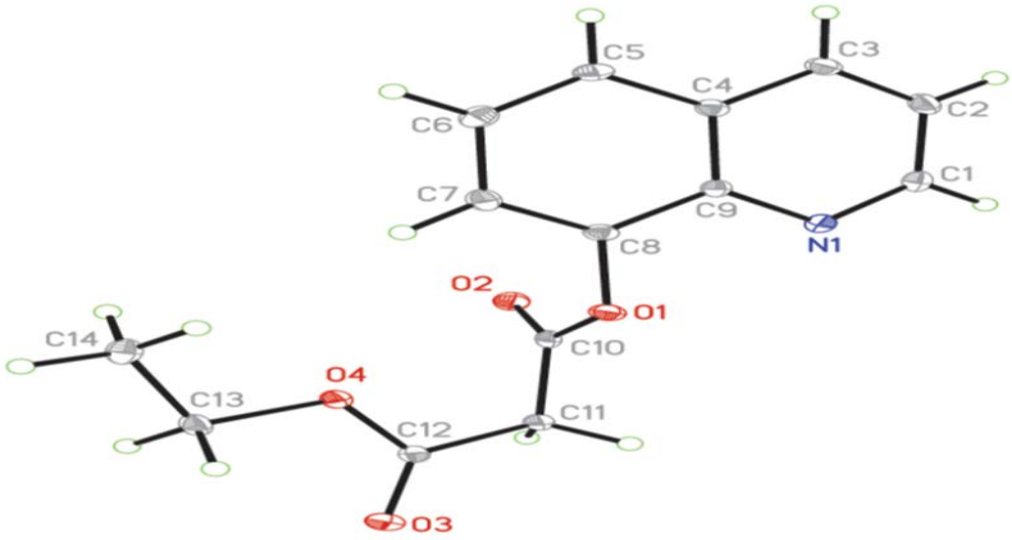


Figure 4.14. The Ortep Molecular Structure of Ligand A

The X-ray structure yielded the following information on bond lengths and bond angles. The following are some of the selected bond lengths and bond angles: C(1)-N(1) is 1.40(1)Å. C(1)-C(2) is 1.414(1) Å , C(2)-C(3) is 1.367(1) Å , C(3)-C(4) is 1.417(1) Å, C(4)-C(5) is 1.418(1) Å, C(4)-C(9) is 1.421(1) Å, C(5A)-C(6A) is 1.368(1) Å, O(1)-C(8) is 1.404(1) Å, N(1)-C(1) is 1.40(1) Å, N(1)-C(9) is 1.366(1) Å, O(2)-C(10) is 1.202(1) Å, and O(4)-C(12) is 1.333(1) Å, for C-O; and when carbon is bound to C=O oxygen, O(4)-C(13) is 1.460(1) Å for $sp^3$ carbon, C-H is 0.95Å for $sp^2$ carbon and C-H is 0.98 Å for $sp^3$ carbon, O(3)-C(12) is 1.205(1) Å for C=O bond, and C(13)-C(14) is 1.505(1) Å for $sp^3$ carbon. O (1)-C (8) is 1.404(1) Å for $sp^2$ carbon.

The following are the bond angles in degrees (°): C(10)-O(1)-C(8) is 116.78(7), C(1)-N(1)-C(9) is 116.90(8), N(1)-C(1)-C(2) is 124.60(9), C(3)-C(2)-C(1) is 118.58(9), C(7A)-C(8A)-O(1A) is 118.63(8), C(7)-C(8)-O(1) is 118.57(8), O(1)-C(8)-C(9) is 118.99(8), N(1)-C(9)-C(8) is 119.40(8), N(1)-C(9)-C(4) is 123.20(9), C(8)-C(9)-C(4) is 117.40(8), O(2)-C(10)-O(1) is 123.96(9), O(2)-C(10)-C(11) is 125.70(9), O(3)-C(12)-O(4) is 124.71(9), O(3)-C(12)-C(11) is

122.63(9), O(4)-C(12)-C(11) is 112.65(8), and O(4)-C(13)-C(14) is 107.39(8).For more information about bond angles and lengths of Ligand A please see appendix C.

### 4.4.2 Ligand A: X-ray Structural Comparisons

The crystal structure of ligand A was compared with other similar structures found in the literature. The literature search indicates no evidence that anyone has ever made this compound before. It becomes a challenge to find a compound similar to it, but many 8-hydroxyquinoline derivatives and their metal complexes have already been prepared and characterized by X-ray method. This section discusses some of these complexes and how they are related to ligand A. The focus of comparison includes the presence of a quinoline ring in already published structures.

### 4.4.3 Ligand A versus 8-hydroxyquinoline

Roychowdhury[90] reported on the structure of the 8-hydroxyquinoline ligand. Unlike ligand A, 8-hydroxyquinoline crystallizes in an orthorhombic crystal system with the *Fdd2* space group. There are 16 molecules per unit cell. The compound has a tendency to arrange itself in a plane very close to (001). Assignment of both bond lengths and angles from the X-ray structures of both compounds reveals the following similarities and differences in bond length and bond angle: the O-C bond length in 8-hydroxylquinoline was found to be 1.39(2) Å, while the corresponding bond length in ligand A was found to be 1.470(1) Å; addition of acac ligand to the 8-hydroxyquinoline ligand lengthens the bond length somehow. In my opinion this could be due to participation of hydroxyl oxygen in resonance with the C=O of the newly formed ester bond. The resonance weakens the O1-C8 bond while strengthening the O1-C10 bond {1.353(1) Å} in

the ester group. Another difference noted is in the C-N bond length of the quinoline ring: in 8-hydroxylquinoline, the N10-C9 bond is 1.35(2) Å, and its corresponding bond angle in ligand A is 1.319(1) Å; in ligand A the bond length is slightly shorter. The second C-N bond is N10-C1; in 8-hydroxylquinoline, this bond has a value of 1.38(2) Å, slightly larger than its corresponding bond length in ligand A {1.366(1) Å}. In pyridine, the average C-N bond length is about 1.337 Å. This bond has $sp^2$ character as the result of resonance. In contrast, the average bond length of C-N in neutral amine is 1.469 Å.[91]

The bond angles in 8-hydroxyquinoline range from 119-124°, typical for $sp^2$ hybridized atoms. For instance, the angle of C1-N10-C9 in 8-hydroxyquinoline is 119.0(1) °, and its corresponding angle in ligand A is 116.9(8) °. For C6-C1-N10, the bond angle is 121.5(1) °, whereas its corresponding angle in ligand A is 123.20(9) °. In 8-hydroxyquinoline, the bond angle C1-N10-C9 is 119.0(1) °, and in ligand A the same angle is 116.9(8) °. In 8-hydroxyquinoline, the bond angle C4-C5-C6 is 119.8(1) °, whereas in ligand A it is 120.65°.

### 4.4.4 Ligand A Versus 3-(3-Methylphenyl)-5-(quinolin-8-ylmethoxy)-1, 2, 4-oxadiazole monohydrate

Compound 3-(3-methylphenyl)-5-(quinolin-8-ylmethoxy) - 1, 2, 4-oxadiazole monohydrate (as shown in the Figure 4.15), [92] like ligand A, crystallizes in a triclinic crystal system, where the space group is *P1*. As in previous cases, both the bond angle and the length of quinoline were compared in order to determine the relationships between the two compounds. For instance, the N1-C7 bond length is 1.313(3) Å in the latter compound, whereas the same N-C is 1.40 (1) Å in ligand A, which means this bond length in ligand A is slightly larger than in its corresponding compound. The N1-C8 bond length is 1.363(3) Å in latter compound, whereas it is 1.366 Å in ligand A; this difference is not great. The C4-C8 bond length is 1.418(3) Å in the

latter compound, while the same bond length in ligand A is measured to be 1.421(1) Å. The C9-O1 bond length in the latter compound is 1.366(3) Å, whereas the corresponding bond length in ligand A is 1.404 Å. The C10-O1 bond length in the latter compound is 1.415(3) Å, while its equivalent bond length in ligand A is 1.354(1) Å. In ligand A, this bond is shorter because oxygen is connected to the C=O of the ester bond; thus, oxygen is involved in resonance, which makes that bond to have $sp^2$ character due to the contribution of the lone oxygen pair in resonance. By contrast, in the corresponding compound oxygen is connected to methylene carbon, which is $sp^3$ and has no resonance available; this makes the bond have more $sp^3$-like character. The C6-C7 bond length in 3-(3-methylphenyl)-5-(quinolin-8-ylmethoxy)-1,2,4-oxadiazole monohydrate is 1.389(4) Å, whereas the same bond in ligand A is 1.414(1) Å. The C-H bond length in oxadiazole monohydrate is 0.9300 Å, whereas in ligand A it is 0.95 Å.

The bond angle of C8-N1-C7 in quinoline of oxadiazole monohydrate is 117. 4°, which is closer to 116.90(8) ° than that of ligand A. Similarly, the C7-C6-C5 bond angle in the quinoline of the oxadiazole compound is 118.5(3) °, whereas the same angle was found to be 118.75(9)° in ligand A. Another angle which is nearly the same is C4-C3-C2; this angle in the quinoline of oxadiazole is 120.4(3) °, whereas the same angle in ligand A is 120.65°. The molecular structure of oxadiazole monohydrate is given in Figure 4.15.

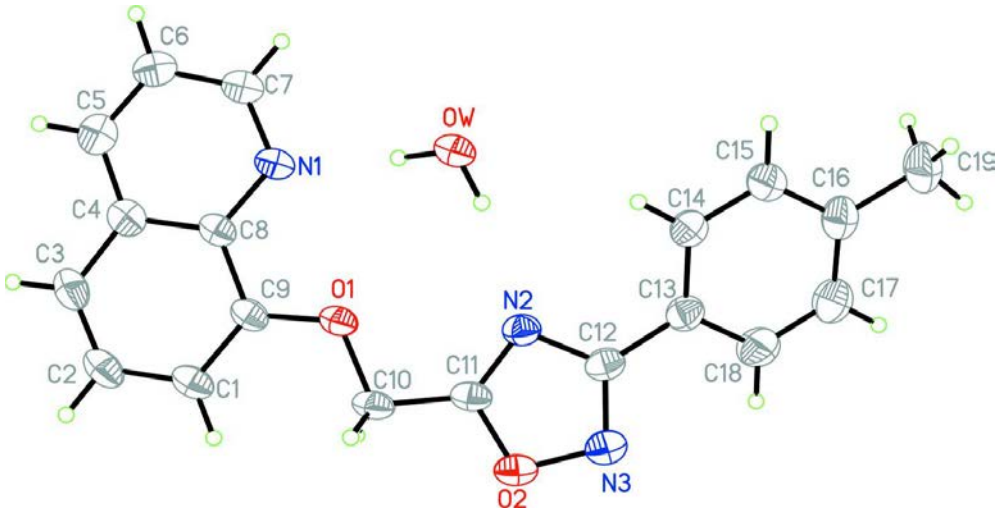


Figure 4.15. The Molecular Structure of 3-(3-methylphenyl)-5-(quinolin-8-ylmethoxy)-1, 2, 4-oxadiazole monohydrate Yang, L et al .*Acta Cryst.* **2013,** E69, o1541.

### 4.4.5 Ligand A versus 8-Hydroxyquinolin-1-ium Hydrogen Sulfate Monohydrate

The two compounds crystallize a in triclinic crystal system with a *P-1* space group. Unlike ligand A, which is neutral, the latter compound is a salt, and therefore it has a positive charge at pyridine nitrogen. The lack of an attaching group allows 8-hydroxyquinolin-1-ium hydrogen sulfate monohydrate[93] to form hydrogen bonding using a hydroxyl group; also, hydrogen bonding can occur between the pyridium proton and the oxygen from sulfate.

For ligand A, the C9-N1 bond length is 1.366(1) Å, while its equivalent bond length in 8-hydroxyquinolin-1-ium salt is 1.360(2) Å; the two are almost the same. The C2-N1 bond length in 8-hydroxyquinolin-1-ium salt is 1.324(2) Å, whereas its equivalent bond in ligand A is 1.40(1) Å. The C1-C2 bond length in ligand A is 1.414(1) Å, whereas the equivalent bond length in hydroxyquinolin-1-ium salt is 1.387(2) Å, and in 8-hydroxyquinoline it is 1.428(2) Å. The C4-C9 bond length is 1.421(1) Å in ligand A, while its equivalent in hydroxyquinolin-1-ium salt is 1.410(2) Å, and in 8-hydroxyquinoline it is 1.45(2) Å. In this case there are no significant differences in bond length. The C8-O1 bond length in ligand A is 1.404(1) Å, and its equivalent bond length in hydroxyquinolin-1-ium salt is 1.344(2) Å, whereas in 8-hydroxyquinoline it is

1.39(2) Å. It is expected the bond length in ligand A will be larger than those of other two compounds. This is attributed to the participation of oxygen lone pairs in the ester bond of the ACAC side arm. This participation weakens the bond strength and lengthens the bond. Lastly, the C5-H5 bond length in ligand A measures 0.95 Å, whereas the same bond length in hydroxyquinolin-1-ium salt measures 0.95 Å.

The C9-N1-C1 bond angle in ligand A is 116.9(8)°, while the same bond angle in hydroxyquinolin-1-ium salt measures 122.9(1)°, and in 8-hydroxyquinoline it is 119.0(1)°. The N1-C1-C2 bond angle in ligand A is 124.6(9)°, while in 8-hydroxyquinolin-1-ium salt the same bond angle measures 120.2(2)°, and in 8-hydroxyquinoline the same angles measures 124.1(1)°. This angle seems to be smaller in 8-hydroxyquinolin-1-ium salt and nearly the same in the other two salts. For ligand A, the N1-C9-C4 bond angle is 123.2(9)°, while its equivalent angle in 8-hydroxyquinolin-1-ium salt is 118.99(1)°, and in 8-hydroxyquinoline the equivalent bond angle measures 121.5(1)°. The bond angle C2-C3-C4 in ligand A measures 119.49(9)°, while the same angle in 8-hydroxyquinolin-1-ium salt measures120.8 (2)°, and in 8-hydroxyquinoline it measures 119.2(1)°. The molecular structure of 8-hydroxyquinolin-1-ium hydrogen sulfate monohydrate is given in Figure 4.16**.**

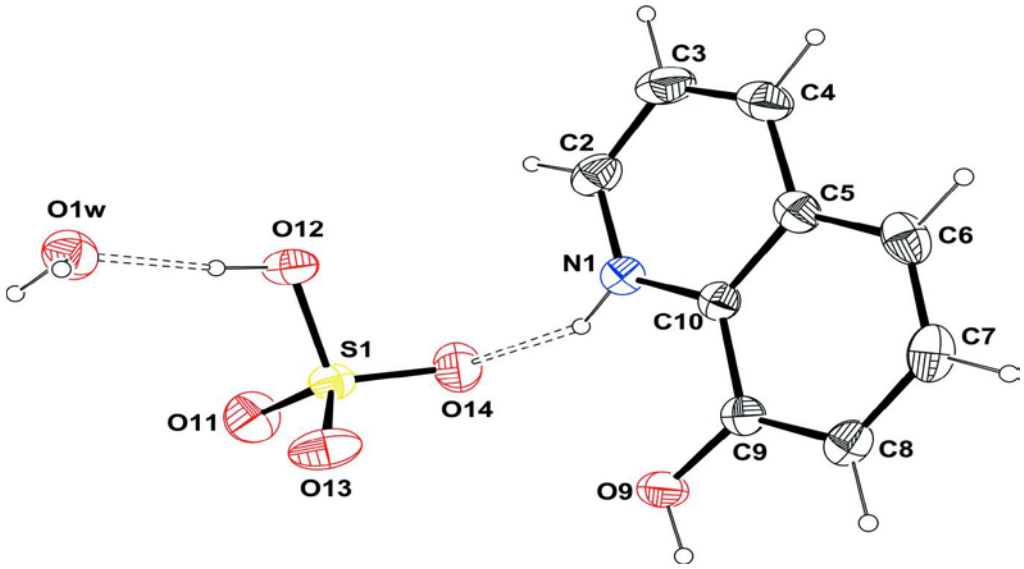


Figure 4.16. The Molecular Structure of 8-Hydroxyquinolin-1-ium Hydrogen Sulfate Monohydrate salt Damous, M et al. *Acta Cryst. Sec E*. **2013**, o1458-o1459.

### 4.4.6 Ligand A versus Non centrosymmetric (quinolin-8-ol-$\kappa^2$-N,O) (quinolin-8-olato-$\kappa^2$-N,O) silver (I) or [Ag($C_9H_6NO$)($C_9H_6NO$)]

[Ag($C_9H_6NO$)($C_9H_6NO$)] crystallizes as a non-centrosymmetric polymorph with an orthorhombic crystal system. The space group for this crystal is $P2_12_12_1$, and Ag (I) exhibits a distorted tetrahedral coordination geometry defined by nitrogen and oxygen from unprotonated 8-quinoliol (8-HQ) from nitrogen and oxygen from deprotonated quinolate anion ($Q^-$). The dihedral angle between the two ligands is 47.0(1) °.[94] The centrosymmetric polymorph crystal of this compound has been reported on by Wu et al.[95]

The bond lengths of [Ag($C_9H_6NO$)($C_9H_6NO$)] were compared with the corresponding ones of ligand A, and the following are some of the selected bonds lengths: the N2-C10 [94] bond length is the shortest in the quinolate ligand in the silver complex and the longest in ligand A. The N2-C14 bond length is the longest in the quinolate ligand in silver (I) complex and the shortest in 8-hydroxyquinolin-1-ium hydrogen sulfate monohydrate (8-HQ ($HSO_4$). The C15-O2

bond length is the longest in ligand A and shortest in the quinolate ligand complexed with silver (I). The bond length and bond angles of all discussed ligands are given tabulated in Table 4.8.

In general, there is a small variation in bond angles and length in the quinoline ligand bonded to metals or bonded to the ACAC ligand as in the case of ligand A. The X-ray structure of [Ag($C_9H_6NO$)($C_9H_6NO$)] is given in Figure 4.17 .

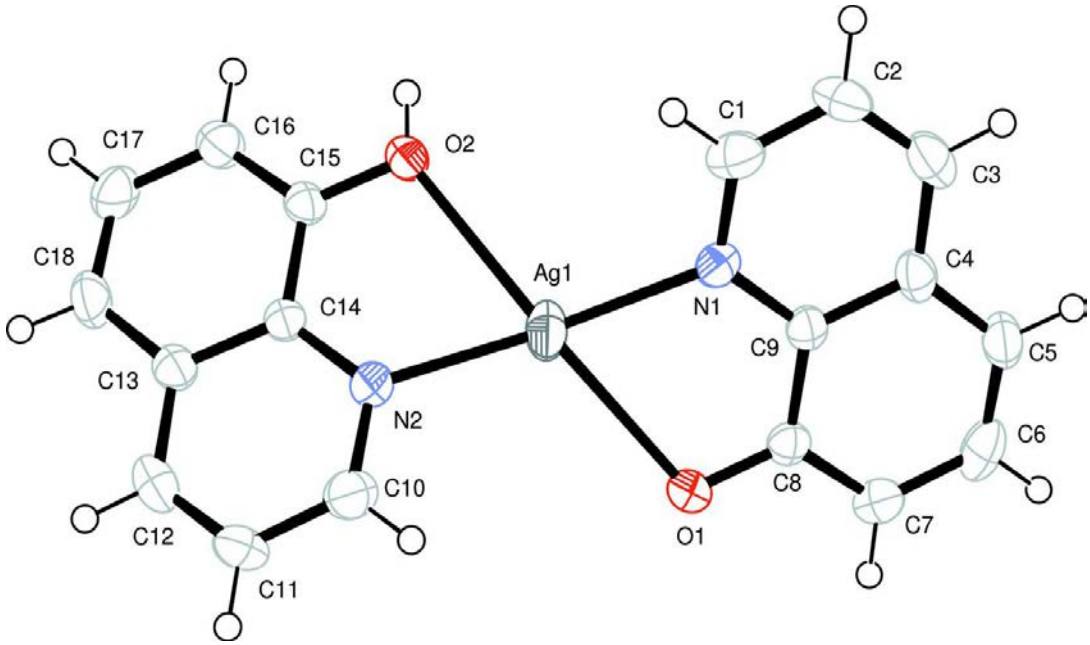


Figure 4.17. The Molecular Structure of [Ag($C_9H_6NO$)($C_9H_6NO$)] Ma, A. Q et al. *Acta Cryst*, E69**, 2013**, m133.

Table 4.8 X-ray data comparison of [$Ag(C_9H_6NO)(C_9H_6NO)$], Ligand A, and 8-hydroxyquinoline compound. The Bond Lengths (Å) and Bond Angles in Degrees (°) are shown

| Parameters | 8-HQ in complex | $Q^-$ in complex) | Ligand A | 8-HQ | 8-HQ($HSO_4$)[93] |
|---|---|---|---|---|---|
| N2-C10 | 1.322(5) | 1.316(5) | 1.40(1) | 1.350(2) | 1.324(2) |
| N2-C14 | | | 1.366(1) | 1.383(2) | |
| C13-C14 | 1.364(4) | 1.370(4) | 1.421(1) | 1.449(2) | 1.3602(2) |
| C12-C13 | | | 1.417(1) | 1.423(2) | |
| C8-C9 | 1.427(5) | 1.434(5) | 1.417(1) | 1.443(2) | 1.410(2) |
| C15-O2 | | | | | |
| C10-N2-14 | 1.403(5) | 1.400(6) | 1.404(1) | 1.390(2) | 1.410(2) |
| N1-C9-C4 | | | | | |
| N1-C1-C2 | 1.427(5) | 1.436(5) | 116.9(8) | 119.0(1) | 1.410(2) |
| C12-C13-C18 | | | | | |
| C15-C16-C17 | 1.336(4) | 1.319(4) | 123.2(9) | 121.5(1) | 1.3438(2) |
| | 118.7(3) | 119.2(3) | 124.6(9) | 124.1(1) | 122.93(1) |
| | 119.8(3) | 121.4(3) | 123.06(9) | 122.7(1) | 118.99(1) |
| | 123.6(4) | 123.1(4) | 119.7(9) | 117.8(1) | 120.19(2) |
| | | | | | 123.86(2) |

| | | | |
|---|---|---|---|
| | 123.1(3) | 123.0(4) | 120.5(1) |
| | 121.6(3) | 121.4(4) | |

The bond length and bond angle parameters used here are from the [Ag($C_9H_6NO$)($C_9H_6NO$)] complex; these were matched with those from other ligands as shown in Table 4.10 . Ligand abbreviations are used in the table; for instance, 8-HQ stands for 8-hydroxyquinoline, and 8-HQ($HSO_4$) stands for 8-hydroxyquinolin-1-ium hydrogen sulfate monohydrate; for more information about [Ag($C_9H_6NO$)($C_9H_6NO$)] please refer to the reference given in Figure 4.17. Also, note that 8-HQ in complex and $Q^-$ in complex belong to [Ag($C_9H_6NO$)($C_9H_6NO$)]; as one can see from Figure 4.17, there is an 8-hydroxyquinoline ring (8-HQ) and a quinolate ring ($Q^-$) in the [Ag($C_9H_6NO$)($C_9H_6NO$)] complex.

## 4.5 Ligand B

Ligand B was prepared from syn-2-peridoxylaldoxime and ethyl malonyl chloride in the same manner as ligand A. Details of the preparation are discussed under the experimental section. Efforts to obtain the crystal structure were unsuccessful because the crystals were not stable in air and decompose at room temperature. The impure ligand is deep red in color but when purified, ligand B turns to golden orange. NMR was used to characterize the structure. The NMR spectra of ligand B are shown in Figure 4.18-4.20.

The NMR of the starting material, syn-2-peridoxylaldoxime, has several chemical shifts. The first peak was observed at 9.325 ppm. The latter was a broad peak likely to be hydroxyl in

the oxime functional group. The proton next to the nitrogen in the pyridine has a chemical shift ranging from 8.646 to 8.627 ppm, and it is a doublet of doublet. This was followed by shifts at 8.445 ppm for a singlet proton outside the pyridine ring and for a doublet that ranged from 7.838 to 7.813 ppm. The last two peaks are both triplets with chemical shifts ranging from 7.751 to 7.701 ppm and from 7.313 to 7.276 ppm. Significant changes were observed in the chemical shift after the reaction. The product's proton chemical shifts were downfield relative to those of the starting material with a broad peak at 9.325 ppm, which was absent in the product. A singlet proton outside the ring in the oxime function group shifted to 8.439 ppm.

Resolution of the NMR spectrum of the product showed the furthest peak to be a doublet of a quartet with numerous chemical shifts δ, 8.657, 8.654, 8.653, and 8.650, dq, J=1.2 and 1.6Hz. The second set of peaks in the same doublet of s quartet include 8.645, 8.642, 8.640, and 8.638, dq, J=1.2 and 1.6Hz. The next peak was found to be a doublet of a triplet with the following chemical shift: δ, 8.045, 8.042, 8.040, 8.025, 8.022, and 8.020, J=0.8, 1.2, and 8.0 Hz. This peak was followed by doublet of a doublet of a triplet 7.778, 7.777, 7.774, and 7.772, ddt, J=0.4, 0.8, 1.6, and 2.0 Hz. Another chemical shift is 7.6, 7.758, and 7.754, d, J=1.6 Hz, and 7.739, 7.738, 7.735, and 7.734, dd, J=0.4, 1.6, and 7.6 Hz. The last peak was found to be very complex in appearance, and it appeared to be a doublet of a doublet of a doublet of a triplet (δ, 7.381, 7.378, d, J=1.2Hz, 7.369, 7.366, 7.362, and 7.359, dd, J=1.2, 2.8 Hz, and 7.350, 7.347, d, J=1.2 Hz).

The side ethyl malonyl side arm derived from ethyl malonyl chloride also showed change in the proton NMR chemical shift. The quartet methylene proton of ester has a chemical shift ranging from 4.218-4.183 ppm. The singlet acidic protons from malonate ester have 3.565 ppm.

Figure 4.18 and 4.19 show the proton NMR of ligand B. Figure 4.20 shows $^{13}C$ NMR of ligand B.

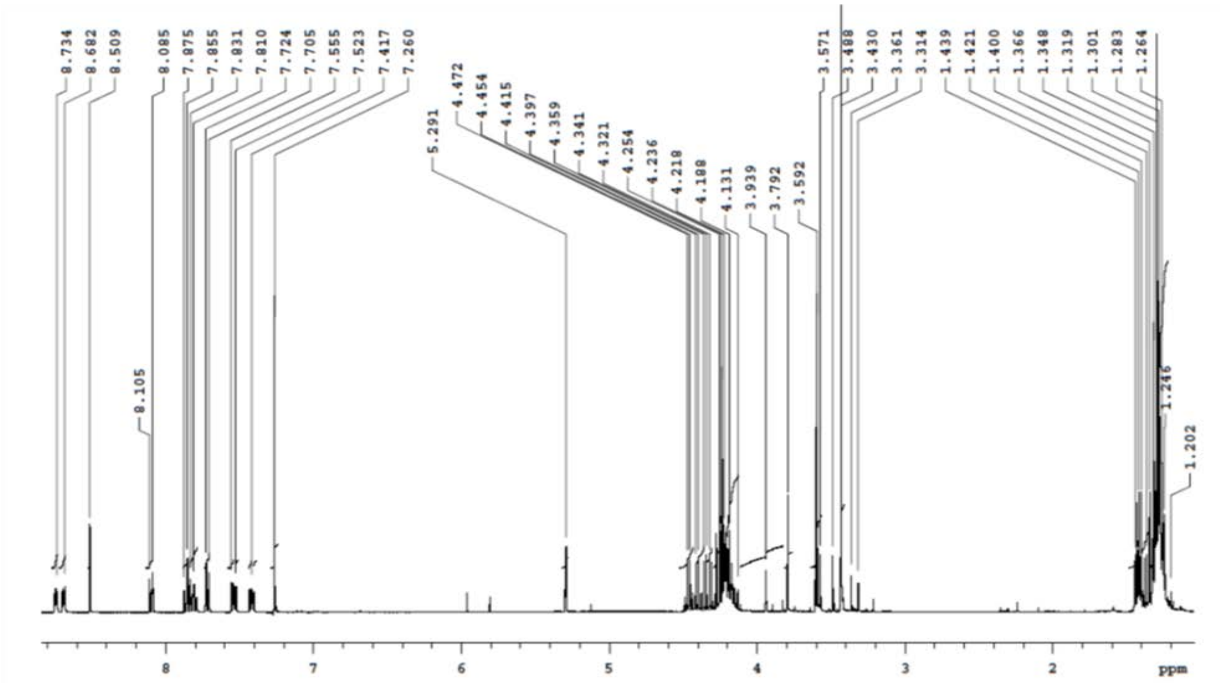


Figure 4.18. $^{1}H$-NMR of Ligand B; $CDCI_3$ was used as a solvent

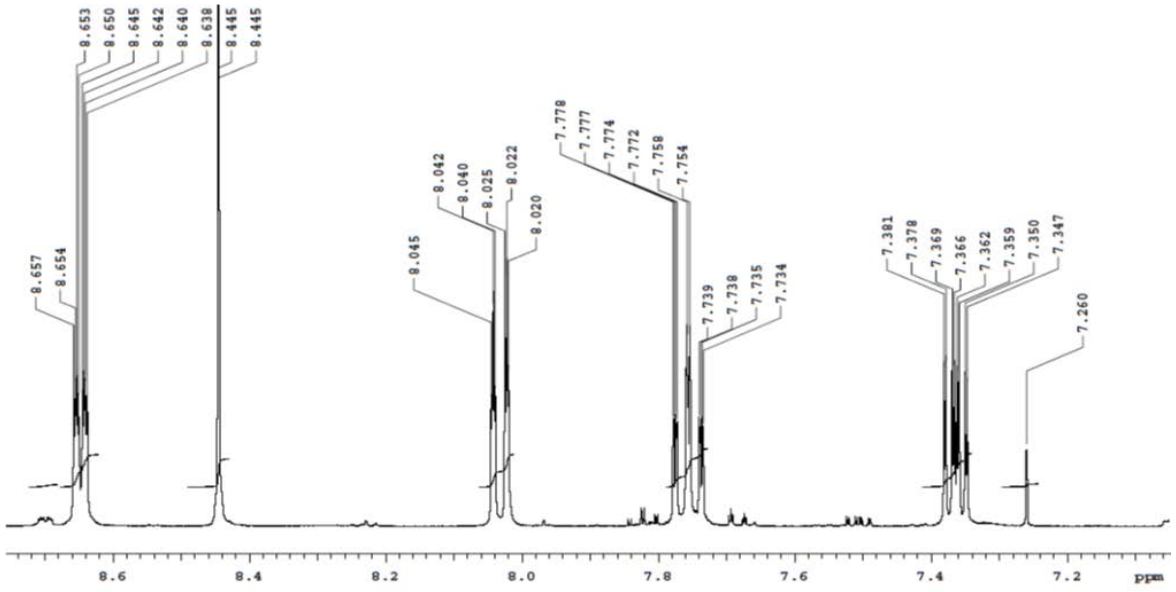


Figure 4.19. $^{1}H$-NMR of ligand B showing the aromatic region; $CDCI_3$ was used as a solvent

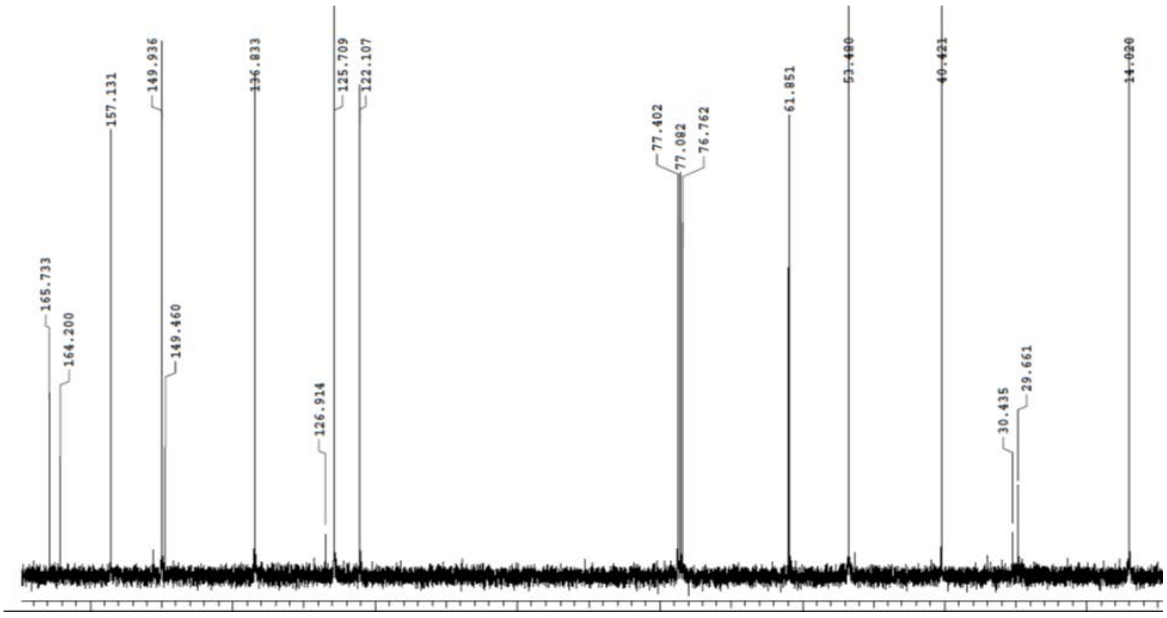


Figure 4.20. $^{13}$C-NMR of Ligand B $CDCI_3$ was used as a solvent

## 4.6 Ligand C

Ligand C was prepared from 2, 6-dipyridinylmethanol and ethyl malonyl chloride as described in the experimental section. Both compounds were studied by means of proton NMR. The proton NMR of 2, 6-dipyridinylmethanol has the following chemical shifts: triplet δ, 7.725, 7.706, and 7.687, t, J=7.6 Hz. There is also another doublet chemical shift, δ, 7.210 and 7.193, d, J=7.6 Hz. The methylene protons have chemical shifts at 4.787 ppm and are downfield due to the effect of electron withdrawal from the two neighbors, viz. the alcohol and the pyridine ring.

The proton NMR spectrum of the product ligand C has different chemical shifts with the same splitting arrangements. The pyridine triplet was found to be more downfield compared to the triplet in the starting material. The chemical shift of the triplet was found to be δ, 7.950, 7.931 and 7.912, t, J=7.6 Hz. The same was true with the pyridine doublet, which has a chemical shift δ, 7.540 and 7.521, d, J=7.6 Hz. By contrast, the methylene proton in the ester group was found to be slightly downfield with a chemical shift of 5.476 ppm. The methylene protons of the

malonate ester shifts up-field with a chemical shift of 4.425 ppm. The acidic α-proton has a chemical shift of 3.684. The $^{13}$C-NMR, done as shown in Figure 4.21, affirmed the existence of the ester carbon bond at 166.321 ppm and 166.17 ppm. Both the carbon and the proton NMR spectra of ligand C are available in Figures 4.21 and 4.22.

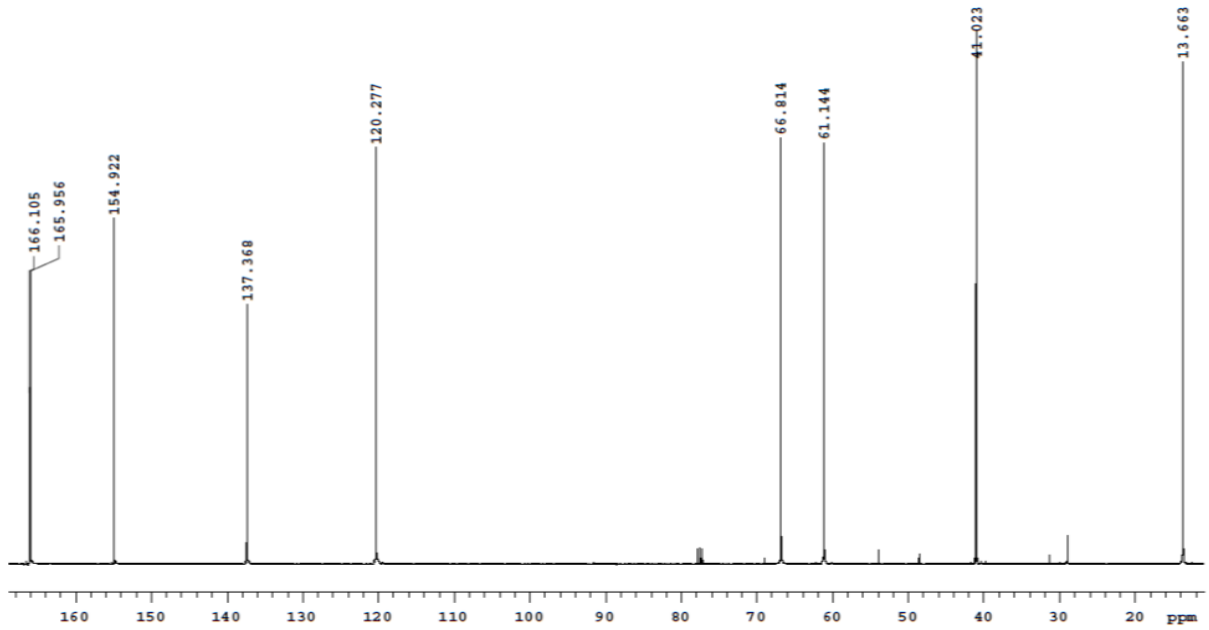


Figure 4.21. $^{13}$C-NMR spectrum of ligand C; $CDCI_3$ was used as a solvent

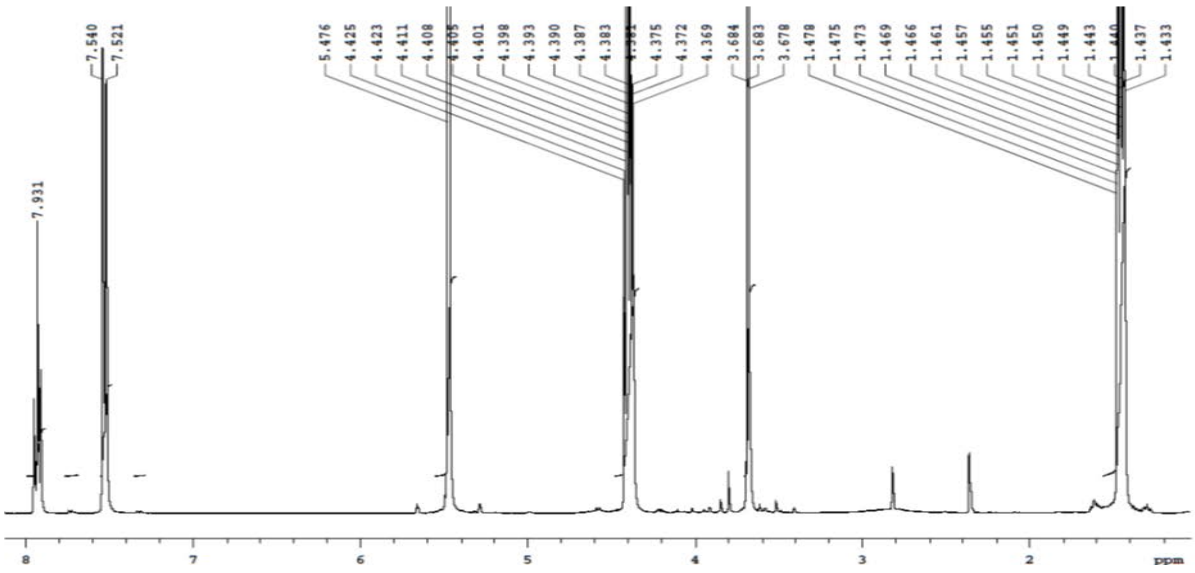


Figure 4.22. $^{1}$H-NMR spectrum of ligand C; $CDCI_3$ was used as a solvent

**4.7** Synthesis of Rhenium Complex 1

The X-ray data and structure of rhenium complex 1 are given in Table 4.11 and Figure 4.23, respectively. The data include the space group, the density, and the number of the reflections collected. Moreover, the X-ray structure shows the crystal to be triclinic. For more detailed information on bond length and bond angle, see Appendix D**.**

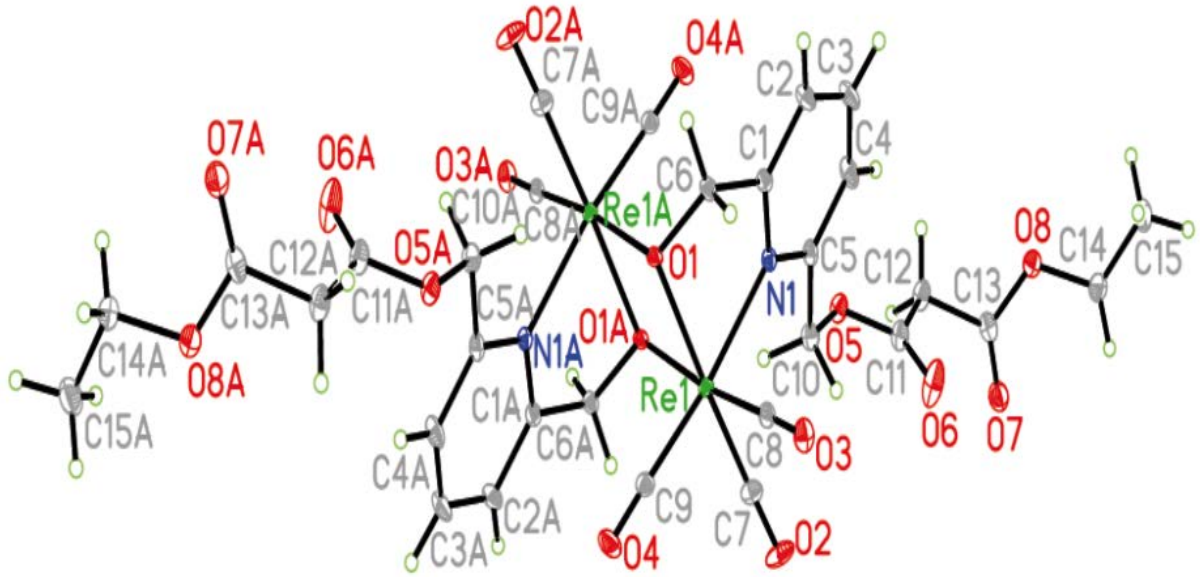


Figure 4.23. The X-ray structure of Rhenium Complex 1

The ORTEP molecular structure of rhenium complex 1 reveals there is no Re-Re interaction, as we have also seen in the gold (I) compounds. Instead, the two rhenium atoms are separated by the oxygen atom which connects the two atoms. The following are some selected bond lengths in angstroms (Å) and angles in degrees (°), starting with selected bond angles: Re(1)-C(8) is 1.898(3), Re(1)-C(9) is 1.911(3), Re(1)-C(7) is 1.913(3), Re(1)-O(1) is 2.152(2), Re(1)-N(1) is 2.224(2), O(1)-C(6) is 1.424(3), N(1)-C(1) is 1.352(4), N(1)-C(5) is 1.357(4), C(1)-C(2) is 1.384(4), C(1)-C(6) is 1.502(4), O(2)-C(7) is 1.150(4), and C(3)-H(3A) is 0.95 for $sp^2$ hybridized carbon in the quinoline ring. O(4)-C(9) is 1.156(4) for the C≡O bond, C(4)-C(5) is 1.381(4) for the C=C bond of the quinoline ring, C(11)-C(12) is 1.509(4) for $sp^3$ carbon of the

ACAC side arm, C(10)-H(10B) is 0.99 for $sp^3$ carbon, and C(14)-C(15) is 1.522(5) for $sp^3$ carbon of the ACAC side arm.

Bond angles (°) include the following: C(8)-Re(1)-C(9) is 83.68(12) , C(8)-Re(1)-C(7) is 86.86(12), C(9)-Re(1)-C(7) is 88.25(13), C(8)-Re(1)-O(1) is 97.85(10), C(9)-Re(1)-O(1) is 96.81(10), C(7)-Re(1)-O(1) is 173.42(10), C(8)-Re(1)-O(1) is 173.02(9), C(9)-Re(1)-O(1) is 99.80(10), C(7)-Re(1)-O(1) is 99.25(10), O(1)-Re(1)-O(1) is 75.79(8), C(8)-Re(1)-N(1) is 92.97(10) , Re(1)-O(1)-Re(1) is 104.21(8), and O(1)-Re(1)-N(1) is 73.67(8).

### 4.7.1 $^1$H-NMR Results for Rhenium Complex 1

The X-ray structure affirmed the loss of one ethyl malonyl side arm. This could be due to the de-esterification by 0.1 g of NaOH, which was added to the deprotonate ethyl malonyl. The enolate was expected to react with $ReBr(CO)_5$ using its charged oxygen or its carbanion. As a result of the reaction, the chemical shift of the complex product moved downfield relative to the ligand. For instance, the methylene proton of ethyl ester was found to be at 4.279 ppm, whereas in pure ligand C these protons resonate at 4.196 ppm. The acidic protons between the two carbonyl groups were found to have a chemical shift of 3.731 ppm and 3.567 ppm respectively. In the complex product, these two proton peaks have different chemical environments. In the starting material, the same protons in ligand C appear to have a single shift at 3.467 ppm. Figure 4.24 shows the proton NMR of rhenium complex 1.

In the aromatic region, there were two sets of protons. The first proton set was found to be a triplet with a chemical shift δ, 8.290, 8.270, and 8.250, t, J=8.0 Hz, and the second set of protons was found to be a doublet with a chemical shift δ, 7.773 and 7.753, d, J=8.0 Hz.

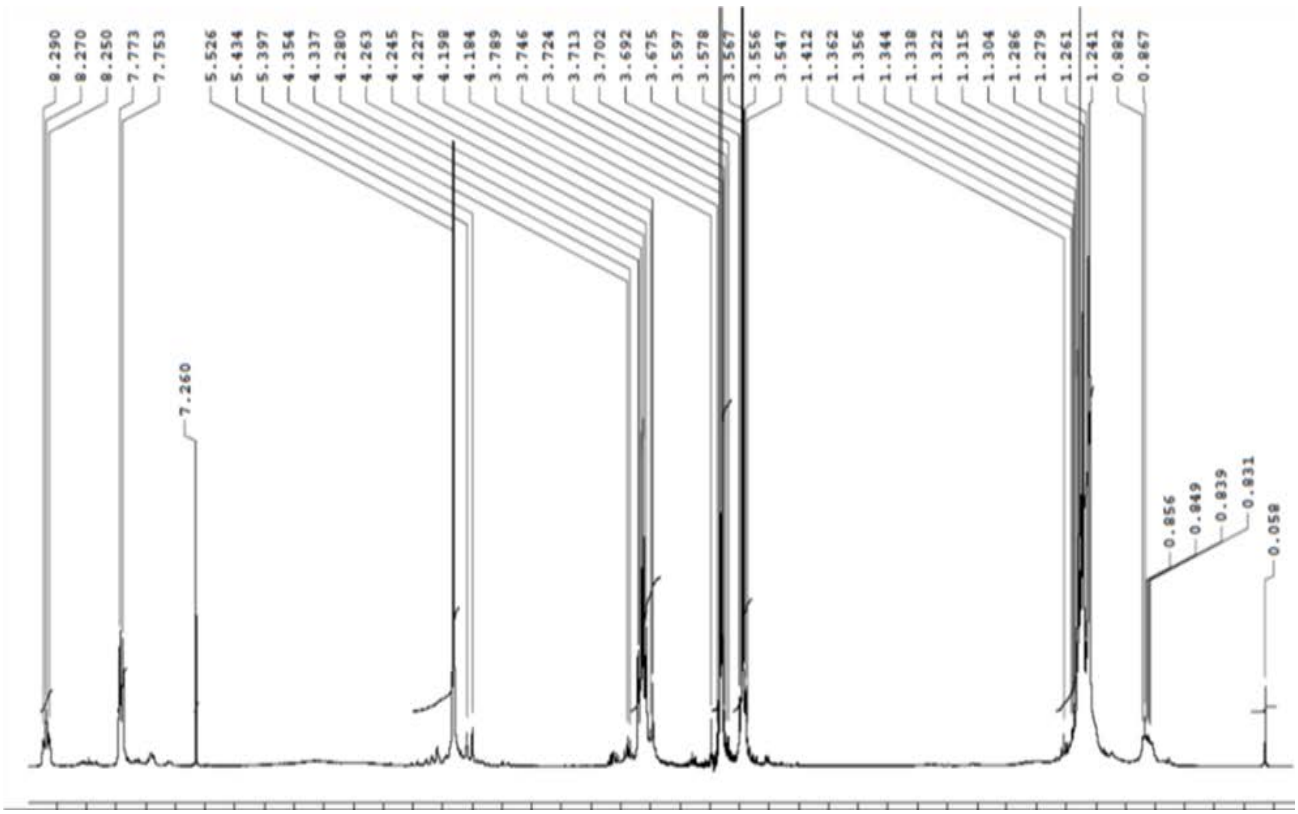


Figure 4.24. $^{1}$H-NMR spectrum result for Rhenium Complex 1

### 4.7.2 Infra-Red Spectrum of Rhenium Complex 1

The IR spectrum affirmed the presence of complex product. Figure 4.25 is an IR spectrum in which the $ReBr(CO)_5$ spectrum is indicated by a red color. The $ReBr(CO)_5$ has two major peaks at 2048cm$^{-1}$ and 1980 cm$^{-1}$. After reflux, the IR spectrum was carried out, and this evinced the disappearance of the two major vibration peaks seen. Instead, smaller vibrational peaks were observed at 1924 cm$^{-1}$, 2023 cm$^{-1}$, and 2253 cm$^{-1}$ in addition to a sharp short peak at 2375 cm$^{-1}$. The IR spectrum of the rhenium complex product is given in Figure 4.26.

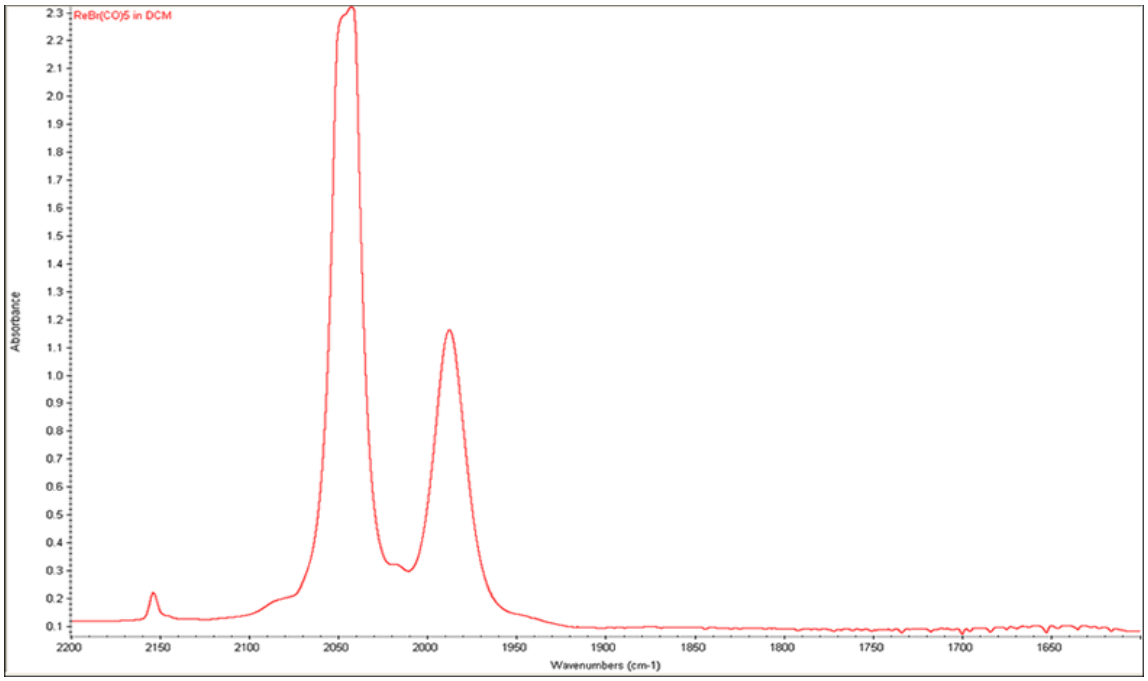


Figure 4.25. IR spectrum of $ReBr(CO)_5$ in DCM

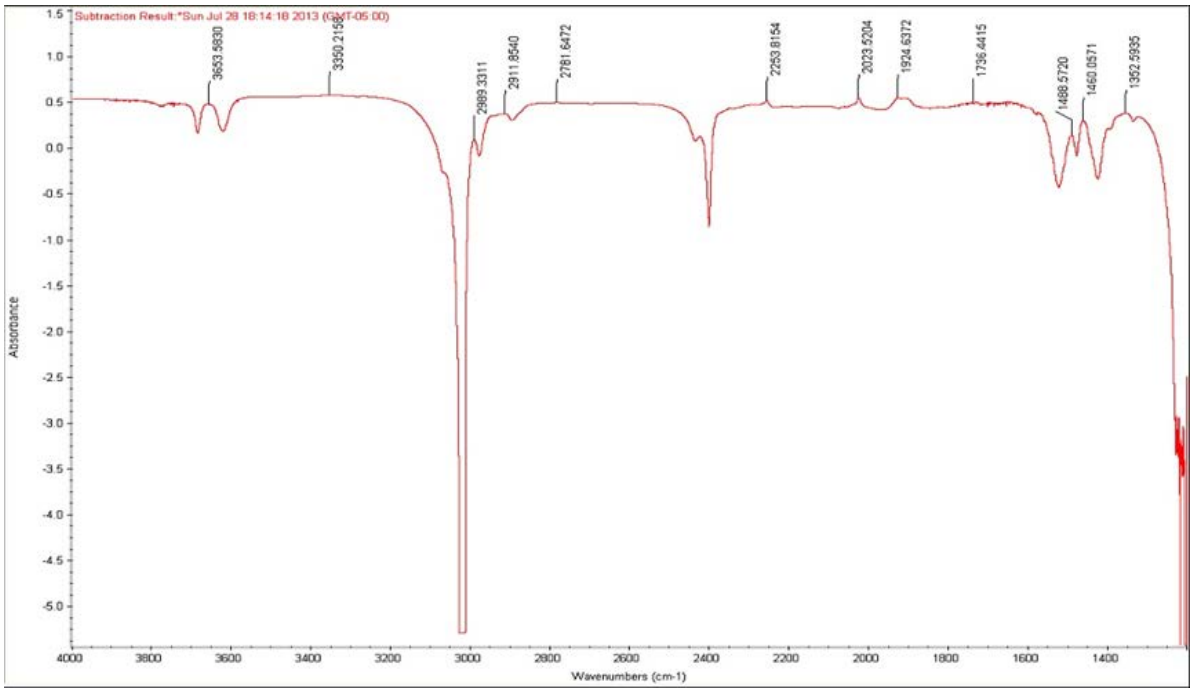


Figure 4.26. IR spectrum of Rhenium Complex 1

Table 4.9 X-ray Crystallographic and Data Processing Parameters for Rhenium Complex 1

| | |
|---|---|
| Crystal system | Triclinic |
| Space Group | *P -1* |
| a, Å | 9.6029(1) Å |
| b,Å | 9.7484(1) Å |
| c,Å | 10.876(2) Å |
| α, deg | 100.711(2)° |
| β, deg | 104.747(2)° |
| V (Å3) | 822.51(2) $Å^3$ |
| Emperical formula | $C_{30}H_{28}N_2O_{16}Re_2$ |
| Formula Weight in g/mol | 1044.94 |
| Formula Unit per cell (Z) | 1 |
| Density, ($Mg/M^3$) | 2.110 |
| abs coeff (μ) mm-1 | 8.965 |
| Reflection Collected | 8405 |
| F(000) | 500 |
| Final R indeces [I>2 | R1 = 0.0168, |
| Sigma(I)] | wR2 = 0.0423 |
| Goodness-of-fit on $F^2$ | 1.037 |
| Crystal Size | 0.20 x 0.11 x 0.08 $mm^3$ |
| Largest diff. peak and hole | 1.542 and -0.864 e.$Å^{-3}$ |
| Temperature | 100(2) K |

### 4.7.2 Rhenium Complex 1: X-ray Structural Comparison

Rhenium complex 1 has not been prepared before. Studies in the literature describe rhenium complexes derived from 2, 6-dipyridinylmethanol, a precursor for the synthesis of ligand C. The lack of descriptions of ligands similar to that seen in the X-ray figure has made comparison of this new structure difficult. In order to overcome this problem, the following criteria were devised so that good rhenium complexes could be used for comparison. These criteria include the following: any complex with rhenium mono, di, or tri-carbonyl ligand, also with a pyridine or quinoline, was considered useful for comparison of the Re-N bond length and the corresponding bond angle. The ligand had to have a Re-O bond in order to make possible the comparison of the Re-O bond angle and bond length. Finally, a nitrogen heterocyclic ligand with an acac side arm was highly preferred.

#### 4.7.2.1 Rhenium Complex 1 versus [*fac*-Re(FOQN)$(CO)_3$](μ-Cl) [*fac*-Re(FOQN)$(CO)_3$]$CH_3C_6H_5$

The two compounds show little resemblance in their chemical structures, but there are a few exceptions; first, both contain a rhenium atom, and the rhenium is directly coordinated to the pyridine ring of the heterocyclic ligand; also, there is a Re-O bond in both compounds. Second, both compounds exist as dimers; there are two ligands and two rhenium metal centers. On the other hand, there are numerous differences between the two compounds; first, rhenium complex 1 crystallizes in a triclinic crystal system with a *P-1* space group. On the other hand, the latter compound crystallizes in a monoclinic crystal system with *P 21/c.* Apart from having different ligands, [*fac*-Re(FOQN)$(CO)_3$](μ-Cl) [*fac*-Re(FOQN)$(CO)_3$]$CH_3C_6H_5$ lacks a aliphatic side arm (acac ligand). In [*fac*-Re(FOQN)$(CO)_3$](μ-Cl) [fac-Re(FOQN)$(CO)_3$]$CH_3C_6H_5$, the two rhenium

atoms are bridged by chloride ligands,[96] whereas in rhenium complex 1, the two rhenium atoms are connected by an oxygen atom.

In [*fac*-Re(FOQN)$(CO)_3$](μ-Cl)[*fac*-Re(FOQN)$(CO)_3$]$CH_3C_6H_5$, the rhenium-carbonmonoxide bond or Re-C bond lengths are1.898 and 1.919 Å, similar to those in rhenium complex 1 [1.898, 1.911(3), and 1.913(3) Å]. This is in agreement with descriptions of other compounds found in the literature.[97] Re-O bond lengths are 2.164 and 2.171 Å in [*fac*-Re(FOQN)$(CO)_3$](μ-Cl)[*fac*-Re(FOQN)$(CO)_3$]$CH_3C_6H_5$, whereas in rhenium complex 1 the same bond lengths are 2.136(2) Å and 2.152(2) Å. This near equality in Re-O bond length in [*fac*-Re(FOQN)$(CO)_3$](μ-Cl) [*fac*-Re(FOQN)$(CO)_3$]$CH_3C_6H_5$ suggests there is an equal sharing of charge at both the Re1 and Re2 metal center. The carbonmonoxide bond length in [*fac*-Re(FOQN)$(CO)_3$](μ-Cl)[fac-Re(FOQN)$(CO)_3$]$CH_3C_6H_5$ ranges from 1.134(5)-1.156(5) Å, whereas in rhenium complex 1 the C≡O bond length ranges from 1.150(4)-1.157(4) Å. In both cases the bond length of C≡O is nearly the same. In free carbonmonoxide, the (C≡O) bond length is around 1.128 Å, slightly shorter than in the two complexes. This indicates there is a decrease in bond order in the C≡O bond; in other words, the C≡O bond is lengthened and weakened by ligand electron donation. Remember that stronger electron donor ligands tend to weaken the C≡O bond, thus leading to a slight increase in bond length.

The carbon-carbon double bonds (C=C) bond lengths of 8-hydroxyquinoline and the pyridine ring in both complexes have more $sp^2$ character due to resonance. For instance, in the pyridine ring of rhenium complex 1the C-C bond length ranges from 1.377(4)-1.384(4) Å, whereas in 8-hydroxyquinoline ring the same C-C has bond length ranges from 1.357(8)-1.417(7) Å. The average C= C bond length in benzene and pyridine is 1.39 Å. For $sp^3$ C-C bond length, slightly longer than in $sp^2$; this is self-evident in the bond length of the C-C side chain.

For instance, C1-C6, C11-C12, and C12-C13 are 1.502(4), 1.509(4), and 1.524(4) Å respectively.

Another important bond length is Re-N; in [*fac*-Re(FOQN)$(CO)_3$](μ-Cl) [fac-Re(FOQN)$(CO)_3$]$CH_3C_6H_5$ the bond lengths are 2.178 and 2.169 Å, whereas in rhenium complex 1, the Re-N bond length is 2.224(2) Å. In rhenium complex 1, the Re-N bond is slightly longer. In comparison to various pyridine containing complexes synthesized by Zubieta and his co-workers, there is slight variation in the Re-N bond length. From the X-ray structures of these complexes, the Re-N bond ranges from 2.136(2)-2.249(7) Å.[97] The X-ray molecular structure of [*fac*-Re(FOQN)$(CO)_3$](μ-Cl) [*fac*-Re(FOQN)$(CO)_3$]$CH_3C_6H_5$ is given in Figure 4.27 . This Figure was obtained from the work of Rochford[96] and his coworker (Rochford, J et al. *Organometallics*, **2013**, 32, 1832-1841) and is used here for clarification of the material discussed. Permission to reproduce has been granted by the publisher, ACS, under strict guidelines. For more information please contact the publisher.

Selective bond angles (°) were also compared in order to understand the impact of steric hindrance caused by the ligand. The following are some examples of comparisons of common bond angles. Carbonyl rhenium carbonyl, C-Re-C, in [*fac*-Re (FOQN)$(CO)_3$](μ-Cl) [*fac*-Re(FOQN)$(CO)_3$]$CH_3C_6H_5$ ranges from 87.2(2)-89.4(2)°, while the same angle in rhenium complex 1ranges from 83.68-88.25°. In rhenium complex 1, the C-Re-C bond angles are relatively small, suggesting increase in overcrowding due to the bulky size of the ligand.

The second angle is carbonyl-rhenium-nitrogen (C-Re-N); in [*fac*-Re(FOQN)$(CO)_3$](μ-Cl)[fac-Re(FOQN)$(CO)_3$]$CH_3C_6H_5$ these angles are 94.8(2)°, 96.2(2)° and 173.1(2)°. In the case of rhenium complex 1, the same angles are 92.97(7) °, 101.61°and 169.44 (1) °.

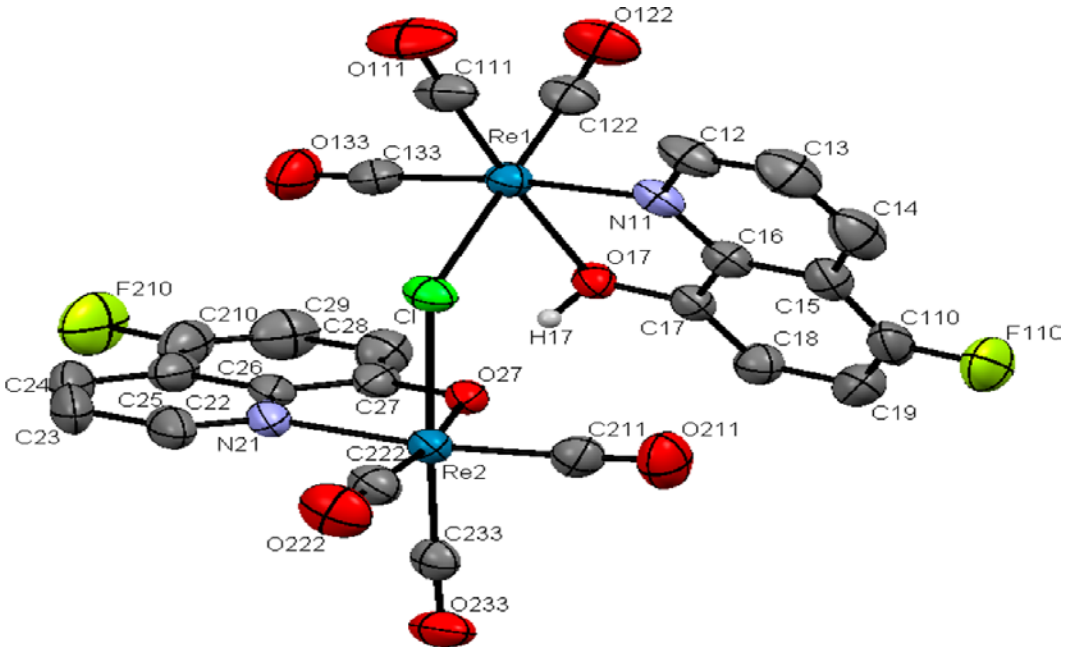


Figure 4.27. The X-ray Molecular Structure of $Re(FOQN)(CO)_3](\mu\text{-}Cl)[fac\text{-}Re(FOQN)(CO)_3]CH_3C_6H_5$

4.7.2.2 Rhenium Complex 1 versus $[fac\text{-}Re(Me_2OQN)(CO)_3]_2$

The second compound to be compared with rhenium complex 1 is $[fac\text{-}Re(Me_2OQN)(CO)_3]_2$ (as shown in Figure 4.28); the latter compound is very similar to the one discussed previously, with two exceptions. The first exception is the absence of the chloride ligand to bridge the two rhenium atoms; instead, oxygen from quinolate does the bridging. The second is the presence of the methyl group in the quinoline ring of $[fac\text{-}Re(Me2OQN)(CO)_3]_2$ instead of the fluorine atom.

There are some similarities between $[fac\text{-}Re(Me2OQN)(CO)_3]_2$ and rhenium complex 1. The first similarity is that in both compounds, rhenium atoms are bridged by an oxygen ligand. Also, the oxygen bridging results in dimers. In both cases, the coordination number around rhenium is 6; therefore, octahedral and carbonyl ligands are located in facial position.

Unlike rhenium complex 1, which crystallizes in a triclinic crystal system with a *P-1* space group, the latter compound crystallizes in a monoclinic crystal system with *P* $2_1/c$. The

rhenium-carbonyl, Re-C bond length in [*fac*-Re(Me2OQN)$(CO)_3]_2$ ranges from 1.897-1.930 Å. This is similar to that in the rhenium complex 1 [1.898, 1.911(3) and 1.913(3) Å].

The Re-O bond lengths in [*fac*-Re(Me2OQN)$(CO)_3]_2$ are 2.216(5) and 2.158(5) Å, whereas in rhenium complex 1, the Re-O bond length is 2.152(2) Å. The longer bond length in [*fac*-Re$(Me_2OQN)(CO)_3]_2$ indicates an increase in π-donating power of the 8-hydroxquinolate ions to the rhenium d orbital. In [*fac*-Re$(Me_2OQN)(CO)_3]_2$, the bond length is slightly shorter, 2.152(2) Å ,which means there is a stronger bond and little electron donation from the ligand. Studies done by Zubieta[97] and his coworkers on mononuclear rhenium complexes containing pyridine found Re-O bond length ranges from 2.113(2)-2.147(4) Å. This is slightly shorter than lengths found in the dinuclear rhenium complexes. This is expected because shorter bonds are stronger bonds; in dinuclear rhenium, the bridge formed by the oxygen ligand between the two rhenium atoms further weakens Re-O bond.

The Re-N bond lengths in [*fac*-Re$(Me_2OQN)(CO)_3]_2$ are 2.195(7) and 2.168 (6) Å, whereas in the rhenium complex 1 the Re-N bond length is 2.224(2) Å. In rhenium complex 1, the bond length is slightly longer. For mononuclear rhenium pyridine complexes, the Re-N bond length ranges from 2.136(2)-2.2249(7) Å according to work done by Zubieta and his group.

The Re-O-Re bond angles in [*fac*-Re$(Me_2OQN)(CO)_3]_2$ are 100.9(2)° and 101.1(2)°, whereas in rhenium complex 1, the Re-O-Re bond angle is 104.21(8)$^o$. The bond angle in rhenium complex 1 is larger than that in [*fac*-Re$(Me_2OQN)(CO)_3]_2$. The stacking π-interaction that exists in 8-hydroxyquinolate rings may hold a key to explaining the difference in the Re-O-Re bond angle. These interactions decrease the space between the two ligands, forcing them into a close proximity, thus minimizing the angle. In rhenium complex 1, there is no stacking interaction, and the presence of the flexible alkoxy side arm of the pyridine further widens the

space between the Re atoms and thereby increases the Re-O-Re angle.

The O-Re-O bond angles in [*fac*-Re($Me_2$OQN)($CO)_3$]$_2$ are 75.9(2)° and 76.2(2)°, whereas in rhenium complex 1 the same angle has a value of 75.79(8)°. In rhenium complex 1, the two monomers have the same bond angle, whereas in [*fac*-Re($Me_2$OQN)($CO)_3$]$_2$ the two angles are slightly different.

The O-Re-N bond angle in [*fac*-Re($Me_2$OQN)($CO)_3$]$_2$ are 75.7(2)° and 76.2(2)°, whereas in rhenium complex 1, same angle has values of 73.67(8)° and 82.53(8)°. X ray structure of dimeric [*fac*-Re($Me_2$OQN)($CO)_3$]$_2$ is given in a Figure 4.28 .

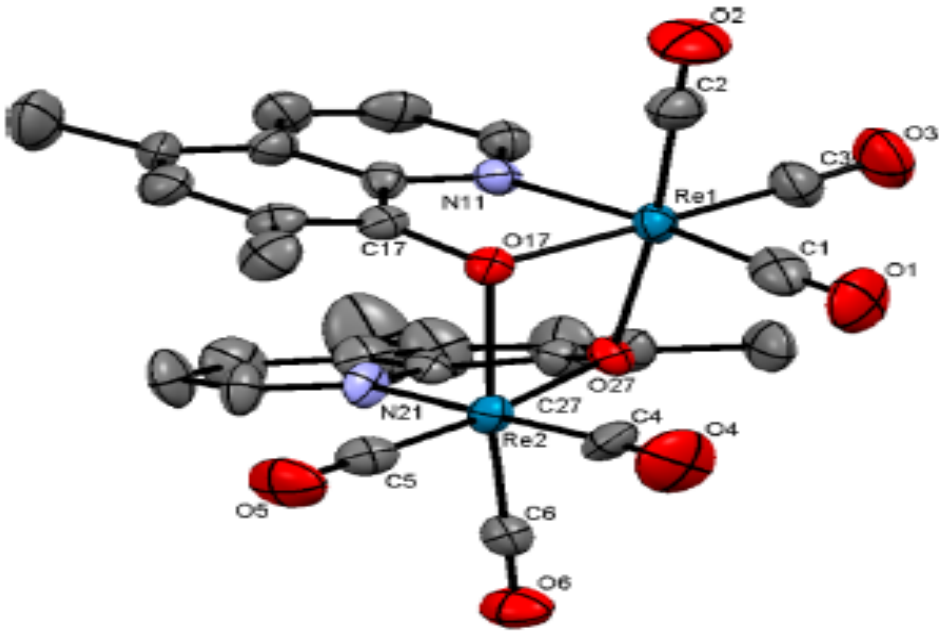


Figure 4.28. The ORTEP stereoscopic structure of dimeric [*fac*-Re($Me_2$OQN)($CO)_3$]$_2$. Rochford, J et al. *Organometallics*, **2013**, 32, 1832-1841). Reproduced with permission from ACS.

4.7.2.3 Rhenium Complex 1 versus *fac*-[ReBr($CO)_3$(pyC(H)=O)] Monomer

The monomer crystallizes in a monoclinic crystal system with a *P21/n* space group, compared to the dimer rhenium complex 1, which crystallizes in a triclinic crystal structure with a *P-1* space group. Also, the monomer has two chiral centers, one at the metal and the other at

the carbon carrying OH group. There is no Re-Re interaction in this monomer; even in the dimer such interaction was not reported.

In the monomer, the rhenium carbon bond length, Re-C, ranges from 1.899(5)-1.914(4) Å, similar to that of rhenium complex 1 [1.898(3)-1.913(3) Å]**.** In the monomer, the Re-N bond length is 2.170 Å, whereas in rhenium complex 1, the bond length is 2.224(2) Å. The monomer has a shorter bond length compared to that of rhenium complex 1.

For the C-Re-C bond angles in the monomer complex, the values range from 86.91(2)-88.3(2)°, whereas in rhenium complex 1, values range from 83.68-88.3(2)°. The C-Re-O bond angle in the monomer is 97.8(2)-171.65(1)°, whereas in rhenium complex 1 the values range from 96.81(1)-173.02(9) °.

The C-Re-N bond angles in the monomer have values ranging from 95.24(2)-172.74(1) °, whereas in rhenium complex 1 the values range from 92.97(1)-169.44(1)°. The O-Re-O bond angle in the monomer complex is 78.61(1) °, whereas in rhenium complex 1, the O-Re-O bond angle is 75.79(8) °. The O-Re-N bond angle in the monomer complex is 75.38(1)°,[98] whereas in rhenium complex 1 the values are 73.67(8)° and 82.53(8)°. The X-ray structure of the monomer complex is given in Figure 4.29.

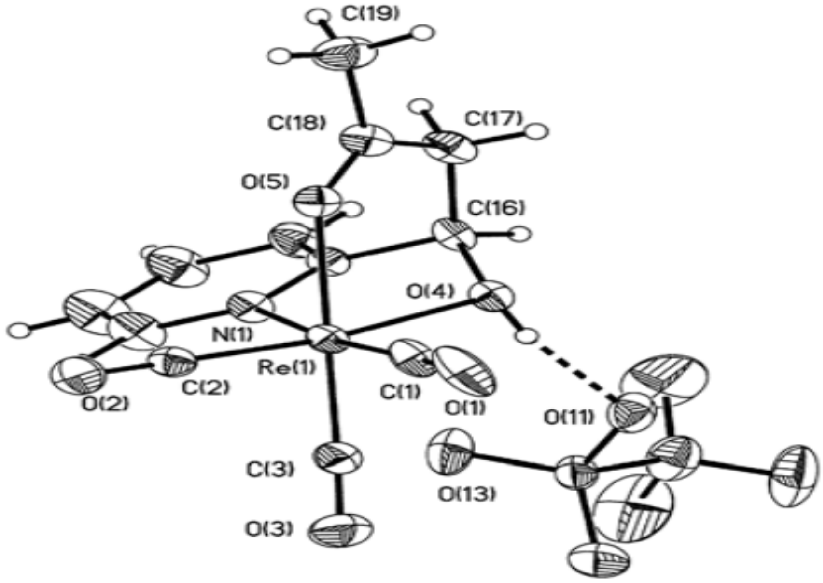


Figure 4.29: The X-ray Structure of the Monomer Complex (*fac*-[ReBr(CO)$_3$(pyC(H)=O)]). Miguel, D, et al. *Chem.Commun.* **2011,** 47, 12765-12767. Reproduced with permission from ACS.

4.7.2.4 Rhenium Complex 1 versus *fac*-[Re(CO)$_3$μ(O)κ$^2$(N,O)-(pyCH(O)CH$_2$COCH$_3$] Dimer

Both compounds are dimers and crystallize in a triclinic crystal system with a *P-1* space group. In both compounds, the two rhenium atoms are bridged by oxygen. The Re-C bond length for *fac*-[Re(CO)$_3$μ(O)κ$^2$(N,O)-(pyCH(O)CH$_2$COCH$_3$]$_2$ ranges from 1.889(7)-1.909(7) Å, similarly to that of rhenium complex 1 [1.898(3)-1.913(3) Å]. The Re-O bond lengths in fac-[Re(CO)$_3$μ(O)κ$^2$(N,O)-(pyCH(O)CH$_2$COCH$_3$]$_2$ range from 2.122(4)-2.174(4) Å. In rhenium complex 1, the Re-O bond is 2.152(2) Å. The Re-N bond lengths in *fac*-[Re(CO)$_3$μ(O)κ$^2$(N,O)-(pyCH(O)CH$_2$COCH$_3$]$_2$ are 2.193(5) Å and 2.195(5) Å, whereas in rhenium complex 1 the same bond has a value of 2.224(2) Å. The latter bond length is longer than the former one. The relationship in bond angle between the two compounds is given in Table 4.12 . *fac*-[Re(CO)$_3$μ(O)κ$^2$(N,O)-(pyCH(O)CH$_2$COCH$_3$]$_2$ is designated as complex A, whereas rhenium

complex 1 is designated as complex B. The X-ray structure of *fac*-$[Re(CO)_3\mu(O)\kappa^2(N,O)$-$(pyCH(O)CH_2COCH_3]_2$ is given in Figure 4.30 .

Table 4.11 Comparisons of Bond Angle and Length of Rhenium Complex 1 and Complex A

| Bond Angle(°) | Complex A | Rhenium Complex 1 (Complex B) |
|---|---|---|
| C-Re-C | 84.5(3), 88.4(3) | 83.7(2), 88.3(3) |
| C-Re-O | 93.7(2),174.3(3) | 96.8(1), 173.0(9) |
| O-Re-O | 73.8(2), 73.8(2) | 75.79(8) |
| C-Re-N | 91.7(3), 175.2(3) | 92.97(1), 169.44(1) |

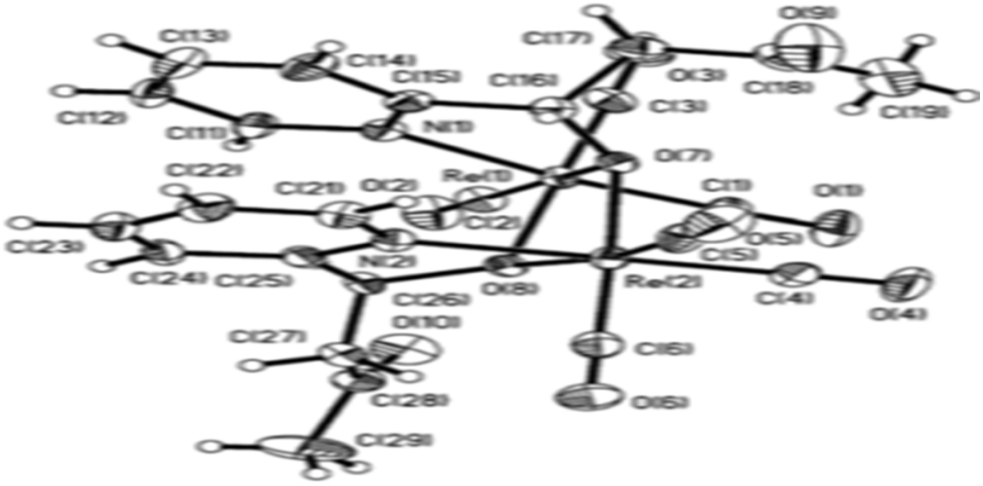


Figure 4.30: The X-ray Structure of *fac*-$[Re(CO)_3\mu(O)\kappa^2$-$(N,O)$-$(pyCH(O)CH_2COCH_3]_2$ Miguel, D, et al. *Chem.Commun.* **2011**, 47, 12765-12767. Reproduced with permission from ACS.

## 4.8 Attempted Synthesis of Rhenium Complex 2

The procedure in the attempted synthesis of rhenium complex 2 has been dealt with in Section 3.1.2. Here I report and explain the spectroscopic results from the experiment.

The crude NMR of the complex product has the following peaks which were not observed in ligand A. All the peaks observed have shifted downfield, indicating that in the complex the ligand protons are de-shielded. The first broad peak was observed and has a chemical shift of 9.272 ppm, followed by three doublet peaks, δ, 9.077 and 9.065, d, J=4.8 Hz. The second peak is δ, 8.863 and 8.830, d, J=8.0 Hz, the third peak is δ, 8.365 and 8.344, d, J=8.4 Hz ppm. There was another broad doublet peak observed, δ, 7.932 and 7.915, d, J=6.8 Hz. The last doublet peak was found to be upfield, δ, 7.100 and 7.088, d, J=4.8 Hz ppm. For the proton NMR spectra of the crude product, please refer to Figure 4.31. For the starting material ligand A, the proton NMR has the following peaks: the first four doublets resonate at 8.752, 8.144, 7.311, and 7.156 ppm. The last peak is a multiplet with a chemical shift of 7.441 ppm.

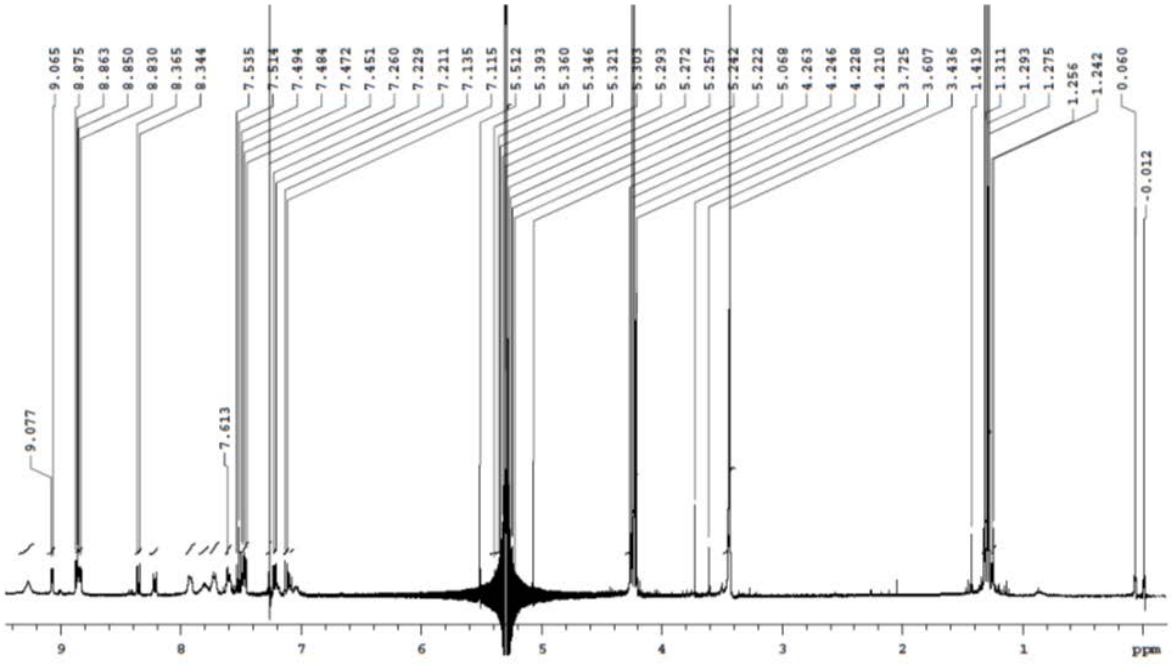


Figure 4.31. Crude $^{1}$H-NMR spectrum of Rhenium Complex 2

Purification of the crude complex was done using a silica column and DCM as a mobile phase. After purification, the NMR of the pure product showed the following peaks. The first two doublet peaks were as follows: the first doublet was δ, 9.035 and 9.025, d, J=4 Hz; and second doublet was δ, 8.332 and 8.311, d, J=8.4 Hz, this was followed by three doublet of doublet, which were δ, 7.959, 7.955, 7.947, and 7.943, dd, J=1.6, 4.8 Hz, the second peak δ, 7.779, 7.776, 7.758, and 7.755, dd, J=1.2, 8.4 Hz, and the third peak δ, 7.423,7.421,7.404, and 7.401, dd, J=0.8, 1.2,8.0 Hz. Figure 4.32 and 4.33 provide the details of each proton NMR spectrum.

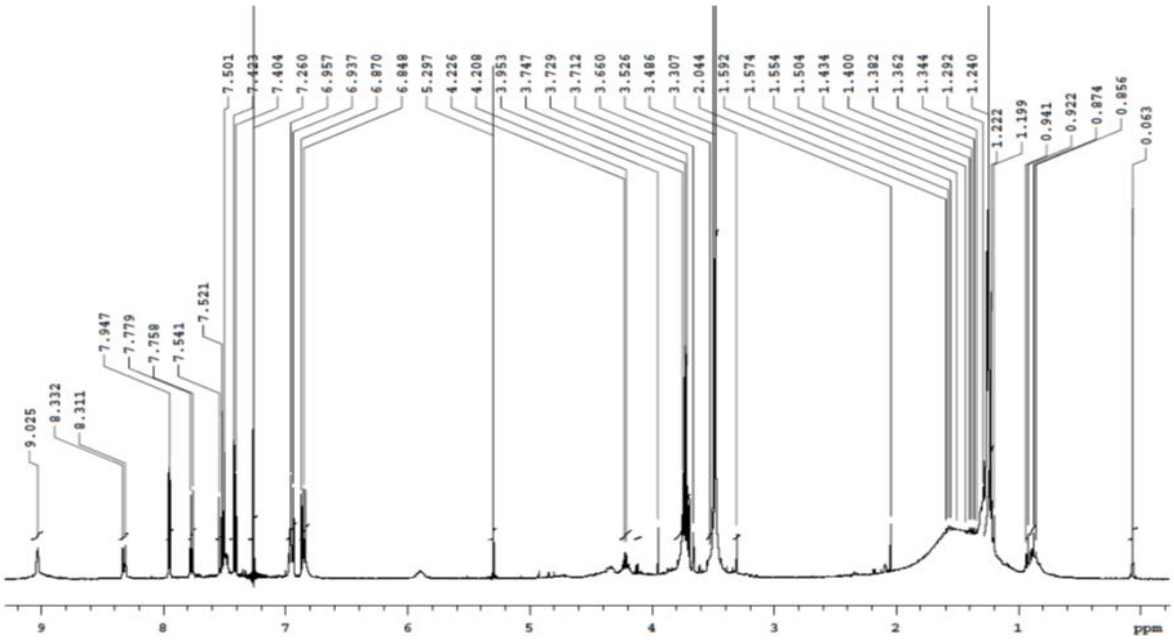


Figure 4.32. $^{1}$H-NMR spectrum of chromatographed rhenium complex 2

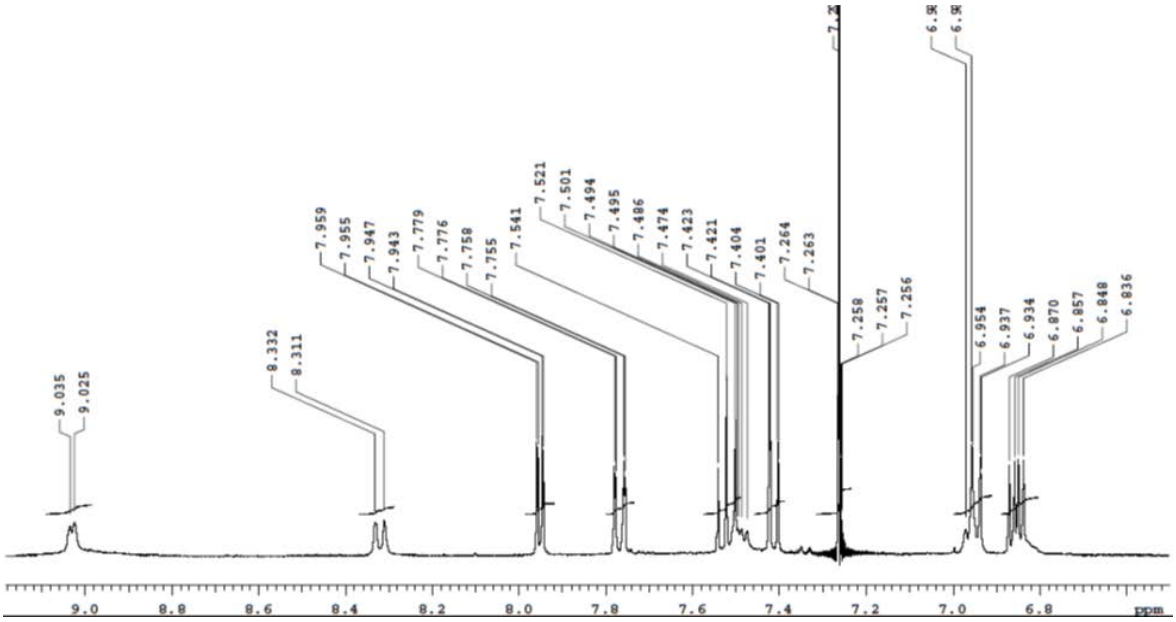


Figure 4.33. $^{1}$H-NMR spectrum of chromatographed Rhenium Complex 2

### 4.7.3 Infra-Red Spectrum of Rhenium Complex 2

Infrared data also supported the fact that there was a reaction between ligand A and $ReBr(CO)_5$. The CO vibrational peaks of $ReBr(CO)_5$ before the reaction were at 2048cm$^{-1}$ and 1980 cm$^{-1}$ as shown in Figure 4.25 , as well as in Figure 4.34 (indicated by the lower red line). After the reaction (from Figure 4.34 ), there were major changes in peaks of the metal carbonyl complex as indicated by the upper blue line. New carbonyl peaks were observed at 1900 cm$^{-1}$ and 2025 cm$^{-1}$, and a small sharp peak was observed at 2300 cm$^{-1}$

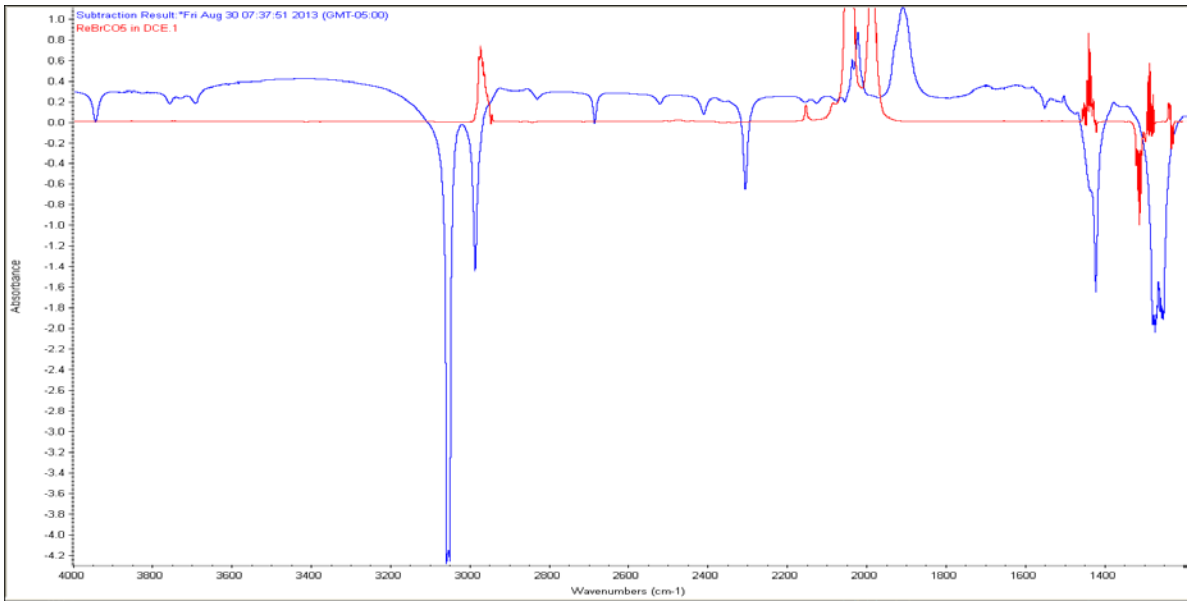


Figure 4.34. The IR Spectrum of Rhenium Complex 2 from Ligand A

# CHAPTER 5

# CONCLUSION

As a study of the synthesis and characterization of transition metal complexes, the first part of this thesis discussed the synthesis of gold (I) complexes from the diphosphine ligands BPCD and BPPM. Both ligands were prepared and characterized by NMR and X-ray crystallography. The second part of the research was to analyze the already prepared heterocyclic acac ligands A, B, and C. All three ligands were successfully prepared and characterized using NMR and X-ray crystallography. The reactions between these heterocyclic ligands and transition metal compounds to produce complexes were investigated using X-ray crystallography, NMR, and IR. One of the complexes characterized by X-ray crystallography revealed no acac side arm involvement in coordination with the metal center. Instead, the heterocyclic pyridine ring was involved in coordination with the metals. Structural comparisons between these newly synthesized four X-ray structures and already published X-ray structures was done. The results showed there were some similarities in bond lengths and angles between the new and old structures.

Further studies are required, particularly with regard to the growth of crystal complexes, to fully determine the bonding between the ACAC ligands and the metal center. NMR and IR alone are not enough to fully determine the structures of these types of complexes.

# APPENDIX A

## X-RAY DATA FOR [$Au_2Cl_2$(bpcd)]

| ATOMS | BOND LENGTH (Å) AND ANGLE ( ° ) | ATOMS | BOND LENGTH(Å) AND ANGLE(° ) |
|---|---|---|---|
| **Au(1)-P(1)** | 2.231(2) | C(3)-H(3A) | 0.99 |
| **Au(1)-Cl(1)** | 2.289(2) | C(3)-H(3B) | 0.99 |
| **Au(1)-Au(2)** | 2.916(4) | C(4)-C(5) | 1.515(8) |
| **P(1)-C(1)** | 1.812(6) | C(7)-H(7A) | 0.95 |
| **P(1)-C(6)** | 1.815(6) | C(8)-C(9) | 1.389(9) |
| **P(2)-C(24)** | 1.799(6) | C(8)-H(8A) | 0.95 |
| **P(2)-C(18)** | 1.819(6) | C(9)-C(10) | 1.389(9) |
| **P(2)-C(5)** | 1.823(6) | C(9)-H(9A) | 0.95 |
| **O(1)-C(2)** | 1.214(8) | C(10)-C(11) | 1.405(9) |
| **O(2)-C(4)** | 1.205(8) | C(10)-H(10A) | 0.95 |
| **C(1)-C(5)** | 1.370(8) | C(11)-H(11A) | 0.95 |
| **C(1)-C(2)** | 1.515(8) | C(12)-C(13) | 1.394(9) |
| **C(2)-C(3)** | 1.483(9) | C(12)-C(17) | 1.397(9) |
| **C(3)-C(4)** | 1.522(8) | C(13)-C(14) | 1.41(1) |
| **C(13)-H(13A)** | 0.95 | C(22)-H(22A) | 0.95 |
| **C(14)-C(15)** | 1.37(1) | C(23)-H(23A) | 0.95 |
| **C(14)-H(14A)** | 0.95 | C(24)-C(29) | 1.393(9) |
| **C(15)-C(16)** | 1.39(1) | C(24)-C(25) | 1.406(9) |
| **C(15)-H(15A)** | 0.95 | C(25)-C(26) | 1.401(9) |
| **C(16)-C(17)** | 1.404(9) | C(25)-H(25A) | 0.95 |
| **C(16)-H(16A)** | 0.95 | C(26)-C(27) | 1.36(1) |
| **C(17)-H(17A)** | 0.95 | C(26)-H(26A) | 0.95 |
| **C(18)-C(23)** | 1.385(9) | C(27)-C(28) | 1.40(1) |
| **C(18)-C(19)** | 1.400(9) | C(27)-H(27A) | 0.95 |
| **C(19)-C(20)** | 1.381(9) | C(28)-C(29) | 1.396(9) |
| **C(19)-H(19A)** | 0.95 | C(28)-H(28A) | 0.95 |
| **C(20)-C(21)** | 1.39(1) | C(29)-H(29A) | 0.95 |
| **C(20)-H(20A)** | 0.95 | Cl(3)-C(1S) | 1.767(8) |
| **C(21)-C(22)** | 1.38(1) | Cl(4)-C(1S) | 1.747(8) |
| **C(21)-H(21A)** | 0.95 | C(1S)-H(1SA) | 0.99 |
| **C(22)-C(23)** | 1.400(9) | C(1S)-H(1SB) | 0.99 |
| **P(1)-Au(1)-Cl(1)** | 173.72(6) | C(5)-C(1)-C(2) | 108.9(5) |
| **P(1)-Au(1)-Au(2)** | 83.37(4) | C(5)-C(1)-P(1) | 125.3(5) |
| **Cl(1)-Au(1)-Au(2)** | 101.55(4) | C(2)-C(1)-P(1) | 125.6(4) |
| **P(2)-Au(2)-Cl(2)** | 172.69(6) | O(1)-C(2)-C(3) | 126.3(6) |
| **P(2)-Au(2)-Au(1)** | 100.46(4) | O(1)-C(2)-C(1) | 124.4(6) |
| **Cl(2)-Au(2)-Au(1)** | 86.85(4) | C(3)-C(2)-C(1) | 109.2(5) |
| **C(12)-P(1)-C(1)** | 110.6(3) | C(2)-C(3)-C(4) | 103.7(5) |

| | | | |
|---|---|---|---|
| **C(12)-P(1)-C(6)** | 103.3(3) | C(2)-C(3)-H(3A) | 111 |
| **C(1)-P(1)-C(6)** | 102.6(3) | C(4)-C(3)-H(3A) | 111 |
| **C(12)-P(1)-Au(1)** | 112.1(2) | C(2)-C(3)-H(3B) | 111 |
| **C(1)-P(1)-Au(1)** | 106.7(2) | C(4)-C(3)-H(3B) | 111 |
| **C(6)-P(1)-Au(1)** | 121.1(2) | H(3A)-C(3)-H(3B) | 109 |
| **C(24)-P(2)-C(18)** | 107.6(3) | O(2)-C(4)-C(5) | 125.2(6) |
| **C(24)-P(2)-C(5)** | 107.7(3) | O(2)-C(4)-C(3) | 127.2(6) |
| **C(18)-P(2)-C(5)** | 103.2(3) | C(5)-C(4)-C(3) | 107.5(5) |
| **C(24)-P(2)-Au(2)** | 110.8(2) | C(1)-C(5)-C(4) | 109.1(5) |
| **C(18)-P(2)-Au(2)** | 109.7(2) | C(1)-C(5)-P(2) | 129.7(4) |
| **C(5)-P(2)-Au(2)** | 117.2(2) | C(4)-C(5)-P(2) | 121.0(4) |
| **C(23)-C(18)-P(2)** | 120.6(5) | C(26)-C(25)-C(24) | 119.0(6) |
| **C(19)-C(18)-P(2)** | 118.8(5) | C(26)-C(25)-H(25A) | 120.5 |
| **C(20)-C(19)-C(18)** | 119.7(6) | C(24)-C(25)-H(25A) | 120.5 |
| **C(20)-C(19)-H(19A)** | 120.2 | C(27)-C(26)-C(25) | 121.5(6) |
| **C(18)-C(19)-H(19A)** | 120.2 | C(27)-C(26)-H(26A) | 119.3 |
| **C(19)-C(20)-C(21)** | 120.6(6) | C(25)-C(26)-H(26A) | 119.3 |
| **C(19)-C(20)-H(20A)** | 119.7 | C(26)-C(27)-C(28) | 119.8(6) |
| **C(21)-C(20)-H(20A)** | 119.7 | C(26)-C(27)-H(27A) | 120.1 |
| **C(22)-C(21)-C(20)** | 119.4(6) | C(28)-C(27)-H(27A) | 120.1 |
| **C(22)-C(21)-H(21A)** | 120.3 | C(29)-C(28)-C(27) | 119.6(6) |
| **C(20)-C(21)-H(21A)** | 120.3 | C(29)-C(28)-H(28A) | 120.2 |
| **C(21)-C(22)-C(23)** | 121.0(6) | C(27)-C(28)-H(28A) | 120.2 |
| **C(21)-C(22)-H(22A)** | 119.5 | C(24)-C(29)-C(28) | 120.5(6) |
| **C(23)-C(22)-H(22A)** | 119.5 | C(24)-C(29)-H(29A) | 119.8 |
| **C(18)-C(23)-C(22)** | 118.9(6) | C(28)-C(29)-H(29A) | 119.8 |
| **C(18)-C(23)-H(23A)** | 120.6 | Cl(4)-C(1S)-Cl(3) | 112.4(4) |
| **C(22)-C(23)-H(23A)** | 120.6 | Cl(4)-C(1S)-H(1SA) | 109.1 |
| **C(29)-C(24)-C(25)** | 119.5(6) | Cl(3)-C(1S)-H(1SA) | 109.1 |
| **C(29)-C(24)-P(2)** | 117.3(5) | Cl(4)-C(1S)-H(1SB) | 109.1 |
| **C(25)-C(24)-P(2)** | 123.0(5) | Cl(3)-C(1S)-H(1SB) | 109.1 |
| | | H(1SA)-C(1S)-(1SB) | 107.9 |

# APPENDIX B

## X-RAY DATA FOR [$Au_2Cl_2$(bppm)]

| | | | |
|---|---|---|---|
| **Au(1)-P(1)** | 2.23(2) | C(2)-C(3) | 1.33(9) |
| **Au(1)-Cl(1)** | 2.293(2) | C(3)-C(4) | 1.514(9) |
| **Au(1)-Au(2)** | 2.298(5) | C(5)-C(6) | 1.39(1) |
| **Au(2)-P(2)** | 2.233(2) | C(5)-C(10) | 1.39(1) |
| **Au(2)-Cl(2)** | 2.289(2) | C(6)-C(7) | 1.36(1) |
| **Au(2)-Au(3)** | 2.96(4) | C(6)-H(6A) | 0.95 |
| **P(1)-C(7A)** | 1.805(7) | C(7)-C(8) | 1.40(1) |
| **P(1)-C(13A)** | 1.812(7) | C(7)-H(7A) | 0.95 |
| **P(1)-C(2A)** | 1.828(7) | C(8)-C(9) | 1.39(1) |
| **C(1A)-O(3)** | 1.194(8) | C(8)-H(8A) | 0.95 |
| **C(1A)-N(2)** | 1.396(8) | C(9)-C(10) | 1.39(1) |
| **C(1A)-C(2A)** | 1.525(8) | C(9)-H(9A) | 0.95 |
| **N(2)-C(1A)** | 1.1397(8) | C(10)-H(10A) | 0.95 |
| **N(2)-C(3A)** | 1.432(1) | C(11)-C(12) | 1.39(1) |
| **C(2A)-C(2A)** | 1 1.336(1) | C(11)-C(16) | 1.42(1) |
| **C(3A)-C(4A)** | 1.383(8) | C(12)-C(13) | 1.38(1) |
| **C(3A)-C(4A)** | 1 1.384(8) | C(12)-H(12A) | 0.95 |
| **C(4A)-C(5A)** | 1.397(9) | C(13)-C(14) | 1.42(1) |
| **C(4A)-H(4AA)** | 0.95 | C(13)-H(13A) | 0.95 |
| **C(5A)-C(6A)** | 1.386(8) | C(14)-C(15) | 1.38(1) |
| **C(5A)-H(5AA)** | 0.95 | C(14)-H(14A) | 0.95 |
| **C(6A)-C(5A)** | 1.19(8) | C(15)-C(16) | 1.38(1) |
| **C(6A)-H(6AA)** | 0.95 | C(15)-H(15A) | 0.95 |
| **C(7A)-C(12A)** | 1.39(1) | C(16)-H(16A) | 0.95 |
| **C(7A)-C(8A)** | 1.411(9) | C(17)-C(18) | 1.39(1) |
| **C(8A)-C(9A)** | 1.40(1) | C(17)-C(22) | 1.396(9) |
| **C(8A)-H(8AA)** | 0.95 | C(18)-C(19) | 1.41(1) |
| **C(9A)-C(10A)** | 1.40(1) | C(18)-H(18A) | 0.95 |
| **C(9A)-H(9AA)** | 0.95 | C(19)-C(20) | 1.37(1) |
| **C(10A)-C(11A)** | 1.39(1) | C(19)-H(19A) | 0.95 |
| **C(10A)-H(10B)** | 0.95 | C(20)-C(21) | 1.38(1) |
| **C(11A)-C(12A)** | 1.39 (1) | C(20)-H(20A) | 0.95 |
| **C(11A)-H(11A)** | 0.95 | C(21)-C(22) | 1.38(1) |
| **C(12A)-H(12B)** | 0.95 | C(21)-H(21A) | 0.95 |
| **C(13A)-C(14A)** | 1.37(1) | C(22)-H(22A) | 0.95 |
| **C(13A)-C(18A)** | 1.41(1) | C(23)-C(28) | 1.39(1) |
| **C(14A)-C(15A)** | 1.42(1) | C(23)-C(24) | 1.399(9) |
| **C(14A)-H(14B)** | 0.95 | C(24)-C(25) | 1.38(1) |
| **C(15A)-C(16A)** | 1.37(1) | C(24)-H(24A) | 0.95 |
| **C(15A)-H(15B)** | 0.95 | C(25)-C(26) | 1.39 (1) |

| | | | |
|---|---|---|---|
| **C(16A)-C(17A)** | 1.36(1) | C(25)-H(25A) | 0.95 |
| **C(16A)-H(16B)** | 0.95 | C(26)-C(27) | 1.39(1) |
| **C(17A)-C(18A)** | 1.40(1) | C(26)-H(26A) | 0.95 |
| **C(17A)-H(17A)** | 0.95 | C(27)-C(28) | 1.39(1) |
| **C(18A)-H(18B)** | 0.95 | C(27)-H(27A) | 0.95 |
| **Au(3)-P(3)** | 2.231(2) | C(28)-H(28A) | 0.95 |
| **Au(3)-Cl(3)** | 2.286(2) | C(29)-C(30) | 1.38(1) |
| **P(2)-C(11)** | 1.800(7) | C(29)-C(34) | 1.39(1) |
| **P(2)-C(2)** | 1.822(7) | C(30)-C(31) | 1.38(1) |
| **P(2)-C(17)** | 1.824(7) | C(30)-H(30A) | 0.95 |
| **P(3)-C(23)** | 1.811(7) | C(31)-C(32) | 1.38(1) |
| **P(3)-C(29)** | 1.823(6) | C(31)-H(31A) | 0.95 |
| **P(3)-C(3)** | 1.830(6) | C(32)-C(33) | 1.39(2) |
| **O(1)-C(1)** | 1.191(8) | C(32)-H(32A) | 0.95 |
| **O(2)-C(4)** | 1.208(8) | C(33)-C(34) | 0.95 |
| **N(1)-C(4)** | 1.389(8) | C(33)-H(33A) | 0.95 |
| **N(1)-C(1)** | 1.394(8) | C(34)-H(34A) | 0.95 |
| **N(1)-C(5)** | 1.435(8) | Cl(1A)-C(1S) | 1.77(1) |
| **C(1)-C(2)** | 1.529(9) | Cl(2A)-C(1S) | 1.72(1) |
| **C(4A)-C(3A)-N(2)** | 85.98(4) | C(3A)-C(4A)-C(5A) | 99.66(4) |
| **C(3A)-C(4A)-H(4AA)** | 172.76(6) | C(5A)-C(4A)-(4AA) | 85.63(4) |
| **C(6A)-C(5A)-C(4A)** | 101.59(5) | C(6A)-C(5A)-(5AA) | 104.4(3) |
| **C(4A)-C(5A)-H(5AA)** | 104.4(3) | C(5A)-C(6A)-C(5A | 106.2(3) |
| **C(5A)-C(6A)-H(6AA)** | 116.9(2) | C(5A)-C(6A)-(6AA) | 110.2(2) |
| **C(12A)-C(7A)-C(8A)** | 113.2(2) | C(12A)-C(7A)-P(1) | 125.8(6) |
| **C(8A)-C(7A)-P(1)** | 127.7(6) | C(9A)-C(8A)-C(7A) | 106.4(6) |
| **C(9A)-C(8A)-H(8AA)** | 110.5(7) | C(7A)-C(8A)-(8AA) | 124.7(4) |
| **C(10A)-C(9A)-C(8A)** | 124.7(4) | C(10A)-C(9A)-9AA) | 108.3(4) |
| **C(8A)-C(9A)-H(9AA)** | 130.2(2) | C(11A)-C(10A)-(9A) | 121.4(5) |
| **C(11A)-C(10A)-(10B)** | 122.1(9) | C(13A)-C(18A)-18B) | 119.5 |
| **P(2)-Au(2)-Cl(2)** | 119.1(7) | P(2)-Au(1)-Au(2) | 120.5 |
| **Cl(2)-Au(1)-Au(2)** | 120.5 | C(11)-P(2)-C(2) | 120.6(7) |
| **C(11)-P(2)-C(17)** | 119.7 | C(2)-P(2)-C(17) | 119.7 |
| **C(11)-P(2)-Au(2)** | 119.5(7) | C(2)-P(2)-Au(2) | 122.5(5) |
| **C(17)-P(2)-Au(2** | 117.9(6) | C(23)-P(3)-C(29) | 120.8(7) |
| **C(23)-P(3)-C(3)** | 119.6 | C(29)-P(3)-C(3) | 119.6 |
| **C(23)-P(3)-Au(3)** | 119.2(8) | C(29)-P(3)-Au(3) | 120.4 |
| **C(3)-P(3)-Au(3)** | 120.4 | C(4)-N(1)-C(1) | 120.6(8) |
| **C(4)-N(1)-C(5)** | 119.7 | C(1)-N(1)-C(5) | 119.7 |
| **O(1)-C(1)-N(1)** | 121.1(8) | O(1)-C(1)-C(2) | 119.5 |
| **N(1)-C(1)-C(2)** | 119.5 | C(3)-C(2)-C(1) | 118.9(8) |

| | | | |
|---|---|---|---|
| **C(3)-C(2)-P(2)** | 120.6 | C(9)-C(10)-H(10A) | 119.1(5) |
| **C(5)-C(10)-H(10A)** | 107.8(5) | C(12)-C(11)-P(2 | 123.1(5) |
| **C(12)-C(11)-C(16)** | 128.9(5) | C(16)-C(11)-P(2) | 126.0(6) |
| **C(13)-C(12)-C(11)** | 126.8(6) | C(13)-C(12)-H(12A) | 107.2(5) |
| **C(11)-C(12)-H(12A)** | 120.6(6) | C(12)-C(13)-C(14) | 119.6(6) |
| **C(12)-C(13)-H(13A)** | 119.8(6) | C(14)-C(13)-H(13A) | 119.6(7) |
| **C(15)-C(14)-C(13)** | 120.2 | C(15)-C(14)-H(14A) | 120.2 |
| **C(13)-C(14)-H(14A)** | 121.3(7) | C(14)-C(15)-C(16) | 119.4 |
| **C(14)-C(15)-H(15A)** | 119.4 | C(16)-C(15)-H(15A) | 118.9(7) |
| **C(15)-C(16)-C(11)** | 120.5 | C(15)-C(16)-H(16A) | 120.5 |
| **C(11)-C(16)-H(16A)** | 120.5(7) | C(18)-C(17)-C(22) | 119.8 |
| **C(18)-C(17)-P(2)** | 119.8 | C(22)-C(17)-P(2) | 119.1(7) |
| **C(21)-C(22)-H(22A)** | 119.9(7) | C(17)-C(22)-H(22A) | 120.1 |
| **C(28)-C(23)-C(24)** | 120.1 | C(28)-C(23)-P(3) | 118.9(8) |
| **C(24)-C(23)-P(3)** | 120.6 | C(25)-C(24)-C(23) | 120.6 |
| **C(25)-C(24)-H(24A)** | 121.3(8) | C(23)-C(24)-H(24A) | 119.4 |
| **C(24)-C(25)-C(26)** | 119.4 | C(24)-C(25)-H(25A) | 120.6(7) |
| **C(26)-C(25)-H(25A)** | 119.7 | C(27)-C(26)-C(25 | 119.7 |
| **C(27)-C(26)-H(26A)** | 119.1(7) | C(25)-C(26)-H(26A) | 119.7 |

# APPENDIX C

## X-RAY DATA FOR LIGAND A [$C_{14}H_{13}NO_4$]

| | | | |
|---|---|---|---|
| **O(1A)-C(10A)** | 1.353(1) | O(1)-C(10) | 1.354(1) |
| **O(1A)-C(8A)** | 1.407(1) | O(1)-C(8) | 1.404(1) |
| **N(1A)-C(1A)** | 1.319(1) | N(1)-C(1) | 1.40(1) |
| **N(1A)-C(9A)** | 1.366(1) | N(1)-C(9) | 1.366(1) |
| **C(1A)-C(2A)** | 1.415(1) | C(1)-C(2) | 1.414(1) |
| **C(1A)-H(1AA)** | 0.95 | C(1)-H(1A) | 0.95 |
| **O(2A)-C(10A)** | 1.202(1) | O(2)-C(10) | 1.202(1) |
| **C(2A)-C(3A)** | 1.366(1) | C(2)-C(3) | 1.367(1) |
| **C(2A)-H(2AA)** | 0.95 | C(2)-H(2A) | 0.95 |
| **O(3A)-C(12A)** | 1.203(1) | O(3)-C(12) | 1.205(1) |
| **C(3A)-C(4A)** | 1.415(1) | C(3)-C(4) | 1.417(1) |
| **C(3A)-H(3AA)** | 0.95 | C(3)-H(3A) | 0.95 |
| **O(4A)-C(12A)** | 1.332(1) | O(4)-C(12) | 1.333(1) |
| **O(4A)-C(13A)** | 1.4642(1) | O(4)-C(13) | 1.460(1) |
| **C(4A)-C(5A)** | 1.417(1) | C(4)-C(5) | 1.418(1) |
| **C(4A)-C(9A)** | 1.421(1) | C(4)-C(9) | 1.421(1) |
| **C(5A)-C(6A)** | 1.368(1) | C(5)-C(6) | 1.368(1) |
| **C(5A)-H(5AA)** | 0.95 | C(5)-H(5A) | 0.95 |
| **C(6A)-C(7A)** | 1.413(1) | C(6)-C(7) | 1.412(1) |
| **C(6A)-H(6AA)** | 0.95 | C(6)-H(6A) | 0.95 |
| **C(7A)-C(8A)** | 1.363(1) | C(7)-C(8) | 1.362(1) |
| **C(7A)-H(7AA)** | 0.95 | C(7)-H(7A) | 0.95 |
| **C(8A)-C(9A)** | 1.416(1) | C(8)-C(9) | 1.417(1) |
| **C(10A)-C(11A)** | 1.507(1) | C(10)-C(11) | 1.508(1) |
| **C(11A)-C(12A)** | 1.518(1) | C(11)-C(12) | 1.519(1) |
| **C(11A)-H(11A)** | 0.99 | C(11)-H(11C) | 0.99 |
| **C(11A)-H(11B)** | 0.99 | C(11)-H(11D) | 0.99 |
| **C(13A)-C(14A)** | 1.505(1) | C(13)-C(14) | 1.505(1) |
| **C(13A)-H(13A)** | 0.99 | C(13)-H(13C) | 0.99 |
| **C(13A)-H(13B)** | 0.99 | C(13)-H(13D) | 0.99 |
| **C(14A)-H(14A)** | 0.98 | C(14)-H(14D) | 0.98 |
| **C(14A)-H(14B)** | 0.98 | C(14)-H(14E) | 0.98 |
| **C(14A)-H(14C)** | 0.98 | C(14)-H(14F) | 0.98 |
| **C(1A)-N(1A)-C(9A)** | 116.75(8) | C(1)-N(1)-C(9) | 116.9(8) |
| **N(1A)-C(1A)-C(2A)** | 124.55(9) | N(1)-C(1)-C(2) | 124.6(9) |
| **N(1A)-C(1A)-H(1AA)** | 117.7 | N(1)-C(1)-H(1A) | 117.7 |
| **C(2A)-C(1A)-H(1AA)** | 117.7 | C(2)-C(1)-H(1A) | 117.7 |
| **C(3A)-C(2A)-C(1A)** | 118.75(9) | C(3)-C(2)-C(1) | 118.58(9) |
| **C(3A)-C(2A)-H(2AA)** | 120.6 | C(3)-C(2)-H(2A) | 120.7 |
| **C(1A)-C(2A)-H(2AA)** | 120.6 | C(1)-C(2)-H(2A) | 120.7 |
| **C(2A)-C(3A)-C(4A)** | 119.36(9) | C(2)-C(3)-C(4) | 119.49(9) |
| **C(2A)-C(3A)-H(3AA)** | 120.3 | C(2)-C(3)-H(3A) | 120.3 |
| **C(4A)-C(3A)-H(3AA)** | 120.3 | C(4)-C(3)-H(3A) | 120.3 |
| **C(12A)-O(4A)-(13A)** | 115.63(7) | C(12)-O(4)-C(13) | 116.19(7) |
| **C(3A)-C(4A)-C(5A)** | 122.84(9) | C(3)-C(4)-C(5) | 123.06(9) |
| **C(3A)-C(4A)-C(9A)** | 117.27(8) | C(3)-C(4)-C(9) | 117.24(9) |

| | | | |
|---|---|---|---|
| **C(5A)-C(4A)-C(9A)** | 119.89(9) | C(5)-C(4)-C(9) | 119.70(9) |
| **C(6A)-C(5A)-C(4A)** | 120.51(9) | C(6)-C(5)-C(4) | 120.65(9) |
| **C(6A)-C(5A)-H(5AA)** | 119.7 | C(6)-C(5)-H(5A) | 119.7 |
| **C(4A)-C(5A)-H(5AA)** | 119.7 | C(4)-C(5)-H(5A) | 119.7 |
| **C(5A)-C(6A)-C(7A)** | 120.29(9) | C(5)-C(6)-C(7) | 120.2(9) |
| **C(5A)-C(6A)-H(6AA)** | 119.9 | C(5)-C(6)-H(6A) | 119.9 |
| **C(7A)-C(6A)-H(6AA)** | 119.9 | C(7)-C(6)-H(6A) | 119.9 |
| **C(8A)-C(7A)-C(6A)** | 119.62(9) | C(8)-C(7)-C(6) | 119.73(9) |
| **C(8A)-C(7A)-H(7AA)** | 120.2 | C(8)-C(7)-H(7A) | 120.1 |
| **C(6A)-C(7A)-H(7AA)** | 120.2 | C(6)-C(7)-H(7A) | 120.1 |
| **C(7A)-C(8A)-O(1A)** | 118.63(8) | C(7)-C(8)-O(1) | 118.57(8) |
| **C(7A)-C(8A)-C(9A)** | 122.43(9) | C(7)-C(8)-C(9) | 122.33(9) |
| **O(1A)-C(8A)-C(9A)** | 118.86(8) | O(1)-C(8)-C(9) | 118.99(8) |
| **N(1A)-C(9A)-C(8A)** | 119.43(8) | N(1)-C(9)-C(8) | 119.40(8) |
| **N(1A)-C(9A)-C(4A)** | 123.31(8) | N(1)-C(9)-C(4) | 123.20(9) |
| **C(8A)-C(9A)-C(4A)** | 117.26(8) | C(8)-C(9)-C(4) | 117.40(8) |
| **O(2A)-C(10A)-O(1A)** | 123.98(8) | O(2)-C(10)-O(1) | 123.96(9) |
| **O(2A)-C(10A)-(11A)** | 125.43(9) | O(2)-C(10)-C(11) | 125.70(9) |
| **O(1A)-C(10A)-(11A)** | 110.58(8) | O(1)-C(10)-C(11) | 110.33(8) |
| **C(10A)-C(11A)-(12A)** | 114.01(8) | C(10)-C(11)-C(12) | 113.30(8) |
| **C(10A)-C(11A)-(11A)** | 108.8 | C(10)-C(11)-H(11C) | 108.9 |
| **C(12A)-C(11A)-(11A)** | 108.8 | C(12)-C(11)-H(11C) | 108.9 |
| **C(10A)-C(11A)-(11B)** | 108.8 | C(10)-C(11)-H(11D) | 108.9 |
| **C(12A)-C(11A)-(11B)** | 108.8 | C(12)-C(11)-H(11D) | 108.9 |
| **H(11A)-C(11A)-(11B)** | 107.6 | H(11C)-C(11)-H(11D) | 107.7 |
| **O(3A)-C(12A)-O(4A)** | 124.68(9) | O(3)-C(12)-O(4) | 124.71(9) |
| **O(3A)-C(12A)-(11A)** | 122.29(9) | O(3)-C(12)-C(11) | 122.63(9) |
| **O(4A)-C(12A)-(11A)** | 113.02(8) | O(4)-C(12)-C(11) | 112.65(8) |
| **O(4A)-C(13A)-(14A)** | 107.00(8) | O(4)-C(13)-C(14) | 107.39(8) |
| **O(4A)-C(13A)-(13A)** | 110.3 | O(4)-C(13)-H(13C) | 110.2 |
| **C(14A)-C(13A)-(13A)** | 110.3 | C(14)-C(13)-H(13C) | 110.2 |
| **O(4A)-C(13A)-(13B)** | 110.3 | O(4)-C(13)-H(13D) | 110.2 |
| **C(14A)-C(13A)-(13B)** | 110.3 | C(14)-C(13)-H(13D) | 110.2 |
| **H(13A)-C(13A)-(13B)** | 108.6 | H(13C)-C(13)-H(13D) | 108.5 |
| **C(13A)-C(14A)-(14A)** | 109.5 | C(13)-C(14)-H(14D) | 109.5 |
| **C(13A)-C(14A)-(14B)** | 109.5 | C(13)-C(14)-H(14E) | 109.5 |
| **H(14A)-C(14A)-(14B)** | 109.5 | H(14D)-C(14)-H(14E) | 109.5 |
| **C(13A)-C(14A)-(14C)** | 109.5 | C(13)-C(14)-H(14F) | 109.5 |
| **H(14A)-C(14A)-(14C)** | 109.5 | H(14D)-C(14)-H(14F) | 109.5 |
| **H(14B)-C(14A)-(14C)** | 109.5 | H(14E)-C(14)-H(14F) | 109.5 |

# APPENDIX D

## X-RAY DATA FOR RHENIUM COMPLEX 1 [$C_{30}H_{28}N_2O_{16}Re_2$]

| **Re(1)-C(8)** | **1.898(3)** | **O(5)-C(11)** | **1.339(4)** |
|---|---|---|---|
| **Re(1)-C(9)** | 1.911(3) | O(5)-C(10) | 1.447(3) |
| **Re(1)-C(7)** | 1.913(3) | C(5)-C(10) | 1.509(4) |
| **Re(1)-O(1)** | 2.136(2) | O(6)-C(11) | 1.188(4) |
| **Re(1)-O(1)** | 2.152(2) | C(6)-H(6A) | 0.99 |
| **Re(1)-N(1)** | 2.224(2) | C(6)-H(6B) | 0.99 |
| **O(1)-C(6)** | 1.424(3) | O(7)-C(13) | 1.160(4) |
| **O(1)-Re(1)** | 2.152(2) | O(8)-C(13) | 1.342(4) |
| **N(1)-C(1)** | 1.352(4) | O(8)-C(14) | 1.457(4) |
| **N(1)-C(5)** | 1.357(4) | C(10)-H(10A) | 0.99 |
| **C(1)-C(2)** | 1.384(4) | C(10)-H(10B) | 0.99 |
| **C(1)-C(6)** | 1.502(4) | C(11)-C(12) | 1.509(4) |
| **O(2)-C(7)** | 1.150(4) | C(12)-C(13) | 1.524(4) |
| **C(2)-C(3)** | 1.377(4) | C(12)-H(12A) | 0.99 |
| **C(2)-H(2A)** | 0.95 | C(12)-H(12B) | 0.99 |
| **O(3)-C(8)** | 1.157(4) | C(14)-C(15) | 1.522(5) |
| **C(3)-C(4)** | 1.385(5) | C(14)-H(14A) | 0.99 |
| **C(3)-H(3A)** | 0.95 | C(14)-H(14B) | 0.99 |
| **O(4)-C(9)** | 1.156(4) | C(15)-H(15A) | 0.98 |
| **C(4)-C(5)** | 1.381(4) | C(15)-H(15B) | 0.98 |
| **C(4)-H(4A)** | 0.95 | C(15)-H(15C) | 0.98 |
| **C(8)-Re(1)-C(9)** | 83.68(1) | C(1)-C(6)-H(6A) | 109.7 |
| **C(8)-Re(1)-C(7)** | 86.86(1) | O(1)-C(6)-H(6B) | 109.7 |
| **C(9)-Re(1)-C(7)** | 88.25(1) | C(1)-C(6)-H(6B) | 109.7 |
| **C(8)-Re(1)-O(1)** | 97.85(1) | H(6A)-C(6)-H(6B) | 108.2 |
| **C(9)-Re(1)-O(1)** | 96.81(1) | O(2)-C(7)-Re(1) | 177.8(3) |
| **C(7)-Re(1)-O(1)** | 173.42(1) | C(13)-O(8)-C(14) | 114.6(2) |
| **C(8)-Re(1)-O(1)** | 173.02(9) | O(3)-C(8)-Re(1) | 177.7(3) |
| **C(9)-Re(1)-O(1)** | 99.80(1) | O(4)-C(9)-Re(1) | 175.0(3) |
| **C(7)-Re(1)-O(1)** | 99.25(1) | O(5)-C(10)-C(5) | 109.5(2) |
| **O(1)-Re(1)-O(1)** | 75.79(8) | O(5)-C(10)-H(10A) | 109.8 |
| **C(8)-Re(1)-N(1)** | 92.97(1) | C(5)-C(10)-H(10A) | 109.8 |
| **C(9)-Re(1)-N(1)** | 169.44(1) | O(5)-C(10)-H(10B) | 109.8 |
| **C(7)-Re(1)-N(1)** | 101.61(1) | C(5)-C(10)-H(10B) | 109.8 |
| **O(1)-Re(1)-N(1)** | 73.67(8) | H(10A)-C(10)-H(10B) | 108.2 |
| **O(1)-Re(1)-N(1)** | 82.53(8) | O(6)-C(11)-O(5) | 124.5(3) |
| **C(6)-O(1)-Re(1)** | 107.87(2) | O(6)-C(11)-C(12) | 125.1(3) |
| **C(6)-O(1)-Re(1)** | 118.6(2) | O(5)-C(11)-C(12) | 110.3(3) |
| **Re(1)-O(1)-Re(1)** | 104.21(8) | C(11)-C(12)-C(13) | 110.6(2) |
| **C(1)-N(1)-C(5)** | 118.9(2) | C(11)-C(12)-H(12A) | 109.5 |
| **C(1)-N(1)-Re(1)** | 111.62(2) | C(13)-C(12)-H(12A) | 109.5 |
| **C(5)-N(1)-Re(1)** | 129.4(2) | C(11)-C(12)-H(12B) | 109.5 |
| **N(1)-C(1)-C(2)** | 122.1(3) | C(13)-C(12)-H(12B) | 109.5 |
| **N(1)-C(1)-C(6)** | 115.0(2) | H(12A)-C(12)-H(12B) | 108.1 |
| **C(2)-C(1)-C(6)** | 122.9(3) | O(7)-C(13)-O(8) | 126.2(3) |
| **C(3)-C(2)-C(1)** | 118.7(3) | O(7)-C(13)-C(12) | 123.6(3) |

| | | | |
|---|---|---|---|
| **C(3)-C(2)-H(2A)** | 120.6 | O(8)-C(13)-C(12) | 110.1(3) |
| **C(1)-C(2)-H(2A)** | 120.6 | O(8)-C(14)-C(15) | 106.6(3) |
| **C(2)-C(3)-C(4)** | 119.3(3) | O(8)-C(14)-H(14A) | 110.4 |
| **C(2)-C(3)-H(3A)** | 120.3 | C(15)-C(14)-H(14A) | 110.4 |
| **C(4)-C(3)-H(3A)** | 120.3 | O(8)-C(14)-H(14B) | 110.4 |
| **C(5)-C(4)-C(3)** | 119.7(3) | C(15)-C(14)-H(14B) | 110.4 |
| **C(5)-C(4)-H(4A)** | 120.1 | H(14A)-C(14)-H(14B) | 108.6 |
| **C(3)-C(4)-H(4A)** | 120.1 | C(14)-C(15)-H(15A) | 109.5 |
| **C(11)-O(5)-C(10)** | 117.2(2) | C(14)-C(15)-H(15B) | 109.5 |
| **N(1)-C(5)-C(4)** | 120.9(3) | H(15A)-C(15)-H(15B) | 109.5 |
| **N(1)-C(5)-C(10)** | 116.7(2) | C(14)-C(15)-H(15C) | 109.5 |
| **C(4)-C(5)-C(10)** | 122.4(3) | H(15A)-C(15)-H(15C) | 109.5 |
| **O(1)-C(6)-C(1)** | 109.7(2) | H(15B)-C(15)-H(15C) | 109.5 |
| **O(1)-C(6)-H(6A)** | 109.7 | | |

REFERENCES


1. Mehrotra, R. C.; Bohra, R.; Gaur, D. *Metal β-diketonates and Allied Derivatives;* Academic Press: 1978; . New York **1978**, 268-275.

2. Stephen, A.; Hashmi, K. Homogeneous Catalysis by Gold. *Gold Bulletin* **2004**, *37*, 51-65.

3. Stephen, A.; Hashmi, K. Homogeneous Catalysis by Gold. *Gold Bulletin* **2004**, *37*, 51-65.

4. Shi, F.; Deng, Y.; Yang, H.; SiMa, T. The First Syntheses of Diformamides by Carbonylation of Aliphatic Diamines with Au (I) Complex Catalysts. - *J.Chem.Soc.Chem. Commun.*, **2001**, 345-346.

5. Mizushima, E.; Hayashi, T.; Tanaka, M. Au (I)-Catalyzed Highly Efficient Intermolecular Hydroamination of Alkynes. *Org. Lett.* **2003**, *5*, 3349-3352.

6. Ito, H.; Yajima, T.; Tateiwa, J.; Hosomi, A. An Unprecedented Catalytic Reaction Using gold (I) complexes. *Tetrahedron Lett.* **1999**, *40*, 7807-7810.

7. Ito, H.; Yajima, T.; Tateiwa, J.; Hosomi, A. First gold Complex-Catalysed Selective Hydrosilylation of Organic Compounds Studies on Organosilicon Chemistry: no. 152. For no. 151, see K. Miura, K. Tamaki, T. Nakagawa and A. Hosomi, *Angew. Chem., Int. Ed*., 2000, in press. *Chemical Communications* **2000**, 981-982.

8. Roembke, P.; Schmidbaur, H.; Cronje, S.; Raubenheimer, H. Application of (phosphine)gold(I) Carboxylates, Sulfonates and Related Compounds as Highly Efficient Catalysts for the Hydration of Alkynes. *Journal of Molecular Catalysis.A, Chemical* **2004**, *212*, 35-42.

9. Miyaura, N.; Suzuki, A. Palladium-Catalyzed Cross-Coupling Reactions of Organoboron Compounds. *Chem. Rev.* **1995**, *95*, 2457-2483.

10. Alhanash, F. *Reaction of Tertiary Phosphine with group 15 trihalides and related systems.* University of Manchester, 2012.

11. Tolman, C. A. Steric Effects of Phosphorus Ligands in Organometallic Chemistry and Homogeneous Catalysis. *Chem. Rev.* **1977**, *77*, 313-348.

12. Crabtree, R. H. *The Organometallic Chemistry of Transition Metals Third Edition;* Wiley Interscience: New York, 2001; 92.

13. Streitwieser, A.; McKeown, A. E.; Hasanayn, F.; Davis, N. R. Basicity of Some Phosphines in THF. *Org. Lett.* **2005**, *7*, 1259-1262.

14. Hartwig, J. F. *Organotransition Metal Chemistry: From Bonding to Catalysis;* United Science Books, 1964, pp 35.

15. Bush, R. C.; Angelici, R. J. Phosphine Basicities as Determined by Enthalpies of Protonation. *Inorg. Chem.* **1988**, *27*, 681-686.

16. Crabtree, R. H.; Mihelcic, J. M.; Quirk, J. M. Iridium Complexes in Alkane Dehydrogenation. *J. Am. Chem. Soc.* **1979**, *101*, 7738-7740.

17. Uttley, J. *J. Chem. Soc. Dalton Trans* **1976**, 2069.

18. Tolman, C. A. Phosphorus Ligand Exchange Equilibriums on Zerovalent Nickel. Dominant Role for Steric Effects. *J. Am. Chem. Soc.* **1970**, *92*, 2956-2965.

19. Hartwig, J. F. *Organotransition Metal Chemistry: From Bonding to Catalysis;* United States, 2010; .University Science Books, **1964**, pp 35

20. Miyashita, A.; Yasuda, A.; Takaya, H.; Toriumi, K.; Ito, T.; Souchi, T.; Noyori, R. Synthesis of 2,2'-Bis(diphenylphosphino)-1,1'-Binaphthyl (BINAP), an Atropisomeric Chiral Bis(triaryl)phosphine, and its Use in the Rhodium(I)-Catalyzed Asymmetric Hydrogenation of Alpha (acylamino)acrylic acids. *J. Am. Chem. Soc.* **1980**, *102*, 7932-7934.

21. Shimizu, H.; Nagasaki, I.; Matsumura, K.; Sayo, N.; Saito, T. Developments in Asymmetric Hydrogenation from an Industrial Perspective. *Acc. Chem. Res.* **2007**, *40*, 1385-1393.

22. Knowles, J. P.; Whiting, A. The Heck–Mizoroki Cross-Coupling Reaction: A Mechanistic Perspective. *Organic & Biomolecular Chemistry* **2007**, *5*, 31-44.

23. Baudry, D.; Ephritikhine, M.; Felkin, H.; Holmes-Smith, R. The Selective Catalytic Conversion of Cycloalkanes Into Cycloalkenes Using a Soluble Rhenium Polyhydride System. *Journal of the Chemical Society, Chemical Communications* **1983**, 788.

24. Jensen, C. Iridium PCP Pincer Complexes: Highly Active and Robust Catalysts for Novel Homogeneous Aliphatic Dehydrogenations. *Chemical Communications* **1999**, 2443-2449.

25. Herrmann, W. A.; Böhm, V. P.; Reisinger, C. Application of Palladacycles in Heck Type Reactions. *Journal of Organometallic Chemistry* **1999**, *576*, 23-41.

26. Reisinger, C.-P. PhD thesis, TU Munchen, 1997

27. Hennings, D. D.; Iwasa, S.; Rawal, V. H. Anion-Accelerated Palladium-Mediated Intramolecular Cyclizations: Synthesis of Benzofurans, Indoles, and a Benzopyran. *Tetrahedron Lett.* **1997**, *38*, 6379-6382.

28. Louie, J.; Hartwig, J. A Route to Pd-0 from Pd-II Metallacycles in Amination and Cross-Coupling Chemistry. *Angewandte Chemie-International Edition* **1996**, *35*, 2359-2361.

29. Duffy, N.; Nelson, R.; Richmond, M.; Rieger, A.; Rieger, P.; Robinson, B.; Tyler, D.; Wang, J.; Yang, K. An EPR Study of 2, 3-bis (diphenylphosphino) maleic Anhydride (BMA) Complexes and the BMA Radical Anion. *Inorg. Chem.* **1998**, *37*, 4849-4856.

30. Watson, W.; Wu, G.; Richmond, M. Diphosphine Isomerization and C-H and P-C Bond Cleavage Reactivity in the Triosmium Cluster Os-3(CO)(10)(bpcd): Kinetic and Isotope Data for Reversible Ortho Metalation and X-ray structures of the Bridging and Chelating Isomers of Os-3(CO)(10)(bpcd) and the Benzyne-Substituted Cluster $HOs_3(CO)_8$(mu(3)-$C_6H_4$)[mu(2),eta(1)-PPhC=C(PPh2)C(O)CH2C(O)]. *Organometallics* **2006**, *25*, 930-945.

31. Becher, H. J.; Fenske, D.; Heymann, M. Radikalanionen des Bis(diphenylphosphino)maleinsäureanhydrid und Seiner Derivate Polarographische und ESR-Messungen Präparative Anwendungen. *Zeitschrift für anorganische und allgemeine Chemie* **1981**, *475*, 27-34.

32. Mao, F.; Tyler, D.; Keszler, D. Mechanism Of The Substitution-Reactions Of The 19-Electron Co(Co)3l2 Complex [L2=2,3-Bis(Diphenylphosphino)Maleic Anhydride. *J. Am. Chem. Soc.* **1989**, *111*, 130-134.

33. Atim, S.; Wang, X.; Richmond, M. G. Synthesis of the Donor-Acceptor Ligand 2-(4-dimethylaminobenzylidene)-4,5-bis(diphenylphosphino)-4-cyclopenten-1,3-dione (dbpcd) and X-ray Diffraction Structure of the Platinum(II) Compound $PtCl_2$(dbpcd)1.5$CH_2Cl_2$. *Inorg. Chim. Acta* **2010**, *363*, 418.

34. Hunt, S.; Yang, L.; Wang, X.; Nesterov, V.; Richmond, M. New Pt(II)(dithiolate) Compounds Possessing an Energetically Accessible Diphosphine-Based LUMO: Syntheses, Redox Properties, and Solid-State Structures of PtCl2(pbpcd), Pt(tdt)(pbpcd), and Pt(tdt)(bpcd). *Journal of Inorganic and Organometallic Polymers and Materials* **2010**, *20*, 457-467.

35. Lingafelter, E. t.; Braun, R. Interatomic Distances and Angles in Metal Chelates of Acetylacetone and Salicylaldimine. *J. Am. Chem. Soc.* **1966**, *88*, 2951-2956.

36. Bennett M.A; Mitchell T.R; Stevens M.R; Willis A.C Mono- and bis-(acetylacetonato) complexes of Arene-Ruthenium(II) and Arene-Osmium(II): Variation of the Binding Mode of Acetylacetonate with the Nature of the Arene. *Canadian Journal of Chemistry* **2001**, *79*, 655-655.

37. Koda, S. e. a. *J. C. S. Chem. Commun* **1971**, 1321.

38. Haigh, J. M.; Thornton, D. A. Acetylacetone and ß-Ketoimine Solvates of dioxobis(acetylacetonato) Uranium(VI). *Inorganic and Nuclear Chemistry Letters* **1970**, *6*, 231-235.

39. Shalhoub, G. M. $Co(acac)_3$: Synthesis, Reactions and Spectra: An Experiment for General Chemistry. *J. Chem. Educ.* **1980**, *57*, 525.

40. Hynes, M. J. *Rev. Inorg. Chem.* **1990**, *11*, 121.

41. Wenzel, T. J.; Williams, E. J.; Haltiwanger, R. C.; Sievers, R. E. Studies of Metal Chelates with the Novel Ligand 2,2,7-Trimethyl-3,5-octanedione. *Polyhedron* **1985**, *4*, 369-378.

42. Hauser, C. P.; Thielemann, D. T.; Adlung, M.; Wickleder, C.; Roesky, P. W.; Weiss, C. K. *Macromol. Chem. Phys.* **2011**, *212*, 286.

43. Czerwiński, M.; Narbutt, J. Outer-Sphere Hydration and Liquid− Liquid Partition of Metal (III) Chelates− Density Functional Calculations. *European Journal of Inorganic Chemistry* **2005**, *2005*, 555-562.

44. Hansen, B.; Hybertson, B.; Barkley, R.; Sievers, R. Supercritical Fluid Transport Chemical-Deposition of Films. *Chemistry of Materials* **1992**, *4*, 749-752.

45. Laintz, K. E.; Tachikawa, E. Extraction of Lanthanides from Acidic Solution Using Tributyl Phosphate Modified Supercritical Carbondioxide. *Anal. Chem.* **1994**, *66*, 2190.

46. Cullen, W. R.; Wickenheiser, E. B. Rhodium (I) Complexes of β-Diketonates and Related Ligands as Hydrosilylation Catalysts. *Journal of Organometallic Chemistry* **1989**, *370*, 141-154.

47. Lewis, F.; Miller, A.; Salvi, G. Spectroscopy And Photochemistry Of Nickel(II), Palladium(Ii), And Platinum(II) Beta-Diketonates. *Inorg. Chem.* **1995**, *34*, 3173-3181.

48. Dhar, S.; Park, B.; Arnold, C. Dioxygen Activation By Acetylacetone And Salicylaldehyde Complexes Of Fe(Ii). *Microchemical Journal* **1993**, *47*, 14-18.

49. Eng, S. J.; Motekaitis, R. J.; Martell, A. E. The Effect of End-Group Substitutions and Use of a Mixed Solvent System on ß-Diketones and their Iron Complexes. *Inorg. Chim. Acta* **1998**, *278*, 170-177.

50. Kimberly D M Charleton; Ernest M Prokopchuk Coordination Complexes as Catalysts: The Oxidation of Anthracene by Hydrogen Peroxide in the Presence of $VO(acac)_2$. *J. Chem. Educ.* **2011**, *88*, 1155.

51. Menshikov, S.; Vurasko, A.; Petrov, L.; Molochnikov, L.; Novoselova, A.; Skryabina, Z.; Saloutin, V. Liquid-Phase Oxidation Of Anthracene By Hydrogen-Peroxide In The Presence Of Heterogenized Vanadyl Acetylacetonate. *Bulletin of the Russian Academy of Sciences-Division Of Chemical Science* **1992**, *41*, 619-622.

52. Bouyahyi, M.; Roisnel, T.; Carpentier, J. Aluminum Complexes of Fluorinated beta-Diketonate Ligands: Syntheses, Structures, Intramolecular Reduction, and Use in Ring-Opening Polymerization of Lactide. *Organometallics* **2010**, *29*, 491-500.

53. Morin, A.; Detrembleur, C.; Jerome, C.; De Tullio, P.; Poli, R.; Debuigne, A. Effect of Head-to-Head Addition in Vinyl Acetate Controlled Radical Polymerization: Why is $Co(acac)_2$-Mediated Polymerization so Much Better *Macromolecules* **2013**, *46*, 4303-4312.

54. Wang, J.; Liu, Z.; Wang, D.; Guo, D. Syndiospecific Polymerization of Styrene Based on Dichlorobis(1,3-diketonato)titanium/methylaluminoxane Catalyst System: Effects of Substituents on Catalyst Activity. *Polym. Int.* **2000**, *49*, 1665-1669.

55. Jeong, N.; Hwang, S.; Lee, Y.; Chung, Y. Catalytic Version of The Intramolecular Pauson-Khand Reaction. *J. Am. Chem. Soc.* **1994**, *116*, 3159-3160.

56. Lee, N.; Chung, Y. Synthesis of Cyclopentenones: The New Catalytic Cyclization Reaction of Alkyne, Alkene, and Carbonmonoxide Employing Catalytic $Co(acac)_2$ and $NaBH_4$. *Tetrahedron Lett.* **1996**, *37*, 3145-3148.

57. Yu, W.; Fuhr, O.; Fenske, D. Derivatives of Bis(diphenylphosphino)maleic Anhydride as Ligands in Polynuclear Gold(I) Complexes. *Journal of Cluster Science* **2012**, *23*, 753-766.

58. Zhao, H.; Mello, B.; Fu, B.; Chowdhury, H.; Szalda, D.; Tsai, M.; Grills, D.; Rochford, J. Investigation of Monomeric versus Dimeric fac-Rhenium(I) Tricarbonyl Systems Containing the Noninnocent 8-Oxyquinolate Ligand. *Organometallics* **2013**, *32*, 1832-1841.

59. Jorgensen, C. K. *Coord. Chem. Rev.* **1966**, 164-178.

60. Allgeier, A.; Mirkin, C. Ligand Design for Electrochemically Controlling Stoichiometric and Catalytic Reactivity of Transition Metals. *Angewandte Chemie-International Edition* **1998**, *37*, 894-908.

61. Wada, T.; Tsuge, K.; Tanaka, K. Oxidation of Hydrocarbons by Mono- and Dinuclear Ruthenium Quinone Complexes via Hydrogen Atom Abstraction. *Chem. Lett.* **2000**, *29*, 910-911.

62. Chaudhuri, P.; Wieghardt, K. In *Phenoxyl radical complexes;* John Wiley & Sons Inc: New York, 2001; Vol. 50, 151-216.

63. Hino, T.; Wada, T.; Fujihara, T.; Tanaka, K. Redox Behavior of New Ru-dioxolene-ammine Complexes and Catalytic Activity toward Electrochemical Oxidation of Alcohol under Mild Conditions. *Chem. Lett.* **2004**, *33*, 1596-1597.

64. Sumathi, S.; Tharmaraj, P.; Sheela, C. D.; Anitha, C. Synthesis and Studies on Cu(II), Co(II), Ni(II) complexes of Knoevenagel ß-diketone ligands. *Spectrochimica Acta Part A: Molecular and Biomolecular Spectroscopy* **2012**, *97*, 377-383.

65. Rowe, R. A.; Jones, M. M. *Inorg. Synth.* **1957**, *5*, 114-115.

66. Bryant, B. E.; Fernelius, W. C. *Inorg. Synth.* **1957**, *5*, 115.

67. Bhattacharjee, M. An Efficient And Direct Synthesis Of Bis(Acetylacetonato)-Oxovanadium(Iv). *Journal of Chemical Research-S* **1992**, 415-415.

68. Bruker APEX 2 Bruker Advanced Analytical X ray Systems, Inc. Copyright. **2007,** Madison, WI.

69. Bruker, S. Bruker Advanced Analytical X-ray System, Inc. **2007,** Madison, WI.

70. Bruker, S. Bruker Advanced Analytical X-ray System, Inc. **2007,** Madison, WI.

71. A.L. Spek, P. A Multipurpose Crystallographic Tool. Ultrecht University. **2006,** The Netherlands.

72. Sheldrick, G. M. S. *Bruker Advanced Analytical X-ray Systems, Inc. Copyright* . **2008,** Madison, WI.

73. Davila, R.; Elduque, A.; Grant, T.; Staples, R.; Fackler, J. Syntheses And Characterization Of Dinuclear Gold(I) Ring And Open-Ring Complexes Containing Saturated And Unsaturated Dithiol Bridging Ligands And Phosphine Or Bis(Diphosphine) Donor Ligands - Crystal-Structures Of $[Au_2(Mu\text{-}S(CH_2)_3)(Mu\text{-}Dppm)]$,[Au2(Mu-Mnt)$(PPh_3)$2], $[Au_2(Mu\text{-}S_2C_6H_4)(PPh_3)_2]$, And $[Au_4(Mu\text{-}S_2C_6H_3CH_3)_2(PEt_3)_2]$. *Inorg. Chem.* **1993**, *32*, 1749-1755.

74. Deak, A.; Megyes, T.; Tarkanyi, G.; Kiraly, P.; Biczok, L.; Palinkas, G.; Stang, P. Synthesis and Solution- and Solid-State Characterization of Gold(I) rings with Short Au Center Center Au Interactions. Spontaneous Resolution of a Gold (I) Complex. *J. Am. Chem. Soc.* **2006**, *128*, 12668-12670.

75. Berners-Price, S. J.; Bowen, R. J.; Fernandes, M. A.; Layh, M.; Lesueur, W. J.; Mahepal, S.; Mtotywa, M. M.; Sue, R. E.; van Rensburg, C. E. Gold (I) and Silver (I) Complexes of 2, 3-bis (diphenylphosphino) maleic acid: Structural Studies and Antitumour Activity. *Inorg. Chim. Acta* **2005**, *358*, 4237-4246.

76. Hussain, M. S.; Schlemper, E. Chloro (triphenylphosphine sulfide) gold (I). *Acta Crystallographica Section C: Crystal Structure Communications* **1987**, *43*, 450-453.

77. Tiekink, E. R. Chloro (triethylphosphine) gold (I). *Acta Crystallographica Section C: Crystal Structure Communications* **1989**, *45*, 1233-1234.

78. Yu, W.; Fuhr, O.; Fenske, D. Derivatives of Bis(diphenylphosphino)maleic Anhydride as Ligands in Polynuclear Gold(I) Complexes. *Journal of Cluster Science* **2012**, *23*, 753-766.

79. Schmidbaur, H.; Schier, A. Aurophilic Interactions as a Subject of Current Research: An Up-date. *Chem. Soc. Rev.* **2011**, *41*, 37-412.

80. Serrano-Becerra, J.; Paradies, J.; Maier, A.; Gonzalez-Gallardo, S.; Moos, E.; Kaub, C.; Gaffga, M.; Niedner-Schatteburg, G.; Roesky, P.; Breher, F. Mono- vs. Dinuclear Gold-Catalyzed Intermolecular Hydroamidation. *European Journal of Organic Chemistry* **2014**, 4515-4522.

81. Baenziger, N. C.; Dittemore, K. M.; Doyle, J. R. Crystal and Molecular Structure of Chlorobis(triphenylphosphine) gold(I) hemibenzenate. *Inorg. Chem.* **1974**, *13*, 805-811.

82. Attar, S.; Bearden, W.; Alcock, N.; Alyea, E.; Nelson, J. Phosphole Complexes Of Gold (I) Halides - Comparison Of Solution And Solid-State Structures By a Combination of Solution And Cp Mas P-$^{31}$NMR-Spectroscopy And X-Ray Crystallography. *Inorg. Chem.* **1990**, *29*, 425-433.

83. Kriechbaum, M.; List, M.; Himmelsbach, M.; Redhammer, G. J.; Monkowius, U. Peptide Coupling Between Amino Acids and the Carboxylic Acid of a Functionalized Chloride - gold(I)-phosphane. *Inorg. Chem.* **2014**, *53*, 10602-10610.

84. Guidez, E.; Hadley, A.; Aikens, C. Initial Growth Mechanisms of Gold-Phosphine Clusters. *Journal of Physical Chemistry C* **2011**, *115*, 6305-6316.

85. Smith, M. B.; Dale, S. H.; Elsegood, M. R. J. *Acta. Cryst. E* **2006**, m 1850-m1852.

86. Schmidbaur, H.; Schier, A. Aurophilic Interactions as a Subject of Current Research: An Up-date. *Chem. Soc. Rev.* **2011**, *41*, 37-412.

87. Jones, P. G. μ-cis-1, 2-Bis (diphenylphosphino) ethylene-bis [chlorogold (I)]. *Acta Crystallographica Section B: Structural Crystallography and Crystal Chemistry* **1980**, *36*, 2775-2776.

88. Kriechbaum, M.; List, M.; Himmelsbach, M.; Redhammer, G. J.; Monkowius, U. Peptide Coupling Between Amino Acids and the Carboxylic Acid of a Functionalized Chloride - gold(I)-phosphane. *Inorg. Chem.* **2014**, *53*, 10602-10610.

89. Ahrland, S.; Dreisch, K.; Noren, B.; Oskasson, A. Crystal Structure of Iodo(triphenylphosphine)gold(I) and Bis[iodo(trimethylphosphine)gold(I)]. *Acta. Chemica Scandinavia A* **1987**, *41*, 173-177.

90. Roychowdhury, P.; Das, B. N.; Basak, B. Crystal and Molecular Structure of 8-Hydroxyquinoline. *Acta Crystallographica Section B: Structural Crystallography and Crystal Chemistry* **1978**, *34*, 1047-1048.

91. Allen, F.; Kennard, O.; Watson, D. G.; Brammer, L.; Orpen, A. G. *J. Chem. Soc. Perkin Trans II* **1987**, S1-S9.

92. Yang, L.; Liu, W.; Wang, H.; Chen, X.; Wang, H. 3-(3-Methylphenyl)-5-(quinolin-8-ylmethoxy)-1, 2, 4-Oxadiazole Monohydrate. *Acta Crystallographica Section E: Structure Reports Online* **2013**, *69*, o1541-o1541.

93. Damous, M.; Dénes, G.; Bouacida, S.; Hamlaoui, M.; Merazig, H.; Daran, J. 8-Hydroxyquinolin-1-ium hydrogen sulfate monohydrate. *Acta Crystallographica Section E: Structure Reports Online* **2013**, *69*, 1458-1459.

94. Jia, Z.; Zhao, Y.; Wen, Q.; Ma, A. The Non-Centrosymmetric Polymorph of (Quinolin-8-ol-2N, O) (Quinolin-8-olato-2N, O) silver (I). *Acta Crystallographica Section E: Structure Reports Online* **2013**, *69*, m133-m133.

95. Wu, H.; Dong, X.; Liu, H.; Ma, J. (Quinolin-8-ol-2N, O)(quinolin-8-olato-2N, O) silver (I). *Acta Crystallographica Section E: Structure Reports Online* **2006**, *62*, m281-m282.

96. Zhao, H.; Mello, B.; Fu, B.; Chowdhury, H.; Szalda, D.; Tsai, M.; Grills, D.; Rochford, J. Investigation of Monomeric versus Dimeric fac-Rhenium(I) Tricarbonyl Systems Containing the Noninnocent 8-Oxyquinolate Ligand. *Organometallics* **2013**, *32*, 1832-1841.

97. Banerjee, S.; Levadala, M.; Lazarova, N.; Wei, L.; Valliant, J.; Stephenson, K.; Babich, J.; Maresca, K.; Zubieta, J. Bifunctional Single Amino Acid Chelates for Labeling of Biomolecules with the{Tc(CO)(3)}+ and {Re(CO)(3)}+ Cores. Crystal and Molecular Structures of [ReBr(CO)(3)($H_2NCH_2C_5H_4N$)], [Re(CO)(3){($C_5H_4NCH_2$)(2)NH}]Br, [Re(CO)(3){($C_5H_4NCH_2$)(2)$NCH_2CO_2H$}]Br, [Re(CO)(3){X(Y)$NCH_2CO_2CH_2CH_3$}]Br (X = Y=2-pyridylmethyl; X=2-pyridyimethyl, Y=2-(1-methylimidazolyl)methyl; X = Y=2-(1-methylimidazolyl)methyl), [ReBr(CO)(3){($C_5H_4NCH_2$)NH($CH_2C_4H_3S$)}], and [Re(CO)(3){($C_5H_4NCH_2$)N($CH_2C_4H_3S$)($CH_2CO_2$)}]. *Inorg. Chem.* **2002**, *41*, 6417-6425.

98. Alvarez, C.; Carrillo, R.; Garcia-Rodriguez, R.; Miguel, D. pH-driven Dynamic Stereoinduction: Epimerization Upon Dimerization in Rhenium (I) Complexes. *Chemical Communications* **2011**, *47*, 12765-12767.